POLITECNICO DI MILANO

Facoltà di Ingegneria Industriale

Corso di Laurea in
Ingegneria Aeronautica

Non modal linear stability analysis of an EHD channel flow

Relatore: Prof. Maurizio Quadrio
Co-relatori: Fulvio Martinelli
Peter J. Schmid

Tesi di Laurea di:
Emanuele BEZZECCHI Matr. 720618

Anno Accademico 2009 - 2010

Abstract

This work studies the stability properties of a dielectric liquid confined between two indefinite plane electrodes, the so-called electro-hydrodynamic (EHD) electroconvection problem, that presents a full coupling between the electric field and the velocity field. The EHD stability has been already studied in the past, owing to its practical importance and theoretical interest, but several open problems still exist. In fact, very simple analytical and/or numerical models have been employed, with sometimes far-reaching simplifying assumptions like that of neglecting the charge diffusion process altogether. As a matter of fact, discrepancies exist between the critical values of the governing parameters measured in experiments as compared to those educed from theoretical analysis.

This work reports on several, substantial improvements of the state-of-the-art in the study of EHD electroconvection. The effect of charge diffusion is taken into account, and a cross-flow is explicitly considered in the form of a laminar Poiseuille flow. Moreover, and perhaps most importantly, we apply to the EHD problem the recent theoretical tools of non-modal stability analysis. After a physically sound norm is defined to quantify the disturbance amplitude, the non-modal stability analysis allows us to describe the non-normality of the underlying stability operator, which implies that the EHD system is capable to support transient growth, albeit of mild intensity, in both the hydrostatic case and in the case with shear. The important role of charge diffusion is described, which enhances instability through increased mixing, and is connected to wall-based modes. The EHD-Poiseuille system is found to be unstable to perturbations that at low Re are dominated by the electrical parameters.

Sommario

A causa della sua importanza pratico-teorica, nel corso degli ultimi decenni i fenomeni di instabilità riguardanti l'accoppiamento fluido-elettrodinamico sono stati oggetto di numerose indagini. In questo campo, conosciuto sotto l'acronimo di EHD, uno dei fenomeni più studiati è quello dell'*elettroconvezione*. Una delle configurazioni più classiche prevede l'azione di un campo elettrico su di un liquido dielettrico attraverso l'utilizzo di due elettrodi piani, paralleli ed indefiniti.
Nonostante col passare degli anni si sia aquisita una notevole conoscenza dei processi scatenanti l'elettroconvezione restano ancora alcuni interrogativi da risolvere. L'accoppiamento EHD ha infatti una natura molto complessa ed i modelli semplificati utilizzati fino ad oggi hanno sempre trascurato sia gli effetti della diffusività elettrica molecolare sia la presenza di un una corrente laminare. A causa di ciò esiste una notevole dicrepanza tra i criteri di stabilità lineare ricavati dalla teoria e quelli osservati sperimentalemente.
Si sono quindi reinterpretati i suddetti criteri, includendo per la prima volta ad oggi sia la diffusività elettrica che il flusso laminare. Nondimeno, grazie alla teoria dell'analisi non modale ed alla definizione di una norma che quantifica l'energia associata ai disturbi, è stato possibile dimostrare che l'operatore EHD linearizzato manifesta crescite energetiche transitorie anche quando la semplice analisi agli autovalori predice il contrario. Tali crescite sono legate sia a meccanismi fluiddinamici (*Orr* e *Lift-up*) che elettrici.
Siamo quindi in grado di affermare che sono stati portati notevoli miglioramenti allo studio dell'elettroconvezione così come inteso fino ad oggi.

CAPITOLO 1

Ringraziamenti

Credo di avervi già ringraziati più e più volte ma *verba volant, scripta manent*, perciò...

Innanzitutto ringrazio il Politecnico di Milano. In questa Sparta dello studio ho imparato che nella vita nulla viene regalato, anzi, ma ho anche capito che in ognuno di noi alberga una forza che ci spinge a non riposarci mai, fino a quando possiamo andare un po' più in là.

Ufficialmente, ma non perchè imposti dall'etichetta, ringrazio il Professor Maurizio Quadrio che mi ha dato fiducia, tempo, e soprattutto l'irripetibile possibilità di capire che, da qualche parte là fuori, la cultura è ancora un bene inestimabile. Con la speranza nel cuore di ritornare a Parigi per poterlo fare di persona ringrazio Fulvio Martinelli e Peter J. Schimd per la paterna pazienza dimostrata nei miei confronti. Soprattutto Fulvio, Grazie di tutto!

Vorrei poi ringraziare chi in questi anni di studio mi ha comunque *comunicato* qualcosa, che siano stati insegnamenti o semplici regole di vita. Ringrazio perciò il professor Luigi Quartapelle per lo stupendo pomeriggio passato a parlare di Termodinamica davanti ad uno Spritz, per avermi insegnato il concetto di *persona per bene*, e per avermi dato la possibilitá di aiutarlo con il suo libro. Nondimeno vorrei ringraziare lui ed il professor Alberto Guardone per aver discusso con noi dei problemi di questa Nostra Italia.
So che chiunque stia leggendo strabuzzerà gli occhi ma vorrei ringraziare Lui, il professor Paolo Mantegazza per avermi fatto capire, nel suo modo tutto particolare, che non si finisce mai di imparare[1].

Finiti i ringraziamenti di rito vorrei passare a voi.
Innanzitutto Mamma Vittoria e papà Giuseppe *Peppone*. Grazie. Grazie. Grazie. Lo dovrei scrivere almeno 10^{1000} volte e non basterebbe ancora. Grazie. So che avete nè avete passate tante per darmi questa opportunità quindi grazie.
Patata, tu più di tutti, forse anche più di me hai dovuto sopportare il peso di quest'ultimo anno. La lontananza, i week end da sola, solo una voce al telefono e mai una persona da abbracciare...grazie per non avermi mai fatto sentire il peso delle mie decisioni. Dopo otto anni passati assieme riesci ancora a stupirmi con la tua forza e

[1] Lei scrive, scrive, ma non capisce un $*****$!

con il coraggio che sai dimostrare nelle situazioni più difficili[2]. Dio solo sa quanto ti amo e quanto mi è spiaciuto renderti triste. Riparerò a tutto. Nel frattempo però *baciami donna! Si va a festeggiare!*

Amici, non vogliatemene se siete dopo Mamma, Papà e Ale. Ringrazio Giovanni e Luca per avermi insegnato come sopravvivere in questa Sparta. Elmetto in testa e coltello in bocca. Grazie Gio, senza di te non sarei arrivato alla specialistica, non mi sarei mai deciso ad andare all'estero e non avrei mai finito in tempo di scrivere questa tesi. Grazie Luca, senza di te non avrei mai capito, *e forse* entrambi non l'abbiamo ancora capito, come delle *brave persone* affrontano i problemi. Lo sai che aldilà dei voti tu sei il più bravo di tutti. È l'unica certezza che ho.
Grazie Nicholas Sebastian Fantini detto Montenegrolas, Skifolas, Vomitolas. Fratello di altra Madre, Tu mi hai insegnato tanto, e parlo di come essere un uomo nelle situazioni difficili. Tu hai più cultura, voglia di fare e forza di volontà del 99% delle persone che conosco. Vedi di non gettare via questo dono. Spacca. Ora.

Ciuffo, Coppa, Giovi, Jorge, Marco, Nuwan, so che ormai il tempo trascorso assieme è sempre meno ma avete un posto di rigurado nel mio cuore. Tutti. E sarebbe meglio TUTTI ASSIEME. Voi sapete di cosa parlo. Thomas tieni duro, sei arrivato ormai. Grazie per il tuo supporto, i mitici messaggi di motivazione del Tommy non si scordano mai. Fede, sai che ti invidio un sacco per quello che hai fatto vero??? Dai che ci si becca a Parigi! Giulio, ah *Cecchetto*, è stato un onore servire con lei in quest'ultima battaglia. Roby, Bubu, grazie per aver supportato la mia causa con l'Ale. Leti, il tuo primo paziente ancora vivente, ti ringrazia di tutto, dei consigli, e delle risate che mi fai fare pensando alle tue vicissitudini amorose. vedrai che troverai la persona giusta, eh eh!Sopratutto grazie del tempo che impieghi ogni volta a venire alla mia laurea, spero di poter ricambiare il più presto possibile! I ragazzi di RESET!, Alex, Rocco, Simo, Teo e Zizzo, grazie di cuore per avermi reso partecipe del vostro progetto. WE CAN MAKE IT TOGETHERE IF WE TRY. Ladhyx crew, thanks for making me feel at home. Eletta, grazie per non avermi fatto fare il barbone a Parigi e per avermi fatto capire quanto *noi italiani* spacchiamo!

Avrò dimenticato sicuramente qualcuno. Mi dispiace ma ho scritto tutto questo mezz'ora prima di stampare la tesi. In puro stile Bezzecchi. Non vogliatemene!

Se sembra esserci una facile soluzione, preoccupati. Se sembra non esserci soluzione, preoccupati.
Emanuele e Luca parafrasando Aristotele.

[2]bhè quasi sempre a parte quando bisogna portare i gatti altrui dal veterinario

Contents

List of Figures

CHAPTER 2

INTRODUCTION

ELECTROHYDRODYNAMICS (EHD) is the particular domain of electrodynamics of moving media concerned with the action of electric forces on dielectric fluids. Since the dielectric fluids are usually characterized by very low electrical conductivity they can sustain very high electric fields without strong currents and this permits to neglect the induced magnetic fields (A)

Two electric forces can be distinguished which can give rise to a permanent fluid motion, namely the *Coulomb force* and the dielectric force. On another hand, two categories of problems can be defined. Only the Coulomb force distributed in the bulk of fluids will be considered here.

Unfortunately the complex and most often strongly nonlinear coupling between force and motion makes EHD a difficult subject. In fact, the charge distribution involves much smaller spatial scales, which are strongly influenced by minimal variations of the velocity field. This intrinsic complexity forced the early numerical simulations of EHD flows to use simplified model of flow-charge interaction and charge transport, neglecting the charge diffusion.

2.1 Electroconvection

The classical EHD problem deals with the simple and idealized case of unipolar injection of identical ions into a liquid layer bounded between two parallel electrodes almost exclusively without cross flow. The unipolar injection assumption implies that the density of injected charge is uniform on the injecting electrode. For this configuration the question of hydrodynamic instability arises. Nevertheless, in this

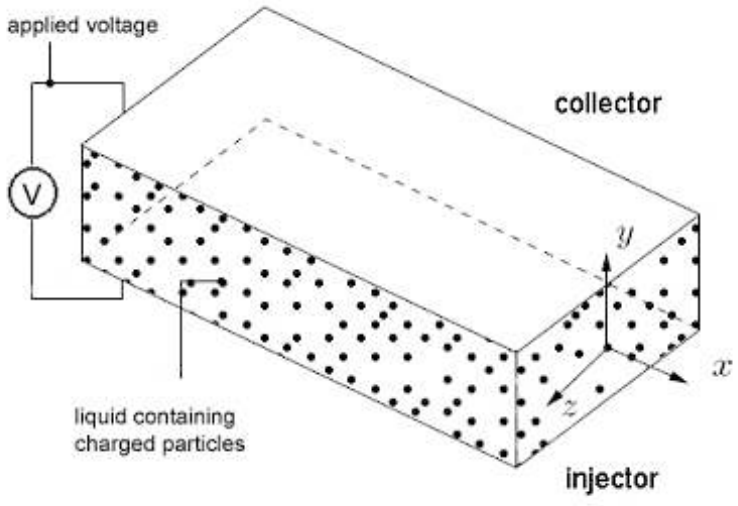

Figure 2.1: Introduction: *Framework*

.

domain, the Naiver-Stokes equations have *two equilibrium* solutions: the motionless state and the Poiseuille flow.
The instability problem is then to determine in what conditions the fluid mechanics equilibrium solutions destabilize under electric field effect examining the time evolution of perturbation of vanishingly small amplitude and determining the critical conditions for which at least one perturbation begin to grow exponentially. If instability arises, it has been proven that this growing perturbation produces coherent convective structures (called *rolls*) between two electrodes that show an *electroconvective* effect.

Fundamental studies into the onset of electroconvection in insulating liquid have been carried out by Watson et al. [25], [4] starting from the 70's. Till now both theoretical and experimental studies have been carried out implying the motionless state of the basic flow and steady charge transport dominated by ionic drift. Nevertheless after [16] the charge diffusion term has been ignored at all.
The first important result figures out by these studies is the role played by the dimensionless parameter T, which is described as the ratio of electrical energy supplied to the system to the energy dissipated by viscous force. It could be viewed as the directly analogous to the Rayleigh number in hydrodynamics.

Atten [1] shows that the simple Ohmic law that relates voltage and current density tends to fail as T increases above a critical value. This deviation suggests the sets in of a liquid convection which affects the charge transport.
Performing a modal linear stability analysis, a dimensionless wavenumber K also appears in [25] and a neutral stability curve can be plotted relating the critical values of T and K.
For strong injection, the autonomous *injection assumption* is valid. In this regime instability is only dependent on T, and it occurs for $T^{\star} \approx 161$.
Physically, the charge density decreases from the emitter into insulating liquid and and this creates a potentially unstable situation. Considering a fluid portion under a velocity perturbation which conserves the charge, if it will be pushed toward collector it will be subjected to a greater Coulomb force than the fluid in its neighborhood which has a lower charge. Therefore it will have a tendency to continue to swing towards the collector.This tendency is counteracted by viscous drag and by relaxation of charge [6]. This excesses charge relaxation takes place via two physical mechanisms, i.e. molecular charge diffusion and Coulomb repulsion.
As many authors such as [3], [6] suggested, neglecting the diffusion term, is possible to obtain from the charge continuity a simplified but clear model of the charge relaxation. This model gives the decay of space-charge (Figure 2.2) along specific trajectories. The obvious limitation of this analysis is that it does not couple charge and velocity.

2.1.1 Rayleigh-Benard analogy and fluid-charge interaction

It has been proven as in the stationary state of pure unipolar injection, due to coulombic repulsion the charge density decreases from the injector to the collector. Therefore it suggests an analogy between the pure unipolar injection problem in plane parallel electrodes geometry and the Rayleigh-Bernard problem of horizontal fluid layer heated from below. In the latter case the unstable density gradient brings about fluid motion when the temperature differences is large enough for buoyancy to overcome the damping action of viscous forces. Above the critical value of the Rayleigh number, instability sets in and heat is partially transferred by convection. Although this analogy is not strictly correct because it does not take into account all three mechanisms which transport the charge carriers: mass flux, the molecular charge diffusion and the finite drift velocity of charge carriers with respect to the fluid.
In absence of fluid motion, Felici [10] developed a simple model, known as *hydraulic model*, in the weak injection regime. Felici modeled a convective cell as two columns of equal radius R in whose the liquid velocity is assumed to be constant in magnitude and to have a direction respectively identical and opposite to that of the electric field. In these assumptions the *time of flight* t_s of the ions between the injector ($y = 0$) and a point at height $\overline{y}$ has been computed as

$$t_s = \frac{\overline{y}}{KE_0} \tag{2.1}$$

where K is the ionic mobility of the dielectric and E_0 is the equilibrium solution of the electric field. Let us consider a convective motion in the form of two dimensional rolls as shown in Figure 2.2. a positive velocity component w along the field line

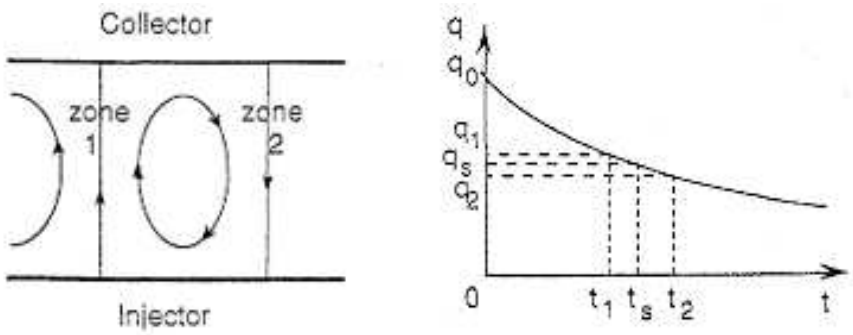

Figure 2.2: Introduction: *Two dimensional rolls and charge relaxation law*

(zone 1) results in a decrease of the time t_1 required for the ions to reach the height y because

$$t_1 = \frac{\overline{y}}{(KE_0 + v)}. \tag{2.2}$$

Coulomb repulsion therefore acts during a time smaller than the motionless time t_s and the charge density Q_1 is higher than the value Q_s which exists at rest (Figure 2.2). In zone 2, the liquid velocity diminishes resulting an opposite effect. Therefore the convective motion gives rise to a net torque which tends to accelerate it. Because of this positive coupling between velocity and charge perturbations, the stationary charge distribution is potentially unstable. The destabilizing force is proportional to $Q_1 - Q_2$ and consequently to the mean charge gradient.
This unstable character of space charge distribution does not imply that any velocity perturbations will be amplified. Indeed a sustained motion implies that an energy source can provide for dissipation due to viscous forces and it is clear that for low enough applied voltages the system remains stable.
As the liquid velocity reaches the value ($v = KE_0$), two separate regions are formed in the cell pattern. The charges are indeed denied to enter in zones where the liquid velocity in the electric field direction equals the ion mobility velocity. If the diffusion has been neglected the two region are separated by a discontinuity line called *separatrix*. If the charge diffusion works [8] the two regions still exist with the same geometry but the separatrix becomes an high charge gradient layer. The linear stability analysis gives the critical conditions but cannot predict the planform of the convective cells which will appear. Therefore non-linear analysis has been developed to explain both cells shape behavior and hysteresis loop in current-voltage law [1], [7]. The great features of the non-linear instability mechanism have been derived by Felici [10] and consists in its *hydraulic model*. This simple model has been extended by several authors using information about the shape of convective cells risen by experimental results. The typical shapes are 2D rolls and 3D hexagonal

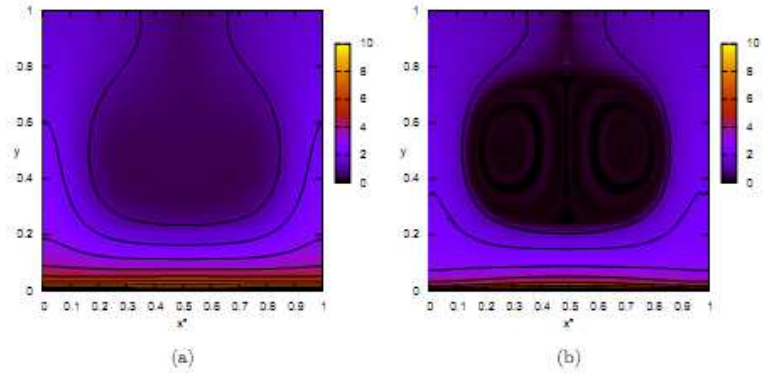

Figure 2.3: Introduction: *Charge density contour from [8] (a) accounting for diffusion (b) neglecting diffusion*

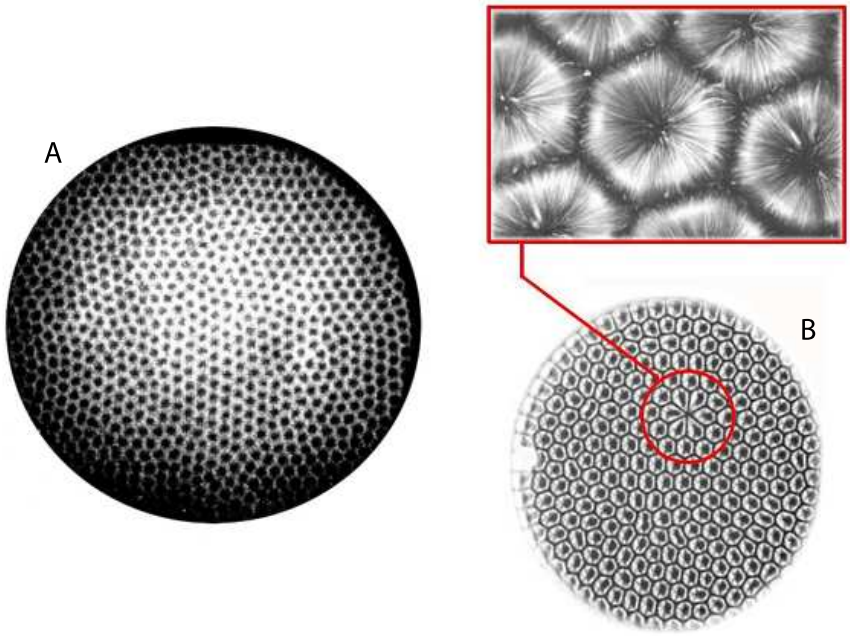

Figure 2.4: Introduction: . A) Schlierenphotograph of the motion pattern in *pyralene 1460* under strong injection from [27], B) Visualization of hexagonal convective cells for the 3d Rayleigh-Benard problem

cells [27]. By theoretical studies the non linear instability threshold agrees with experimental results.
With the intent to better understand both linear and non linear EHD processes, a computer code for the Direct Numerical Simulation of wall turbulent flows has been recently modified during an earlier thesis work by S. Ceccon [22] to account for the full set of equations which describe an EHD flow.
From this starting point, D. Cerizza [8] has done 3D DNS of EHD parallel plates flow with full account of charge diffusivity effects. Being the first 3D EHD flow simulation ever realized it has allowed us to investigate the diffusivity's role, always neglected till now.
In 2D case [8] has brought to light the limits of the simplified models used until the present day.
In particular, accounting for charge diffusion, the estimate critical values of linear and non linear analysis are significantly lower than the values reported in others papers.
Moreover in 3D case [8] has been able to show for the first time hexagonal cells with details made possible only by a numerical simulation.

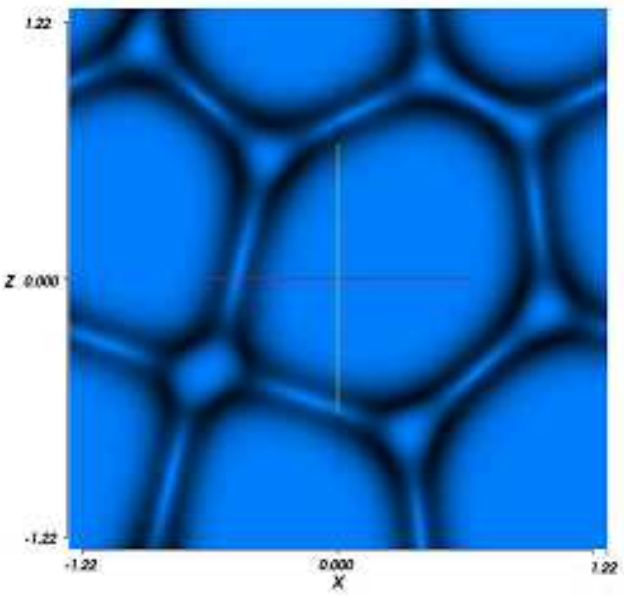

Figure 2.5: Introduction: *Stable pattern.* Visualizations for the first stable convective to charge pattern for a value of Q = 1.4 from [8]

Cerizza in [8] underlines that a simple order of magnitude analysis does not take into account of several effects related to the diffusion charge mechanism which affects the density charge distribution.

2.1.2 The cross flow effect

The cross flow effect has been studied in [7] only in weak injection regime and neglecting the EHD coupling. From this study emerges that a flow with a mean velocity parallel to the electrodes generally interacts with the convection generated by unipolar injection. For a low enough applied voltage the ions injected have a vertical velocity $K\mathbf{E}_0(y)$ due to the electric field and an horizontal velocity due to the velocity profile $\mathbf{U}_0(y)$. When the instability sets in the flow pattern depends on the ratio of ionic velocity to the mean flow velocity and it could be 3-dimensional (modulated transverse rolls or hexagonal cells) or, for higher values of Reynolds number, it could appears as longitudinal rolls which later destabilize. Although no furthers studies have been done about the cross flow effect and many interrogatives about EHD and cross flow coupling still remain.

2.2 Brief summaries of EHD applications

EHD flows are implied in many devices actually in use and still in development. In the first case the study of the electric-velocity field interaction can explain undiscovered aspects about EHD flows, defining new path of technological improvement. In the latter situation it defines a brand of new applications of the physical theory.

- **EHD and heat transfer**
  The most classical topic is how the EHD convective structures influence the fluid properties. Superimposing a simple EHD flow on the fluid in an enclosure domain, the convective rolls can enhance heat transfer at the wall. The heat transfer for a given Rayleigh number could be augmented by EHD processes, in particular using a non-uniform injection. For instance, experimental results have shown an increasing 1000 % in heat transfer coefficients for the refrigerant R-134a [15]. The improvements in heat transfer are dramatic, especially at lower refrigerant qualities (more liquid and less vapor). This allows manufacturers to produce highly compact heat exchangers with less complicated surfaces without sacrificing heat transfer efficiency. From a safety and cost point of views, to use EHD seems to have some troubles because of an electrical voltage needs to be added to the heat transfer device. However,using typically dielectric materials, very little current is generated, despite the high voltage.

- **EHD and MEMS technology**
  The utility of electrohydrodynamics (EHD) has an effective mean for the microdrop generation. The electric field developed between the charged liquid sample and the ground electrode cause the electrical body force at the air/liquid interface. The microdrop size can be controlled either by the gap between the electrode and the microchannel or the strength of the electric field. Recently, the EHD method are especially applied to small scale diagnostic devices such as massive parallel drug discovery and DNA microarray.

- **EHD and micropumps**
  EHD pump are usually feasible only at microscale as the forces generated are generally unable to move large quantity of fluids unless one is looking at input in order of some tens of kilovolts. The fundamental phenomenon that allows the transduction of electrical to mechanical energy in an EHD pump is an electric field acting on induced charges in a fluid. In EHD pumping, fluid forces are generated by the interaction of electric field with the charges injected in the fluid. The fluid must be dielectric in order to permit EHD pumping to occur. This idea is not a new one. In fact, EHD pump were first proposed and built back in the 1960's.

- **EHD and flow control**
  Until the present day the main processes that generate electroconvective motions have been dealt in hydrostatic conditions. However combining the EHD set up and a cross flow, a boundary flow control technique via injection distribution could be developed.

2.3 Present work

Despite the remarkable accomplishments seen till here, many questions were left unanswered including the discrepancy between the computed critical $T^\star$ and the observed one. The common simplifications in the previous works are the assumptions of an exponential time dependence (normal-mode approach) and a negligible charge diffusion. The limiting nature of the above-mentioned approaches was underlined by [18] and confirmed by [8].

Although, after being dominated by modal (eigenvalue) analysis for many decades, a different perspective has emerged, allows the quantitative description of short-term disturbance behavior.
Stability has been redefined in a broader sense as the response behavior of the governing equations to general input variables [17].
A remarkable result of the non modal stability is that the temporal behavior of a non linear operator substantially deviates from the asymptotic behavior dictated by its eigenvalues. Therefore any conclusions drawn from the eigenvalues can easily misrepresent the general disturbance behavior over the course of time, and the dynamics of the least stable mode are, at worst, entirely irrelevant to the temporal behavior of the linear system at finite time.

The aim of this work is to provide valuable answers to the following questions throughout a non modal linear stability analysis of an EHD parallel plane problem with and without cross flow and charge diffusion.

- What is the role played by the charge diffusion in the instability set in?
- Can it solve the discrepancy between computed and theoretical critical value of T?
- What happens when combing a cross flow with the EHD parallel plane system?
- Is the EHD problem affected by a short time amplification?
- If yes, which are the growth mechanisms?

As can be seen by gathering all the previous investigations and theoretic studies available in literature, the cross flow in strong injection, the charge diffusion effects and the short time behavior have never been investigated before.

The thesis is structured (Figure 2.6) as follows:

- **Chapter 1**: INTRODUCTION.
  Introduction to the EHD planar plan problem and reviews of the most remarkable literature results.

- **Chapter 2**: MODAL STABILITY ANALYSIS.
  Introduction to the specific problem considered in the present work. Definition of the equation set, its adimensionalization and its linearization. Discussion of dimensionless electrical parameters and electrical time scale. Definition of the eigenvalue problem for the linear modal analysis.

- **Chapter 3**: NON MODAL STABILITY ANALYSIS.
  Introduction to the non modal analysis tools as initial value problem, energy definition and its related norm, maximum transient growth, maximum growth rate, harmonically forced response and optimal initial conditions.

- **Chapter 4**: HYDROSTATIC CASE.
  Application of the modal e non modal analysis tools to the hydrostatic case. A direct comparison with available data is possible and shows a good agreement, even if several differences are observed thanks to the full accounting of the physical processes related to the charge diffusion. A weak transient growth has been observed.

- **Chapter 5**: POISEUILLE CASE Application of the modal e non modal analysis tools to the EHD planar plane problem combined with a cross flow. In the viscous dominated regime ($Re \to 0$) the stability is strongly affected by electric field while as the Reynolds number increase the fluid dynamics mechanisms dominate the transition. A strong transient growth has been observed especially when $\alpha = 0$.

- **Chapter 6**: CONCLUSION

- **Appendixes**.
  Brief summaries of the mathematical tools used as Quasi-steady-Maxwell equation and Spectral methods. Moreover there are the benchmark cases used to test the numerical code.

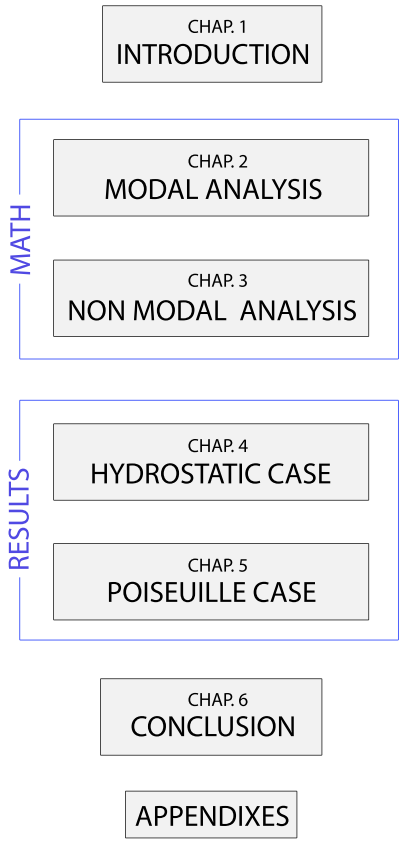

Figure 2.6: Introduction: *Presentation plan*

CHAPTER 3

MODAL STABILITY

3.1 Introduction

An isothermal flow of incompressible and perfectly insulating liquid, contained between two metallic electrodes of infinite extent and subject to unipolar injection, is a classical configuration useful to study the effect of charge diffusion upon the Coulomb-driven finite amplitude convection. This motion,named *electroconvection*, depends on the strength of the electric field, the ionic purity of the liquid, and the geometry of the electrodes. Both electrical and fluid-mechanical equations are necessary to study this problem, and the electric-motive force is the coupling term between the fluid's motion field and the electric equations system. In fact for liquids, ionic convection may not be negligible and a two way coupling will exist between the flow field and the electrical-force field. How to write the equation set for the linear modal stability analysis is the goal of this chapter.
Hydrodynamic stability theory is concerned with the response of a laminar flow to a disturbance of small amplitude and deals with the mathematical analysis of evolution of disturbance superposed on a laminar base-flow. In the EHD problem, the instabilities results in a convective motion similar to Rayleigh-Benard's instability. A linear equation governing the the evolution of disturbance is necessary.

3.2 Basic equations

3.2.1 Fluid mechanics equations

The plane electrodes are along the coordinates x, z and are placed at $y = -\ell$ (*injector*) and $y = \ell$ (*collector*) where y is associated to the electrodes-normal direction. The fluid is assumed to be incompressible, Newtonian, with no-slip conditions at the walls and driven by a pressure gradient along x direction. The fluid's ions are subjected to electrical-force that drive them towards the collector. In this process the ions collide with fluid molecules, transferring momentum. This is equivalent to a *body force* which acts directly on the fluid. Calling ρ the density and ν the cinematic viscosity, the time evolution of the velocity vector $\mathbf{V}$ is described by the solenoidal condition stemming from mass conservation and the Navier-Stokes equations complemented by a suitable driving term related to the electric field, represented by $\mathbf{F}$. A cinematic constrain for the modified pressure could be found solving the momentum equation's divergence so it is implied by continuity equation.

$$\begin{cases} \nabla \cdot \mathbf{V} = 0, \\ \\ \dfrac{D\mathbf{V}}{Dt} = -\dfrac{1}{\rho}\nabla P + \nu\nabla^2\mathbf{V} + \dfrac{1}{\rho}\mathbf{F}. \end{cases} \tag{3.1}$$

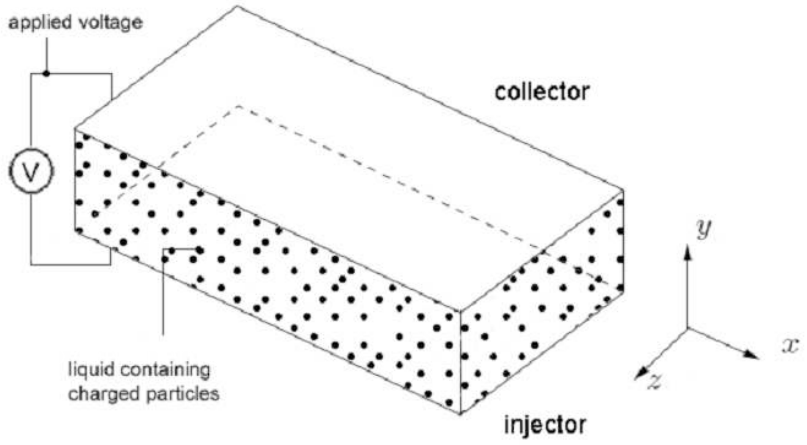

Figure 3.1: Poiseuille simulation set up

3.2.2 Electric field equations: Quasi-steady Maxwell equations

To investigate the effect of the charge injection upon the first instabilities in the EHD flow the Maxwell equation set is required. Since the electrical current in dielectric liquids is much small, the magnetic induction can be ignored yielding the electro-quasi-statics Maxwell's equations (A). In this limit the effect of density charge evolution still remains by the charge continuity equation, but the electrodynamics laws are submitted to the Gauss law and the irrotational nature of the electric field.

$$\begin{cases} \nabla \cdot \mathbf{D} = Q, \\ \\ \mathbf{E} = -\nabla \Phi, \end{cases}$$

where $\mathbf{E}$, $\mathbf{D}$, Φ, Q are the electric field, displacement, potential and the charge density respectively. As usual, the electrical displacement is given by $\mathbf{D} = \varepsilon \mathbf{E}$ with ε being the permittivity.

3.2.3 Electric field equations: Charge continuity

Electric charge is a fundamental property of subatomic particles. The charges of free-standing particles are integer multiples of the elementary charge[1] $e = -1.602 \cdot 10^{-19} C$. The electric charge of a macroscopic object is the sum of the electric charges of the particles that make it up. This charge is often small, because matter is made of atoms, and atoms have typically equal numbers of protons and electrons, making the atoms neutral.
The conservation law for the charge is

$$\frac{\partial Q}{\partial t} + \nabla \cdot \mathbf{J} = 0.$$

In dielectric liquids of high resistivity, as afterward specified, the Ohm's law

$$\mathbf{J} = \sigma \mathbf{E}$$

often fails to be valid and a new constitutive law for the current density is needed. The injection mechanism controls the ions species injected in the system and the nature of the force which drive them so it is strictly correlated to the current density's law.
Moreover, as shown in several papers [6], [12], [28], the injection mechanism depends on the nature of the electrode-liquid interface. For example in [27] metal electrodes act as blocking contact than a injecting one causing non-uniform ionic emission and so local pumping.
Therefore focus is needed on the simplest case where only one species of charge carriers is injected into a perfectly insulating fluid (conductivity $\sigma = 0$) with unipolar

[1] Charge of an electron or proton

autonomous injection.

There are several factors influencing the transport of charge and each are discussed in turn below.

Convective transport by fluid motion

Naturally, if charge is present in a convected fluid the convective flux, i.e. the current flux, for a specific species is simply that carried by the bulk motion of the fluid

$$\mathbf{J}_{conv} = Q\mathbf{V}$$

Mobility and the Drift term

Generally in a conductor or in a dielectric, an electron will 'rattle around' at the Fermi velocity randomly. Since a dielectric material is a substance that is a poor conductor but an efficient supporter of electric fields, when these are applied, a small net velocity to the electron's random motion results. This net velocity is called *drift velocity* v_{drift}.
Ionic mobility is therefore classified as a *material property* closely related to the ratio between free and blocked charges, describing the ability of the charge carriers (such as electrons or ions[2]) to move through a medium in response to an electric field.

$$\mathbf{V}_{drift} = K\mathbf{E}$$

The ionic mobility of a fluid is usually assumed to be both isotropic and constant, and varies depending on the physical properties of the charge carriers and medium. For negative ions the typical Walden's rule give

$$K = 1.5\frac{10^{-11}}{\mu}$$

If it is assumed that the charged fluid element is traveling at its terminal velocity, then it is said to have reached the *mobility limit* and the flux of current can be expressed as

$$\mathbf{J}_{mob} = QK\mathbf{E}$$

The conduction term is proportional to the Coulomb force so, theoretically, for high

[2]An *ion* is an atom (or group of atoms) that has lost one or more electrons, giving it a net positive charge (*cation*), or that has gained one or more electrons, giving it a net negative charge (*anion*).

electric fields, it could permit to the charge carriers (ions) to move in the upstream direction and create free charge zones.

Diffusion and the Debye length

As explained in [6] the diffusion could be considerated in both boundary layers or internal layers. The typical length scale of these layers is the *Debye length*. It is defined as the distance over which the potential developed by separating a charge density from the background charge of the opposite polarity is equal to the Thermal Voltage $\ell_D = K_B\Gamma/e$. The simplest formula to get the charge diffusion is the Nernst-Einstein equation [26], which relates diffusion to ions mobility for a given ionic specie i:

$$D_i = K_i \ell_{Di} \tag{3.2}$$

where Γ is the absolute temperature in Kelvin and K_i the mobility for the specified ionic specie. As explained by [26], ℓ_D is important when the ratio of ionic diffusion timescale to the charge relaxation timescale is considerable. Which is the reason why diffusion is signified in EHD processes occurring close to the charge injecting electrode. The current flux due to diffusion can be written as

$$\mathbf{J}_{diff} = -D\nabla Q$$

Typically, D diffusion coefficient's range is $10^{-8} \sim 10^{-10}$. The diffusion term is usually eliminated only if bulk effects are of interest. According to [1] it is possible to formulate a magnitude analysis regarding the drift and diffusion term

$$\frac{D\nabla Q}{QK\mathbf{E}} \sim \frac{0.025}{\Phi_0}\frac{\ell}{\ell_D}$$

Thus the diffusion term is of interest only if the ratio of diffusion and drift currents accords to unity's order. For the most common EHD applications D is very low and it is usually neglected [4], [2], [**?**], [29] but as shown in [8], it has a strong influence, in particular for the 2D case. In fact [8] has demonstrated that its presence enhances the instability of the flow throughout an augmented mixing. Moreover within the linear-stability analysis, the absence of diffusion term creates a critical layer making the numerical solution more complex (D).

Charge conservation

The total steady-state current flux can be defined by combining the previews contributes. Therefore, the constitutive laws for the current density results as:

$$\mathbf{J} = Q\mathbf{V} + QK\mathbf{E} - D\nabla Q. \tag{3.3}$$

It's clear that generally, three charge distribution mechanisms are present in (3.3).

3.2.4 The electrical-force

The body force **F** has an electrical origin and is the only term that permits EHD coupling, and it is a force per volume unit. The most general expression for **F** is:

$$\mathbf{F} = Q\mathbf{E} - \frac{E^2}{2}\nabla\varepsilon + \nabla\left[\frac{E^2}{2}\rho\frac{\partial\varepsilon}{\partial\rho}\right] + \mathbf{J}\wedge\mathbf{B} + (\mathbf{P}\cdot\nabla)\mathbf{E} \tag{3.4}$$

For the previous hypotheses, the magnetic induction (**B**) and the polarization (**P**) are negligible. The first term is the Coulomb force on a medium containing free electric charge. It is the strongest EHD force in these kind of systems. The second term, called the dielectric force, is due to the force exerted on a non-homogeneous dielectric liquid by an electric field so, assuming ε steady and homogeneous, it doesn't exist.
The third term, called the *electrostrictive term*, is a gradient of a scalar. It is treated as the gravitational force, so it is possible to considerate it modifying the pressure term.
Equation (3.4) simplifies to:

$$\mathbf{F} = Q\mathbf{E} \tag{3.5}$$

3.2.5 The complete sets and its boundary conditions

Substituting (3.5) in (3.1) and writing (3.3) as function just of Φ is possible to write the complete equation set in five unknowns variables[3].

$$\begin{cases} \nabla \cdot \mathbf{V} = 0, \\ \\ \dfrac{D\mathbf{V}}{Dt} = -\dfrac{1}{\rho}\nabla P + \nu\nabla^2\mathbf{V} + \dfrac{\varepsilon}{\rho}\nabla^2\Phi\nabla\Phi, \\ \\ \dfrac{\partial}{\partial t}\nabla^2\Phi + \nabla\cdot(\nabla^2\Phi\mathbf{V} - K\nabla^2\Phi\nabla\Phi - D\nabla^2(\nabla^2\Phi)) = 0. \end{cases} \tag{3.6}$$

The differential problem is closed when an initial condition for all the fluid variables and electric potential are specified, and suitable boundary conditions are chosen. At the wall the no-slip condition is physically meaningful.

$$\mathbf{V}(x,\ell,z,t) = 0, \qquad \mathbf{V}(x,-\ell,z,t) = 0. \tag{3.7}$$

Periodic conditions are usually employed in the x and z directions, where either the problem is homogeneous in wall-parallel planes. From now on this assumption will be considerated.
The third equation of (3.6) is a forth order differential equation and so it needs four boundary conditions. Assuming that the injection is autonomous, i.e., independent by electric field, the electrical boundary conditions, consist in imposing the potential on the electrodes.

$$\Phi(x,\ell,z,t) = 0, \qquad \Phi(x,-\ell,z,t) = \overline{\Phi}_0, \tag{3.8}$$

Specifying the way in which charge is injected into the liquid on one boundary and removed from the opposite, the last two conditions will be revealed. The assumption of autonomous injection provides (3.9). Moreover, in the case where the charge diffusion coefficient is not negligible, the dielectric nature of the medium ($\mathbf{E}(\ell) = 0$) suggests a Neumann boundary condition for the charge density on the collector (3.10).

$$\nabla^2\Phi(\mathbf{x},t)\big|_{y=-\ell} = -\varepsilon\overline{Q}_0, \tag{3.9}$$

$$\left.\frac{\partial\nabla^2\Phi(\mathbf{x},t)}{\partial y}\right|_{y=\ell} = 0. \tag{3.10}$$

[3] the operator $\dfrac{D}{Dt}(.)$ is defined as substantial derivative t.c. $\dfrac{D}{Dt}(.) = \dfrac{\partial}{\partial t}(.) + \mathbf{V}\dot{\nabla}(.)$

3.3 Non-dimensional EHD equations and parameters

3.3.1 Dimensionless sets and boundary conditions

Before any kind of analysis, a dimensionless form of preview set is more likely desidered. The mechanical and electrical equations may be written as (3.11) taking ℓ, $\overline{\Phi}_0$, $\overline{Q}_0$, $(K\overline{\Phi}_0)/\ell$ as the dimensional units for distance, potential, charge density and velocity respectively[4][5]. The EHD set is:

$$\begin{cases} \nabla \cdot \tilde{\mathbf{V}} = 0, \\ \\ \dfrac{D\tilde{\mathbf{V}}}{D\tilde{t}} = -\nabla\tilde{P} + \dfrac{M^2}{T}\nabla^2\tilde{\mathbf{V}} + M^2\nabla^2\tilde{\Phi}\nabla\tilde{\Phi}, \\ \\ \dfrac{\partial}{\partial\tilde{t}}\nabla^2\tilde{\Phi} + \nabla\cdot(\nabla^2\tilde{\Phi}\tilde{\mathbf{V}} - \nabla^2\tilde{\Phi}\nabla\tilde{\Phi} + \dfrac{1}{Fe}\nabla^2(\nabla^2\tilde{\Phi})) = 0. \end{cases} \tag{3.11}$$

with its suitable boundary condition:

$$\tilde{\mathbf{V}}(\tilde{x},1,\tilde{y},\tilde{t}) = 0, \quad \tilde{\mathbf{V}}(\tilde{x},-1,\tilde{z},\tilde{t}) = 0, \quad \tilde{\Phi}(\tilde{x},1,\tilde{z},\tilde{t}) = 0, \quad \tilde{\Phi}(\tilde{x},-1,\tilde{z},\tilde{t}) = 1,$$

$$\nabla^2\tilde{\Phi}(\tilde{\mathbf{x}},\tilde{t})\Big|_{\tilde{y}=-1} = -\mathcal{C}, \qquad \frac{\partial\nabla^2\tilde{\Phi}(\tilde{\mathbf{x}},\tilde{t})}{\partial\tilde{y}}\Big|_{\tilde{y}=1} = 0.$$

3.3.2 EHD non-dimensional parameters

Electrical timescales

There are many timescales associated with EHD flow in addition to those by Hydrodynamic definition. For the present purposes they are

→ τ_{SCR}: *Space charge Relaxation*$= \varepsilon/(K\overline{Q_0})$,
Typical for high insulating liquid. By [16] [6] it determines the rate at which charge decay from a given origin.

$$Q(y) = \frac{Q(y_0)}{1 + t/\tau_{SCR}}$$

[4]To let the notation more clear ∇ is the dimensionless differential operator $\tilde{\nabla}$

[5]To let the notation more clear, from now on the dimensionless quantities will be written without $\tilde{(\cdot)}$

→ τ_D:*Ionic diffusion timescale*= D/ℓ_D^2,
Near the electrodes, a thin layer exists where electro-chemical reactions enabling charge to be injected in the fluid. Here the Debye scale is important and defines a diffusion timescale.

→ τ_K:*Ionic transit Timescale*= $\dfrac{\ell^2}{K\overline{\Phi_0}}$,
It is the timescale associated with drift of ions, characterized the bulk of EHD processes.

→ τ_{EV}: *Electro-viscous timescale*= $\dfrac{\mu\ell^2}{\varepsilon\overline{\Phi_0}}$,

→ τ_{EI}:*Electro-inertial timescale*= $\ell^2\sqrt{\dfrac{\rho}{\varepsilon\overline{\Phi_0^2}}}$,

Non dimensional parameters

The EHD parameters are:

→ T : *Taylor's Parameter* = $\dfrac{\varepsilon\overline{\Phi}_0}{\mu K} = \dfrac{\tau_K}{\tau_{EV}}$

It measures the strength of the destabilizing Coulomb force. It could be also viewed as the ratio of electrical energy supplied to the system to the energy dissipated by viscous force, and it plays a role of critical parameter. It is directly analogous to the Rayleigh number in hydrodynamics.

→ M : *Dimensionless ionic mobility* = $\dfrac{1}{K}\sqrt{\dfrac{\varepsilon}{\rho}} = \dfrac{\tau_K}{\tau_{EI}}$.

It s the ratio of the hydrodynamic mobility to the ionic mobility. The character $\sqrt{\varepsilon/\rho}$ as a hydrodynamic mobility can be easily understood by considering a complete conversion of the electric energy supplied to the system into kinetic energy of the liquid [1].

→ $\mathcal{C}$: *Charge injection coefficient* = $\dfrac{\overline{q_0}\ell^2}{\varepsilon\overline{\Phi}_0} = \dfrac{\tau_K}{\tau_{SCR}}$,

When the charge density is uniform on the injector it is a measure of the injection level. It has a relevant influence on the critical value of T. $\mathcal{C} \ll 1$ and $\mathcal{C} \gg 1$ limit both weak and strong injection.

→ Fe : *Dimensionless charge diffusivity* = $\dfrac{K\Phi_0}{D} \propto \dfrac{\tau_K}{\tau_D}$.

It is the ratio of diffusion time to ionic transit time [6]

[6]By [6] it may also be written (for ambient temperature) as $\frac{1}{40}\overline{\Phi_0}$.

It is important to distinguish *material parameters* (M), fixed once the liquid has been chosen, from *flow parameters* (M,C,T) that depend on flow regime. In (3.11) the viscous stress are proportional to M^2/T that is analogous to the Prandtl number.

3.3.3 Weak and strong injection regime

The critical T value, depends on the $\mathcal{C}$ parameter which measures the intensity of charge injection. [1] has expressed charge relaxation (3.3.2) that shows how moving the charge carriers toward the collector, the charge density decreases because of the Coulomb repulsion.
The weak injection limit, corresponds to great τ_{SCR}. By (3.3.2), in this regime, the charge density doesn't change on the trajectory towards the collector. The increasing of the current due to convection could be although considered weak, so the Coulomb repulsion has a weak effect between charge carriers.
In the case of two plane parallel rigid electrodes, the weak injection limit is characterized by the criterion

$$T_c\mathcal{C}^2 = 220.7 \tag{3.12}$$

As ($\mathcal{C} \to +\infty$) [7], the convection has an influence on the passage of current. In this case the charge diffusion plays an important role close to the injector. In this regime the stability criterion is

$$T_c \approx 161. \tag{3.13}$$

Even though, both injections are shown, only the strong injection will be considerate throughout this thesis.

[7] also called (SCL)

3.4 Linear modal analysis

3.4.1 Velocity base flow

The Poiseuille flow assumption has been taken in account. Stream-line parallel to the plates and U as non-null velocity component. Moreover, as the velocity field even the electric field has not dependence by x and z direction and in the equilibrium case there's not EHD coupling because mechanic and electric fields are orthogonal each other. In fact, under the previews assumptions the coupling term are:

$$F_x = M\frac{\partial}{\partial x}\frac{d^2}{dy^2}\Phi_0 = 0, \qquad \nabla(\nabla^2\Phi_0)\cdot\mathbf{V} = 0.$$

Substituting the hypotheses in the (3.11), integrating the x-momentum in y for two time and applying the no-slip boundary condition we get:

$$U_0(y) = \frac{U(y)}{U_{ion}} = \frac{\Pi_{ion}}{2}\frac{T}{M^2}(y^2-1),$$

$$U_0^{'}(y) = \Pi_{ion}\frac{T}{M^2}y,$$

$$U_0^{''}(y) = \Pi_{ion}\frac{T}{M^2}.$$

Where Π_{ion} is the dimensionless pressure gradient taking ionic velocity as reference velocity. Π_{ion} is negative if the velocity is positive and *viceversa*. As we would control the mean velocity flow with a parameter which is independent by electrical parameters M, T and C we choose to get the dimensionless equations set (**??**) with center-line velocity as reference velocity

$$\frac{U(y)}{U_{cl}} = \frac{\Pi_{cl}}{2}Re_{cl}(y^2-1), \qquad \rightarrow \qquad \frac{U(0)}{U_{cl}} = -\frac{\Pi_{cl}}{2}Re_{cl} = 1.$$

$$\Pi_{ion} = \Pi_{cl}\frac{U_{cl}^2}{U_{ion}^2} = -\frac{2}{Re_{cl}}\frac{U_{cl}^2}{U_{ion}^2}$$

and so:

$$U_0(y) = Re_{cl}\frac{M^2}{T}(1-y^2), \quad U_0^{'}(y) = -2Re_{cl}\frac{M^2}{T}y, \quad U_0^{''}(y) = -2Re_{cl}\frac{M^2}{T}. \quad (3.14)$$

3.4.2 Electric potential base flow

As previously explained the coupling term in the charge continuity, the scalar product between the electric field and the velocity, is null in the base flow assumption. In the case where the charge diffusion coefficient is not neglected, the third equation in (3.11) is a fourth order equation, and therefore we need an homogeneous Neumann boundary condition for the charge density. The electric base flow equation is

$$\frac{d\Phi_0}{dy}\frac{d^3\Phi_0}{dy^3} + (\frac{d^2\Phi_0}{dy^2})^2 + \frac{1}{Fe}\frac{d^4\Phi_0}{dy^4} = 0 \tag{3.15}$$

or more simply, as

$$\frac{d}{dy}\left(\frac{1}{Fe}\frac{d^2\Phi_0}{dy^3} + \frac{d\Phi_0}{dy}\frac{d\Phi_0}{dy}\frac{d^2\Phi_0}{dy^2}\right) = 0$$

Eq. (3.15) is readily integrated to give

$$\frac{1}{Fe}\frac{d^3\Phi_0}{dy^3} + \frac{d\Phi_0}{dy}\frac{d^2\Phi_0}{dy^2} = \alpha$$

Upon substituting $A = \dfrac{d\Phi_0}{dy}$ one obtains

$$\frac{1}{Fe}\frac{d^2A}{dy^2} + A\frac{dA}{dy} = \alpha$$

which can be simplified by setting $B = \frac{dA}{dy} + \frac{Fe}{2}A^2$ to yield

$$\frac{dB}{dy} = \alpha Fe$$

Integrating yields directly the new equation

$$\frac{dA}{dy} + \frac{Fe}{2}A^2 = \alpha Fey + \beta$$

which is a Riccati equation. Substituting $A = \frac{2P'}{FeP}$ leads to

$$2P'' - PFe(\alpha Fey + \beta) = 0$$

Solving yields

$$P = \sqrt{y + \frac{\beta}{\alpha Fe}}\left\{\gamma J_{1/3}\left[\frac{2}{3}\left(y + \frac{\beta}{\alpha Fe}\right)^{3/2}\sqrt{-\frac{\alpha Fe}{2}}\right] + \eta Y_{1/3}\left[\frac{2}{3}\left(y + \frac{\beta}{\alpha Fe}\right)^{3/2}\sqrt{-\frac{\alpha Fe^2}{2}}\right]\right\}$$

We select $\eta = 0$ to avoid the singularity due to the Bessel function of the second

kind $Y_{1/3}$. further, nothing that

$$A = \frac{2}{Fe}\frac{P'}{P} = \frac{2}{Fe}(\ln P)' = \phi',$$

that readily integrates to

$$\Phi_0(y) = \delta + \frac{2}{Fe}\ln\left\{\sqrt{y+\frac{\beta}{\alpha Fe}}\left(\gamma J_{1/3}\left[\frac{2}{3}\left(y+\frac{\beta}{\alpha Fe}\right)^{3/2}\sqrt{-\frac{\alpha Fe}{2}}\right]\right)\right\}.$$

where α, β, γ and δ are integration's constants.
To solve the system a spectral method with boundary bordering technique has been used.

3.4.3 Perturbation equations

The evolution equations for the disturbance can be derived by considering a basic state, previously obtained, and a perturbed state , both satisfying the Naiver-Stokes equations.

$$\mathbf{V} = \mathbf{V}_0 + \mathbf{v}, \qquad \hat{P} = \hat{P}_0 + p, \qquad \Phi = \Phi_0 + \phi, .$$

Subtracting the equations for basic and perturbed flow and omitting the non linear terms, the resulting linear equation can be written as

$$\begin{cases} \dfrac{\partial u}{\partial x} + \dfrac{\partial v}{\partial y} + \dfrac{\partial w}{\partial z} = 0 \\ \dfrac{\partial u}{\partial t} + U_0\dfrac{\partial u}{\partial x} + v\dfrac{\partial U}{\partial y} = -\dfrac{\partial p}{\partial x} + \dfrac{M^2}{T}\nabla^2 u + M^2\Phi_0''\dfrac{\partial \phi}{\partial x}, \\ \dfrac{\partial v}{\partial t} + U_0\dfrac{\partial v}{\partial x} = -\dfrac{\partial p}{\partial y} + \dfrac{M^2}{T}\nabla^2 v + M^2\Phi_0''\dfrac{\partial \phi}{\partial y} + M^2\Phi_0'\nabla^2\phi, \\ \dfrac{\partial w}{\partial t} + U_0\dfrac{\partial w}{\partial x} = -\dfrac{\partial p}{\partial z} + \dfrac{M^2}{T}\nabla^2 w + M^2\Phi_0''\dfrac{\partial \phi}{\partial z}, \\ \dfrac{\partial}{\partial t}\nabla^2\phi = \Phi_0'''(\dfrac{\partial \phi}{\partial y} - v) + 2\Phi_0''\nabla^2\phi + \Phi_0'\dfrac{\partial}{\partial y}\nabla^2\phi - U_0\dfrac{\partial}{\partial x}\nabla^2\phi + \dfrac{1}{Fe}\nabla^2\nabla^2(\phi) \end{cases}$$

With its suitable *homogenous* boundary conditions at the wall and periodic in x, z directions

$$\mathbf{v}(x,1,z,t) = 0, \quad \mathbf{v}(x,-1,z,t) = 0, \quad \phi(x,1,z,t) = 0, \quad \phi(x,-1,z,t) = 0,$$

$$\nabla^2\phi(\mathbf{x},t)\big|_{y=-1} = 0, \qquad \frac{\partial}{\partial y}\nabla^2\phi(\mathbf{x},t)\bigg|_{y=1} = 0.$$

The linearized momentum equation's divergence with the continuity equation yields a cinematic constrain for the perturbation pressure

$$\nabla p = -2U_0'\frac{\partial v}{\partial x} + M^2(\Phi_0'\frac{\partial}{\partial y}\nabla^2\phi + 2\Phi_0''\nabla^2\phi + \Phi_0'''\frac{\partial \phi}{\partial y}) \tag{3.16}$$

In order to describe the EHD system in a more efficient way, (3.16) may be used to eliminate the pressure, resulting in an equation for the normal velocity v supplemented by charge continuity and the normal vorticity[8]. If the disturbance pressure is needed it can be recovered from the normal velocity.

$$\begin{cases} \dfrac{\partial}{\partial t}\nabla^2 v = -U_0\dfrac{\partial}{\partial x}\nabla^2 v + U_0''\dfrac{\partial v}{\partial x} + \dfrac{M^2}{T}\nabla^2\nabla^2 v + M^2\left[\Phi_0'\nabla^2\nabla_1^2\phi - \Phi_0'''\nabla_1^2\phi\right], \\ \dfrac{\partial \eta}{\partial_t} = -U_0\dfrac{\partial \eta}{\partial x} - U_0'\dfrac{\partial v}{\partial z} + \dfrac{M^2}{T}\nabla^2\eta, \\ \dfrac{\partial}{\partial t}\nabla^2\phi = \Phi_0'''(\dfrac{\partial\phi}{\partial y} - v) + 2\Phi_0''\nabla^2\phi + \Phi_0'\dfrac{\partial}{\partial y}\nabla^2\phi - U_0\dfrac{\partial}{\partial x}\nabla^2\phi + \dfrac{1}{Fe}\nabla^2\nabla^2(\phi) \end{cases} \tag{3.17}$$

This equations set, together with the homogeneous boundary condition

$$v(x,\pm1,z,t) = 0, \qquad v'(\mathbf{x},t)\big|_{y=\pm1} = 0, \qquad \eta(x,\pm1,z,t) = 0, \qquad \phi(x,\pm1,z,t) = 0,$$

$$\nabla^2\phi(\mathbf{x},t)\big|_{y=-1} = 0, \qquad \frac{\partial}{\partial y}\nabla^2\phi(\mathbf{x},t)\Big|_{y=1} = 0.$$

and the initial conditions

$$v(x,y,z,0) = v_0(x,y,z), \quad \eta(x,y,z,0) = \eta_0(x,y,z), \quad \phi(x,y,z,0) = \phi_0(x,y,z).$$

form a complete description of the evolution in both space and time of an infinitesimal disturbance. In the linear stability analysis the velocity, pressure and potential perturbations have a *wave-like* form

$$g(\mathbf{x},t) = \hat{g}(y)e^{i(\alpha x+\beta z-\omega t)}, \qquad \alpha,\beta \in R, \qquad \omega \in C \tag{3.18}$$

where $\omega = \alpha c$, with c as phase speed and α and β as streamwise and spanwise wave number. The choice of a complex frequency is know as temporal problem where the spatial structure of wavelike perturbation is unchanged and the amplitude of wave grows or decays as time progress. Introducing this representation into (3.17), or equivalently taking the Fourier transform in the horizontal directions, results in the

[8] $\eta = \dfrac{\partial u}{\partial z} - \dfrac{\partial w}{\partial x}, \qquad \nabla_1^2(\cdot) = \nabla^2(\cdot) - \dfrac{\partial}{\partial y}(\cdot).$

following equations for v, η and Φ [9]

$$\begin{cases} \omega(D_2-\mathsf{k}^2)\hat{v} = \left[\alpha U_0(D_2-\mathsf{k}^2) - \alpha U_0'' - \frac{1}{i}\frac{M^2}{T}(D_2-\mathsf{k}^2)^2\right]\hat{v} + \\ \quad + \frac{1}{i}M^2\left[\mathsf{k}^2\Phi_0'(D_2-\mathsf{k}^2) - \mathsf{k}^2\Phi_0'''\right]\hat{\phi}, \\ \omega\hat{\eta} = \left[U_0'\beta\right]\hat{v} + \left[\alpha U_0 - \frac{1}{i}\frac{M^2}{T}(D_2-\mathsf{k}^2)\right]\hat{\eta}, \\ \omega(D_2-\mathsf{k}^2)\hat{\phi} = \Phi_0'''\hat{v} + \\ \quad + \left[\alpha V_0(D_2-\mathsf{k}^2) - \frac{1}{i}(\Phi_0'''D_1 + 2\Phi_0''(D_2-\mathsf{k}^2) + \Phi_0'(D_3-\mathsf{k}^2D_1))\right]\hat{\phi} + \\ -\frac{1}{i}\left[\frac{1}{Fe}(D_2-\mathsf{k}^2)^2\right]\hat{\phi}. \end{cases} \tag{3.19}$$

with its suitable homogeneous boundary condition

$$\hat{v}(\pm1) = 0, \quad \hat{v}'|_{y=\pm1} = 0, \quad \hat{\eta}(\pm1) = 0, \quad \hat{\phi}(\pm1) = 0, \quad \hat{\phi}''\Big|_{y=-1} = 0, \quad \hat{\phi}'''\Big|_{y=1} = 0.$$

[9] $D_n = \dfrac{\partial^{(n)}}{\partial y^{(n)}}(\cdot)$

3.5 Discrete form

To solve the previews problem a spectral collocation method has been used. More details about Chebyshev polynomials and spectral discretization are given in (B), being specific, given a function $f(y)$ defined for $1 \geq y \geq -1$, is possible to approximate it as

$$f(y) = \sum_{n=0}^{N} a_n T_n(y)$$

where

$$T_n(y) = \cos(n\theta), \quad \theta = \cos^{-1}(y)$$

In matrix form

$$\mathbf{f}(y) = \mathbf{D_0}\mathbf{a}_f, \qquad \mathbf{f}^{(n)}(y) = \frac{d^{(n)}}{dy^{(n)}}(\mathbf{D_0})\mathbf{a}_f = \mathbf{D}_n\mathbf{a}_f \tag{3.20}$$

where

$$D_{0(kj)} = \cos(j\cos^{-1}(y_k)).$$

Substituting (3.20) in the complete set with the wavelike perturbations (3.19), the matrix system (3.21) has been obtained. In this form, notation and algebraic manipulation will result easier.

$$\begin{bmatrix} \mathbf{L}_{vv} & 0 & \mathbf{L}_{v\phi} \\ \mathbf{L}_{\eta v} & \mathbf{L}_{\eta\eta} & 0 \\ \mathbf{L}_{\phi v} & 0 & \mathbf{L}_{\phi\phi} \end{bmatrix} \begin{pmatrix} \mathbf{a}_v \\ \mathbf{a}_\eta \\ \mathbf{a}_\phi \end{pmatrix} = w \begin{bmatrix} \mathbf{M}_{vv} & 0 & 0 \\ 0 & \mathbf{M}_{\eta\eta} & 0 \\ 0 & 0 & \mathbf{M}_{\phi\phi} \end{bmatrix} \begin{pmatrix} \mathbf{a}_v \\ \mathbf{a}_\eta \\ \mathbf{a}_\phi \end{pmatrix} \tag{3.21}$$

Where the $M_{(.)}$ and $L_{(.)}$ operators are the follows:

$$\mathbf{M}_{vv} = \mathbf{D}_2 - \mathsf{k}^2\mathbf{D_0}, \tag{3.22}$$
$$\mathbf{M}_{\eta\eta} = \mathbf{D_0}, \tag{3.23}$$
$$\mathbf{M}_{\phi\phi} = \mathbf{D}_2 - \mathsf{k}^2\mathbf{D_0}. \tag{3.24}$$

$$\mathbf{L}_{vv} = \alpha \mathbf{U_0}(\mathbf{D}_2 - \mathsf{k}^2\mathbf{D_0}) - \alpha \mathbf{U}_\mathbf{0}^{''}\mathbf{D_0} - \frac{1}{i}\frac{M^2}{T}(\mathbf{D}_4 - 2\mathsf{k}^2\mathbf{D}_2 + \mathsf{k}^4\mathbf{D_0}), \tag{3.25}$$

$$\mathbf{L}_{v\phi} = + \frac{1}{i}M^2\left[\mathsf{k}^2\mathbf{\Phi}_\mathbf{0}^{'}(\mathbf{D}_2 - \mathsf{k}^2\mathbf{D_0}) - \mathsf{k}^2\mathbf{\Phi}_\mathbf{0}^{'''}\mathbf{D_0}\right], \tag{3.26}$$

$$\mathbf{L}_{\eta v} = \beta \mathbf{U}_\mathbf{0}^{'}\mathbf{D_0}, \tag{3.27}$$

$$\mathbf{L}_{\eta\eta} = \alpha \mathbf{U_0}\mathbf{D_0} - \frac{1}{i}\frac{M^2}{T}(\mathbf{D}_2 - \mathsf{k}^2\mathbf{D_0}), \tag{3.28}$$

$$\mathbf{L}_{\phi v} = \frac{1}{i}\mathbf{\Phi}_\mathbf{0}^{'''}\mathbf{D_0}, \tag{3.29}$$

$$\begin{aligned}\mathbf{L}_{\phi\phi} =& \alpha \mathbf{U_0}(\mathbf{D}_2 - \mathsf{k}^2\mathbf{D_0}) - \frac{1}{i}(\Phi_0^{'''}\mathbf{D} + 2\Phi_0^{''}(\mathbf{D}_2 - \mathsf{k}^2\mathbf{D_0}) + \Phi_0^{'}(\mathbf{D}_3 - \mathsf{k}^2\mathbf{D})) \\ & - \frac{1}{i}\frac{1}{Fe}(\mathbf{D}_4 - 2\mathsf{k}^2\mathbf{D}_2 + \mathsf{k}^4\mathbf{D_0}).\end{aligned} \tag{3.30}$$

The system (3.21) is a first order generalized eigenvalue problem. Introducing compact notation it equals to:

$$\mathbf{Lx} = \omega \mathbf{Mx} \tag{3.31}$$

with $\mathbf{M}$ as a positive definite operator.

3.5.1 Enforcement of boundary conditions

Choosing the boundary bordering technique described in (B) the operative procedure is really simple.
Giving the following system and its boundary conditions

$$\mathbf{Lx} = \omega\mathbf{Mx} \tag{3.32}$$

the trick is to use the first c rows to force the c conditions on the collector and the last i rows to apply the i conditions on the injector. In the charge diffusive case the modified operators will be the following[10]

$$\begin{aligned}
\mathbf{L}_{vv} &= [\xi\mathbf{D_0}(1,:);\xi\mathbf{D}_1(1,:);\mathbf{L}_{vv}(3:N_{dof}-2,:);\xi\mathbf{D}_1(N_{dof},:);\xi\mathbf{D_0}(N_{dof},:)]\,,\\
\mathbf{L}_{v\phi} &= [\mathbf{Zr}(1,N_{dof});\mathbf{Zr}(1,N_{dof});\mathbf{L}_{v\phi}(3:N_{dof}-2,:);\mathbf{Zr}(1,N_{dof});\mathbf{Zr}(1,N_{dof});]\,,\\
\mathbf{L}_{\eta v} &= [\mathbf{Zr}(1,N_{dof});\mathbf{L}_{\eta v}(2:N_{dof}-1,:);\mathbf{Zr}(1,N_{dof});]\,,\\
\mathbf{L}_{\eta\eta} &= [\xi\mathbf{D_0}(1,:);\mathbf{L}_{\eta\eta}(2:N_{dof}-1,:);\xi\mathbf{D_0}(N_{dof},:)]\,,\\
\mathbf{L}_{\phi v} &= [\mathbf{Zr}(1,N_{dof});\mathbf{Zr}(1,N_{dof});\mathbf{L}_{\phi v}(3:N_{dof}-2,:);\mathbf{Zr}(1,N_{dof});\mathbf{Zr}(1,N_{dof});]\,,\\
\mathbf{L}_{\phi\phi} &= [\xi\mathbf{D_0}(1,:);\xi\mathbf{D}_1(1,:);\mathbf{L}_{\phi\phi}(3:N_{dof}-2,:);\xi\mathbf{D}_2(N_{dof},:);\xi\mathbf{D_0}(N_{dof},:)]\,,
\end{aligned}$$

$$\begin{aligned}
\mathbf{M}_{vv} &= [\mathbf{D_0}(1,:);\mathbf{D}_1(1,:);\mathbf{M}_{vv}(3:N_{dof}-2,:);\mathbf{D}_1(N_{dof},:);\mathbf{D_0}(N_{dof},:)]\,,\\
\mathbf{M}_{\phi\phi} &= [\mathbf{D_0}(1,:);\mathbf{D}_1(1,:);\mathbf{M}_{\phi\phi}(3:N_{dof}-2,:);\mathbf{D}_2(N_{dof},:);\mathbf{D_0}(N_{dof},:)]\,,
\end{aligned}$$

where ξ is a imaginary negative constant.
Its function is to map the spurious modes associated to the forced boundary conditions to an arbitrary location in the complex plane guaranteeing the respect of homogenous boundary conditions. In fact ξ *converts-inverts* real and imaginary

[10] A *Matlab style* notation has been used, the generic matrix $\mathbf{A}(i,j)$ has two indices, i for rows and j for columns. As example the notation $\mathbf{A}(1:3,:)$ equals to consider the firsts three rows of $\mathbf{A}$ and all its columns. N_{dof} is the total number of degree of freedom.

part of the unknown coefficients as

$$\begin{cases} \text{Real}(\hat{v}) = |\xi|\text{Imag}(\hat{v}), \\ |\xi|\text{Real}(\hat{v}) = -\text{Imag}(\hat{v}). \end{cases} \longrightarrow \begin{cases} \text{Real}(\hat{v}) = 0, \\ \text{Imag}(\hat{v}) = 0. \end{cases}$$

CHAPTER 4

NON MODAL STABILITY

4.1 Initial value problem

A new to way to investigate the EHD problem has to be developed. Re-examining (3.11) and focusing the attention on its form of initial value problem,it is possible to turn out significant differences about the perturbations's behavior.
In the previous chapter (3.19) has been obtained by assuming a wave-like form perturbation which includes an exponential time dependence. On the other hand, assuming solutions in the form of

$$g(\mathbf{x},t) = \hat{g}(y,t)e^{i(\alpha x+\beta z)}, \qquad \alpha,\beta \in R.$$

and following the same derivation path of (3.31), it is possible to obtain the initial value problem form

$$\begin{cases} \dfrac{\partial}{\partial t}\nabla^2 v = -U_0\dfrac{\partial}{\partial x}\nabla^2 v + U_0''\dfrac{\partial v}{\partial x} + \dfrac{M^2}{T}\nabla^2\nabla^2 v + M^2\left[\Phi_0'\nabla^2\nabla_1^2\phi - \Phi_0'''\nabla_1^2\phi\right], \\ \dfrac{\partial \eta}{\partial_t} = -U_0\dfrac{\partial \eta}{\partial x} - U_0'\dfrac{\partial v}{\partial z} + \dfrac{M^2}{T}\nabla^2\eta, \\ \dfrac{\partial}{\partial t}\nabla^2\phi = \Phi_0'''(\dfrac{\partial\phi}{\partial y} - v) + 2\Phi_0''\nabla^2\phi + \Phi_0'\dfrac{\partial}{\partial y}\nabla^2\phi - U_0\dfrac{\partial}{\partial x}\nabla^2\phi + \dfrac{1}{Fe}\nabla^2\nabla^2(\phi) \end{cases} \tag{4.1}$$

Introducing a spectral method, it yields a first order strictly proper system

$$\begin{cases} \dot{\mathbf{x}} = \mathbf{A}\mathbf{x} \\ \mathbf{y} = \mathbf{C}\mathbf{x}. \end{cases} \tag{4.2}$$

whereas $\mathbf{A} = -i\mathbf{M}^{-1}\mathbf{L} = -i\mathbf{L}_1$

$$\mathbf{x} = \begin{pmatrix} \mathbf{a}_v \\ \mathbf{a}_\eta \\ \mathbf{a}_\phi \end{pmatrix}, \quad \mathbf{A} = -i \begin{bmatrix} \mathbf{D}_2 - \mathsf{k}^2\mathbf{D}_0 & 0 & 0 \\ 0 & \mathbf{D}_0 & 0 \\ 0 & 0 & \mathbf{D}_2 - \mathsf{k}^2\mathbf{D}_0 \end{bmatrix}^{-1} \begin{bmatrix} \mathbf{L}_{os} & 0 & \mathbf{L}_{v\phi} \\ \mathbf{L}_c & \mathbf{L}_{sq} & 0 \\ \mathbf{L}_{\phi v} & 0 & \mathbf{L}_\phi \end{bmatrix},$$

Besides the dimensionless parameters, the evolution of disturbance is influenced by the initial conditions $[u_0, \quad v_0, \quad w_0]^T$. The input and output are in primitive variables (velocity and potential) while the state variables have to be a specified shape in the wall-normal direction.

$$\mathbf{C} = \begin{bmatrix} i\frac{\alpha}{\mathsf{k}^2}\mathbf{D}_1 & -i\frac{\beta}{\mathsf{k}^2}\mathbf{D}_0 & 0 \\ \mathbf{D}_0 & 0 & 0 \\ i\frac{\beta}{\mathsf{k}^2}\mathbf{D}_1 & i\frac{\alpha}{\mathsf{k}^2}\mathbf{D}_0 & 0 \\ 0 & 0 & \mathbf{D}_0 \end{bmatrix}.$$

$$\begin{aligned} \mathbf{x}_0 &= \begin{pmatrix} \mathbf{a}_{v0} \\ \mathbf{a}_{\eta 0} \\ \mathbf{a}_{\phi 0} \end{pmatrix} = \\ &= \begin{bmatrix} \mathbf{D}_2 - \mathsf{k}^2\mathbf{D}_0 & 0 & 0 \\ 0 & \mathbf{D}_0 & 0 \\ 0 & 0 & \mathbf{D}_2 - \mathsf{k}^2\mathbf{D}_0 \end{bmatrix}^{-1} \begin{bmatrix} 0 & \mathbf{D}_0 & 0 & 0 \\ -i\beta\mathbf{D}_0 & 0 & i\alpha\mathbf{D}_0 & 0 \\ 0 & 0 & 0 & \mathbf{I} \end{bmatrix} \begin{pmatrix} \mathbf{a}_{u_0} \\ \mathbf{a}_{v_0} \\ \mathbf{a}_{w_0} \\ \mathbf{a}_{\phi 0} \end{pmatrix} \\ &= \begin{bmatrix} i\alpha\left(\mathsf{k}^2\mathbf{D}_0 - \mathbf{D}_2\right)^{-1} & \left(\mathsf{k}^2\mathbf{D}_0 - \mathbf{D}_2\right)^{-1}\mathsf{k}^2\mathbf{D}_0 & i\beta\left(\mathsf{k}^2\mathbf{D}_0 - \mathbf{D}_2\right)^{-1}\mathbf{D_1} & 0 \\ i\beta\mathbf{D}_0 & 0 & -i\alpha\mathbf{D}_0 & 0 \\ 0 & 0 & 0 & \mathbf{D}_0 \end{bmatrix} \begin{pmatrix} \mathbf{a}_{u_0} \\ \mathbf{a}_{v_0} \\ \mathbf{a}_{w_0} \\ \mathbf{a}_{\phi 0} \end{pmatrix} = \\ &= \mathbf{B} \begin{pmatrix} \mathbf{a}_{u_0} \\ \mathbf{a}_{v_0} \\ \mathbf{a}_{w_0} \\ \mathbf{a}_{\phi 0} \end{pmatrix} = \mathbf{B}\mathbf{v}_0 \end{aligned} \tag{4.3}$$

Assuming the fact that no statements have been made regarding the temporal behavior, the general solution of (4.2) which completely describes the time evolution of initial condition $\mathbf{x}_0$ is

$$\mathbf{x} = e^{\mathbf{A}t}\mathbf{B}\mathbf{v}_o \tag{4.4}$$

while the velocity-potential *input-output* form is

$$\begin{pmatrix} \mathbf{a}_{u_{out}} \\ \mathbf{a}_{v_{out}} \\ \mathbf{a}_{w_{out}} \\ \mathbf{a}_{\phi_{out}} \end{pmatrix} = \mathbf{C}e^{\mathbf{A}t}\mathbf{B} \begin{pmatrix} \mathbf{a}_{u_0} \\ \mathbf{a}_{v_0} \\ \mathbf{a}_{w_0} \\ \mathbf{a}_{\phi 0} \end{pmatrix} \tag{4.5}$$

As shown in [17], [24], systems governed by non-normal matrices can exhibit a large transient amplification of energy contained in the initial condition.

4.1.1 Modal reduction

As usual in many problems it is possible to reduce the numerical efforts projecting the system in a new, and more efficient, base set. Congruence and completeness are two essential properties that the new set required. The eigenfunctions[1] respect the congruence (boundary conditions) by definition. Moreover, for bounded domains, completeness has been proven by [23].
Assuming (3.18), it is to translate from (4.2) to

$$\mathbf{A}\tilde{\mathbf{x}} = -i\omega\tilde{\mathbf{x}}, \qquad w \in C. \tag{4.6}$$

$$\mathbf{L}_1\tilde{\mathbf{x}} = \omega\tilde{\mathbf{x}}, \qquad w \in C. \tag{4.7}$$

Calling $\tilde{\mathbf{x}}$ and $\tilde{\mathbf{y}}$ right and left eigenvectors of n-by-n system and using their properties already cited,it is possible to expand (4.4) as a linear combination of $m \ll n$ eigenvectors . This technique, called modal reduction[2], is a powerful tool to get a new and smaller system instead the original one. As every tool it has several limitations. Its applicability will be tested forwardly in the same manner used by [21].

$$\mathbf{X} = [\tilde{\mathbf{x}}_1, \tilde{\mathbf{x}}_2, ..., \tilde{\mathbf{x}}_m], \qquad \mathbf{X} \in C^{nxm}. \tag{4.8}$$

$$\mathbf{x} = \mathbf{X}\mathbf{q}. \tag{4.9}$$

where $\mathbf{q}$ are the coefficients of modal expansion. Substituting in (4.2) and using

$$\dot{\mathbf{x}} = \mathbf{X}\dot{\mathbf{q}}, \qquad \mathbf{Y}^T(\mathbf{A})\mathbf{X} = -i\mathbf{\Lambda}, \qquad \mathbf{Y}^T\mathbf{X} = \mathbf{I}.$$

[1] Eigenvector in discrete form
[2] Also known as Modal expansion or Modal truncation.

calling $\mathbf{C}_r = \mathbf{CX}$, the reduced problem is

$$\begin{cases} \dot{\mathbf{q}} = -i\mathbf{\Lambda q}, \\ \mathbf{y} = \mathbf{C}_r\mathbf{q} \end{cases} \tag{4.10}$$

whereas

$$\mathbf{q} = \begin{pmatrix} q_1 \\ q_2 \\ . \\ . \\ . \\ q_m \end{pmatrix}, \qquad \Lambda = \begin{bmatrix} \omega_1 & 0 & ... & ... & 0 \\ 0 & \omega_2 & ... & ... & 0 \\ 0 & 0 & . & ... & 0 \\ 0 & 0 & 0 & . & 0 \\ 0 & 0 & 0 & ... & \omega_m \end{bmatrix}, \qquad n, m \in R, \quad m \ll n.$$

The benefits gained are: a smaller dimension of reduced system, minor numerical effort and the power to use a simple diagonal matrix instead the exponential one

$$e^{\mathbf{A}t} = \mathbf{I} + \mathbf{A}t + \frac{1}{2}\mathbf{A}^2t^2 + ... = \mathbf{Y}^T\mathbf{X} - i\mathbf{X\Lambda Y}^Tt + \frac{1}{2}\mathbf{X\Lambda}^2\mathbf{Y}^Tt^2 + ... = \mathbf{X}e^{-i\Lambda t}\mathbf{Y}^T \tag{4.11}$$

Initial condition for the reduced system

Recalling (4.3), the initial conditions available u, v, w and ϕ need to be projected in the Chebyshev space. Although

$$\mathbf{q}_0 = \mathbf{X}^{-1}\mathbf{x}_0$$

does not make sense because $\mathbf{X}$ is a rectangular matrix. A possible solution is given by least square method. Guessing a modal initial condition, it's possible to define a residual as

$$\varepsilon(\mathbf{q}_0) = \mathbf{x}_0 - \mathbf{Xq}_0$$

and then, using LSD the result is

$$\mathbf{q}_0 = \mathbf{W}_{RE}^{-1}\mathbf{X}^*\mathbf{W}_E\mathbf{x}_0 = \mathbf{Z}\mathbf{x}_0 \tag{4.12}$$

and the *input-output reduced form*

$$\begin{pmatrix} u_{out} \\ v_{out} \\ w_{out} \\ \phi_{out} \end{pmatrix} = \mathbf{C}_r e^{-\mathbf{\Lambda}t}\mathbf{ZB} \begin{pmatrix} u_0 \\ v_0 \\ w_0 \\ \phi_0 \end{pmatrix} \tag{4.13}$$

where the matrices $\mathbf{W}_E$ and $\mathbf{W}_{RE}$ will be presented in the next sections.

4.2 Disturbance measure

4.2.1 Total Energy

At the core of the non modal analysis of non-normal operators is the non-orthogonality of the eigenfunctions. The angle between various eigenfunctions is computed by using an inner product. This same inner product provides a norm to measure the size of our state variables. This choice of inner product will quantitatively influence the maximum amplification potential of the underlying operator. Therefore, the norm and inner product have to be chosen carefully[3].
In order to quantify these amplifications a disturbance measure is needed. As it is clear, physically motivated measures are preferred as they suggest realizability and observability for numerical simulation and experiments.
In the present work the charge carriers are the electrons, which dragged by the electric field form zones with different charge densities. [4] In this process no mass displacement is involved since the electron's mass is negligible. Therefore a natural choice of disturbance measure in EHD problems is the system's total energy determined by the sum of kinetic energy produced by liquid velocity perturbations, and potential energy produced by electrical perturbations.
In dimensional units

$$E_k = \frac{1}{2}\rho \int_{\mathcal{V}} |u|^2 + |v|^2 + |w|^2 dV = [J], \tag{4.14}$$

$$E_p = \frac{1}{2} \int_{\mathcal{V}} q\phi dV = [J]. \tag{4.15}$$

which added yield

$$\tilde{E}_{tot} = \frac{1}{2} \int_{\mathcal{V}} |\tilde{u}|^2 + |\tilde{v}|^2 + |\tilde{w}|^2 + M^2 \tilde{q}\tilde{\phi} \quad d\mathcal{V} \tag{4.16}$$

where ℓ, $\overline{\Phi}_0$,$(\overline{\Phi}_0\varepsilon)/\ell^2$ and $(K\overline{\Phi}_0)/\ell$ are taken as reference distance, potential, charge density and velocity respectively. Using Parseval's equality

$$\int_{-\infty}^{+\infty} h^T(x)h(x)dx = \frac{1}{2\pi} \sum_{\alpha=-\infty}^{+\infty} \mathbf{h}^*(i\alpha)\mathbf{h}(i\alpha)$$

and

[3]Orthogonality is strictly connected to the inner product between eigenvectors and so to the norm used to evaluate it. Since from Lyapunov theory in a stable system the energy should decrease or remain constant over time, we can say that if the system is stable, there is a *energy* defined by quadratic form of the state, for which the inner product is zero. Usually these norms have not physics meaning and so are useless for our purpose.

[4]It has been proven by several papers [19], [8]that, when EHD instability sets in, in the charge continuity equation is possible to find regions with null or almost null charge density even with the charge diffusion term.

$$\hat{u} = \frac{i}{\mathsf{k}^2}(\alpha D\hat{v} - \beta\hat{\eta}),$$
$$\hat{w} = \frac{i}{\mathsf{k}^2}(\beta D\hat{v} + \alpha\hat{\eta}),$$
$$\hat{q} = -(\mathbf{D}_2 - \mathsf{k}^2)\phi.$$

Since the Fourier modes are orthogonal, the total energy can be written as follows

$$\tilde{E}_{tot} = \sum_{\alpha}\sum_{\beta} E \quad (\alpha,\beta) = \sum_{\alpha}\sum_{\beta}\int_{-1}^{1} \frac{|Dv|^2}{\mathsf{k}^2} + |v|^2 + \frac{|\eta|^2}{\mathsf{k}^2} + M^2\mathsf{k}^2|\phi|^2 - M^2\phi^* D_2\phi \quad dyd\alpha d\beta \tag{4.17}$$

Integrating per parts E[5], known as total energy density in Fourier space, the energy measure can be related to a weighted inner product

$$E = \frac{1}{2\mathsf{k}^2}\int_{-\infty}^{+\infty} \begin{pmatrix}\hat{v}\\ \hat{\eta}\\ \hat{\phi}\end{pmatrix}^* \begin{bmatrix}\mathsf{k}^2 - D_2 & 0 & 0\\ 0 & 1 & 0\\ 0 & 0 & M^2\mathsf{k}^4 - M^2\mathsf{k}^2 D_2\end{bmatrix} \begin{pmatrix}\hat{v}\\ \hat{\eta}\\ \hat{\phi}\end{pmatrix} \quad dy \tag{4.18}$$

4.2.2 Energy weight in discrete form

Using a spectral method, the total energy results

$$E = \mathbf{x}^* \quad \frac{1}{2\mathsf{k}^2}\int_{-1}^{1} \begin{bmatrix}\mathbf{D}_1^*\mathbf{D}_1 + \mathsf{k}^2\mathbf{D}_0^*\mathbf{D}_0 & 0 & 0\\ 0 & \mathbf{D}_0^*\mathbf{D}_0 & 0\\ 0 & 0 & M^2(\mathsf{k}^4\mathbf{D}_1^*\mathbf{D}_1 + \mathsf{k}^2\mathbf{D}_0^*\mathbf{D}_0)\end{bmatrix} dy \quad \mathbf{x}$$

$$E = \mathbf{x}^* \begin{bmatrix}\mathbf{W}_{vv} & 0 & 0\\ 0 & \mathbf{W}_{\eta\eta} & 0\\ 0 & 0 & \mathbf{W}_{\phi\phi}\end{bmatrix} \mathbf{x} = \mathbf{x}^*\mathbf{W}_E\mathbf{x}. \tag{4.19}$$

As explained in [11] if values of a function at y_i are known, the function can be integrated with spectral accuracy. Using the matrix $\mathbf{O}$ which converts the function's coefficients in the first derivative's coefficients, and integrating the Chebyshev matrices

$$\mathbf{x}_{/y} = \mathbf{D}_1\mathbf{x} = \mathbf{D}_0\mathbf{O}\mathbf{x},$$
$$\mathbf{S} = \int_{-1}^{1} \mathbf{D}_0^*\mathbf{D}_0 dy.$$

[5]Just its first term $|Dv|^2$.

where $\mathbf{O}$ is given by [9] and

$$\mathbf{S}_{ij} = \begin{cases} \dfrac{1}{1-(i+j)^2} + \dfrac{1}{1-(i-j)^2}, & \text{if} \quad i+j = \text{even} \\ 0, & \text{if} \quad i+j = \text{odd} \end{cases} \tag{4.20}$$

Is possible to re-write every term of (4.19) as a matrix product

$$\begin{aligned} \mathbf{W}_{vv} &= \mathbf{O}^*\mathbf{S}\mathbf{O} + \mathsf{k}^2\mathbf{S}, \\ \mathbf{W}_{\eta\eta} &= \mathbf{S}, \\ \mathbf{W}_{\phi\phi} &= M^2\mathsf{k}^2\mathbf{O}^*\mathbf{S}\mathbf{O} + M^2\mathsf{k}^4\mathbf{S}. \end{aligned}$$

4.2.3 Energy modal reduction, inner product and energy norms

A reduced formulation of the scalar product and its associated norm is needed. Substituting (4.9) in (4.18)

$$E = \mathbf{x}^*\mathbf{W}_E\mathbf{x} = \mathbf{q}^*\mathbf{X}^*\mathbf{W}_E\mathbf{X}\mathbf{q} = \mathbf{q}^*\mathbf{W}_{RE}\mathbf{q} \tag{4.21}$$

whereas $\mathbf{W_E}$ is the n-by-n energy weight matrix and $\mathbf{W_{RE}}$ is the m-by-m *reduced* energy weight matrix where $m \ll n$. The weight matrices are both hermitian and definite positive so a Cholesky decomposition could be applied

$$\begin{aligned} \mathbf{W}_E &= \mathbf{F}^*\mathbf{F}, \\ \mathbf{W}_{RE} &= \mathbf{F}_r^*\mathbf{F}_r, \end{aligned} \tag{4.22}$$
$$\tag{4.23}$$

Both $\mathbf{W_E}$ and $\mathbf{W_{RE}}$ are necessary to convert an energy measure to the more standard Eulerian norm. In fact, the integral (4.18) is a inner product, an application $(\ .\ ,\ .\ )_E$ that permits the passage from a vector space to a scalar space. As every inner product it is linear, hermitian, and definite positive. In that way the energy scalar product could be defined as

$$\begin{aligned} (\mathbf{x}_1, \mathbf{x}_2)_E &= \mathbf{x}^*\mathbf{W}_E\mathbf{x} = (\mathbf{F}\mathbf{x}_1, \mathbf{F}\mathbf{x}_2)_2, \\ (\mathbf{q}_1, \mathbf{q}_2)_{RE} &= \mathbf{q}_1^*\mathbf{W}_{RE}\mathbf{q}_2 = (\mathbf{F}_r\mathbf{q}_1, \mathbf{F}_r\mathbf{q}_2)_2, \\ (\mathbf{x}_1, \mathbf{x}_2)_E &= (\mathbf{q}_1, \mathbf{q}_2)_{RE} \end{aligned}$$

from the inner product it is simple to derive its associated energy and eulerian norms

$$(\mathbf{x}, \mathbf{x})_E = \|\mathbf{x}\|_E^2 = \|\mathbf{F}\mathbf{x}\|_2^2, \tag{4.24}$$
$$(\mathbf{q}, \mathbf{q})_{RE} = \|\mathbf{q}\|_{RE}^2 = \|\mathbf{F}_r\mathbf{q}\|_2^2, \tag{4.25}$$
$$\|\mathbf{x}\|_E^2 = \|\mathbf{q}\|_{RE}^2 \tag{4.26}$$

$$\|\mathbf{B}\|_E = \max_{\mathbf{x}} \frac{\|\mathbf{B}\mathbf{x}\|_E}{\|\mathbf{x}\|_E} = \max_{\mathbf{x}} \frac{\|\mathbf{F}\mathbf{B}\mathbf{x}\|_2}{\|\mathbf{F}\mathbf{x}\|_2} = \max_{\mathbf{x}} \frac{\|\mathbf{F}\mathbf{B}\mathbf{F}^{-1}\mathbf{F}\mathbf{x}\|_2}{\|\mathbf{F}\mathbf{x}\|_2} = \|\mathbf{F}\mathbf{B}\mathbf{F}^{-1}\|_2 \tag{4.27}$$

$$\|\mathbf{B}\|_{RE} = \max_{\mathbf{q}} \frac{\|\mathbf{B}\mathbf{q}\|_{RE}}{\|\mathbf{q}\|_{RE}} = \max_{\mathbf{q}} \frac{\|\mathbf{F}_r\mathbf{B}\mathbf{q}\|_2}{\|\mathbf{F}_r\mathbf{q}\|_2} = \max_{\mathbf{x}} \frac{\|\mathbf{F}\mathbf{B}\mathbf{x}\|_2}{\|\mathbf{F}\mathbf{x}\|_2} = \|\mathbf{F}_r\mathbf{B}\mathbf{F}_r^{-1}\|_2 \tag{4.28}$$

4.3 Unforced problem, response to initial condition

4.3.1 Maximum amplification

The linearized EHD problem is defined by a non-normal operator, therefore a large transient growth is possible even when all eigenvalues are confined to the stable half-plane, thus predicting large-time asymptotic decay. In the large-time limit, this analysis recovers the least stable mode, but for intermediate time, the results may be significantly different. After choosing a suitable disturbance measure and its related norms, we are interested to measure the maximum response to varying initial conditions.
Defining G as the maximum possible amplification of the energy density related to an initial condition

$$G(t) = \max \frac{E(t)}{E(t_0)} = \max_{\mathbf{x}_0 \neq 0} \frac{\|\mathbf{x}(t)\|_E^2}{\|\mathbf{x}_0\|_E^2} = \max_{\mathbf{q}_0 \neq 0} \frac{\|\mathbf{q}(t)\|_{RE}^2}{\|\mathbf{q}_0\|_{RE}^2} = \max_{\mathbf{q}_0 \neq 0} \frac{\|e^{-\Lambda t}\mathbf{q}_0\|_{RE}^2}{\|\mathbf{q}_0\|_{RE}^2}$$

with (4.28) it is possible to re-write it as

$$G(t) = \|\mathbf{F}_r e^{\Lambda t} \mathbf{F}_r^{-1}\|_2^2 = \|\mathbf{B}_E\|_2^2 = \sigma_1^2 \tag{4.29}$$

where σ_1 is the principal singular value of $\mathbf{B}_E$. The crucial feature of this formula is that the 2-norm of any matrix can be determined using the singular value decomposition (SVD), which can be computed using standard subroutines available in most software libraries.
Since $\mathbf{F}_r$ implicitly contains information about eigenvectors, it should become clear that a simple eigenvalue analysis misrepresent the transient growth phenomena. As underlined before, the eventual short time amplification will decay as described by the *eigenvalues's asymptotic fate*. It is important to keep in mind that the initial condition that optimizes the amplification $G(t)$ might be different for different times. The curve $\|e^{-i\Lambda t}\|_{RE}^2$ represents the maximum possible energy amplification, which for each instant in time is optimized over all possible initial conditions with unit energy norm.
$G(t)$ is thus an optimization over all initial conditions with unit energy norm for each time.

4.3.2 Optimal disturbances at fixed time T

The most common approach quest of hydrodynamic stability theory is to figure out the most dangerous initial condition that results in the maximum energy amplification. The SVD decomposition yields both $G(t)$ and the coefficient $\overline{\mathbf{q}}$ of the initial condition that achieves this supremo.
Assuming that the initial condition (unknown) has unit energy norm, it will have an energy density of

$$E(\bar{t}) = \|e^{-i\Lambda\bar{t}}\|^2_{RE} = \|\mathbf{F}_r e^{-i\Lambda\bar{t}}\mathbf{F}_r^{-1}\|_2^2 = \|\mathbf{B}_E\|_2^2$$

which yields

$$\mathbf{B}_E\mathbf{q}_0 = \|\mathbf{B}_E\|_2\mathbf{q}(\bar{t}) = \sigma_1(\mathbf{B}_E)\mathbf{q}(\bar{t})$$

On the other hand applying the SVD decomposition to $\mathbf{B}_E$ we obtain

$$\mathbf{B}_E\mathbf{v}_1 = \sigma_1\mathbf{u}_1. \tag{4.30}$$

The equation (4.30) can have a physical key of lecture. The *energy* given by initial condition $\mathbf{v}_1$ (the unknown $\mathbf{q}_0$), is mapped by $\mathbf{B}_E$ at time $\bar{t}$ in the vector $\mathbf{u}_1$ and amplified by σ_1. So the unknown optimal initial disturbance $\mathbf{q}_0$ is simply $\mathbf{v}_1$.
To recovery the the optimal disturbance in u, v, w and ϕ variables is quite simple.

$$\mathbf{v}_{optimal} = \mathbf{CTX}\mathbf{v}_1 \tag{4.31}$$

4.3.3 Maximum growth rate

In this section the disturbance maximum growth rate will be demonstrate. First of all the energy density rate is defined as

$$\begin{aligned}\dot{E}(t) &= \frac{\partial}{\partial t}\|\mathbf{x}(t)\|_E^2 = (\dot{\mathbf{x}},\mathbf{x})_E + (\mathbf{x},\dot{\mathbf{x}})_E = \\ &= (\mathbf{A}\mathbf{x},\mathbf{x})_E + (\mathbf{x},\mathbf{A}\mathbf{x})_E = 2\mathrm{Real}\,(\mathbf{A}\mathbf{x},\mathbf{x})_E = \\ &= 2\mathrm{Imag}\,(\mathbf{L}_1\mathbf{x},\mathbf{x})_E\end{aligned}$$

or for the projected case

$$\begin{aligned}\dot{E}(t) &= \frac{\partial}{\partial t}\|\mathbf{q}(t)\|_{RE}^2 = (\dot{\mathbf{q}},\mathbf{q})_{RE} + (\mathbf{q},\dot{\mathbf{q}})_{RE} = \\ &= (-i\mathbf{\Lambda}\mathbf{q},\mathbf{q})_{RE} + (\mathbf{q},-i\mathbf{\Lambda}\mathbf{q})_{RE} = \\ &= 2\mathrm{Imag}\,(\mathbf{\Lambda}\mathbf{q},\mathbf{q})_{RE}\end{aligned}$$

It is clear that the growth rate depends on how the numerical range $\mathcal{N}(\Lambda)$ extends into the upper complex half-plane. The *numerical range* or *field of values* $(\mathbf{\Lambda}\mathbf{q},\mathbf{q})_{RE}$, is defined as the set of all Rayleigh quotients of Λ t.c.

$$\mathcal{N}(\mathbf{\Lambda}) = \left\{\mathbf{q}^*\mathbf{\Lambda}\mathbf{q} \quad : \quad \mathbf{q}\in C^N, \quad \|\mathbf{q}\|_{RE} = 1\right\},$$

The principal application of the numerical range, i.e. the limit of *pseudospectra* for $\varepsilon\to\infty$, is estimating the behavior of $\|e^{\Lambda t}\|_{RE}$ as a function of t. The norm above cited may have different behaviors in its initial, transient and asymptotic phases. The behavior as $t\to\infty$ is determined by eigenvalues (or *spectral abscissa*) while as $t\to 0^+$ the behavior is determined by *numerical abscissa*. The boundary of the numerical range is easily computed using the following formula [17], [20]

$$z = \frac{\mathbf{v}^*\mathbf{\Lambda}\mathbf{v}}{\mathbf{v}^*\mathbf{v}}$$

where $\mathbf{v}$ are the principal eigenvector of the Hermitian part

$$\mathbf{H}(e^{i\theta}\mathbf{\Lambda}) = \frac{1}{2}\left((e^{i\theta}\mathbf{\Lambda}) + (e^{i\theta}\mathbf{\Lambda})^*\right), \qquad 0\le\theta\le\pi.$$

Since the maximum growth rate can be determined as

$$\max_{\|\mathbf{q}\|_{RE}=1}\dot{G}(t) = \max\left(2\mathrm{Imag}\,(\mathbf{\Lambda}\mathbf{q},\mathbf{q})_{RE}\right) \tag{4.32}$$

we are interested to find the numerical range's maximum protrusion. Following [14], this protrusion is equivalent to the *numerical abscissa* and thus the max growth rate is the max growth rate at time $t = 0^+$. The numerical abscissa is defined as the maximum eigenvalue of $\mathbf{H}(\mathbf{\Lambda})$ for $\theta = 0$.
For last but not least a necessary and sufficient condition for growth of energy is that the numerical range extends into upper complex plane. This is a much stronger condition than eigenvalues's condition for the instability set in.

4.4 Forced Problem

4.4.1 Response to harmonic excitation

Considering the system (4.2) harmonically forced

$$\dot{\mathbf{x}} = \mathbf{A}\mathbf{x} + \mathbf{x}_f e^{i\omega_f t}, \qquad \omega \in R. \tag{4.33}$$

the solution is

$$\mathbf{x}(t) = \mathbf{x}_h(t) + \mathbf{x}_p(t) = e^{\mathbf{A}t}\mathbf{x}_0 + \int_0^T \mathbf{h}(t-\tau)\mathbf{x}_f e^{i\omega\tau} d\tau. \tag{4.34}$$

where $\mathbf{h}(t)$ is system's impulsive response. Assuming that eigenvalues of $\mathbf{A}$ are confined to the stable half-plane the long time response is governed only by its particular solution

$$\mathbf{x}(t) = (i\omega_f \mathbf{I} - \mathbf{A})^{-1}\mathbf{x}_f e^{i\omega t}. \tag{4.35}$$

Proceeding in the same manner for the projected system we obtain

$$\mathbf{q}(t) = (\mathbf{\Lambda} - i\omega_f \mathbf{I})^{-1}\mathbf{q}_f e^{i\omega t}. \tag{4.36}$$

whereas $\mathbf{q}_f = \mathbf{X}\mathbf{x}_f$ and the quantities $(i\omega_f \mathbf{I} - \mathbf{A})^{-1}$, and $(\mathbf{\Lambda} - i\omega_f \mathbf{I})^{-1}$ are known as *the resolvents*. Similarly to the maximum growth rate of an initial condition, it is possible to define a maximum response of the system to a forcing frequency ω_f according to

$$\begin{aligned} R(\omega_f) &= \max_{\mathbf{q}_f} \frac{\|\mathbf{q}(t)\|_{RE}^2}{\|\mathbf{q}_f\|_{RE}^2} = \|(\mathbf{\Lambda} - \omega_f \mathbf{I})^{-1}\|_{RE}^2 = & (4.37)\\ &= \|\mathbf{F}\mathrm{Diag}\left(\frac{1}{\omega_1 - \omega_f}, ..., \frac{1}{\omega_m - \omega_f}\right)\mathbf{F}^{-1}\|_2^2 = & (4.38)\\ &= \|\mathbf{B}_{fh}\|_2^2 = \sigma_1^2. & (4.39) \end{aligned}$$

where σ_1^2 is the principal singular value of $\mathbf{B}_{fh}$.
Since $\mathbf{B}_{fh}$ contains both eigenvectors and eigenvalues's information, there are two different resonance mechanism [24], [13], in fact as shown in

$$\frac{1}{\mathrm{dist}\left\{\omega_{i-esimo} - \omega_f\right\}} \leq R(\omega_f) \leq \frac{\mathrm{cond}(\mathbf{F})}{\mathrm{dist}\left\{\omega_{i-esimo} - \omega_f\right\}}. \tag{4.40}$$

the two distinct ways to get a large response are either forcing with a ω_f close to $\omega_{i-esimo}$ (resonance) or getting a large cond($\mathbf{F}$). This second mechanism is known

as *pseudoresonance* and it's related to the level of nonorthogonality of eigenvectors. Exactly as in the case of optimal disturbance we are able to compute the most responsive disturbances using SVD decomposition as

$$\mathbf{v}_{f-optimal} = \mathbf{CTX}\mathbf{v}_1 \tag{4.41}$$

where, obviously, $\mathbf{v}_1$ is the principal left vector of SVD decomposition of $\mathbf{B}_{fh}$.

CHAPTER 5

HYDROSTATIC CASE

5.1 Equations and Parameters

Physically, the problem has a certain symmetry in the x-z directions due to the domain's geometry. Thus by a geometrical point of view it is possible to confuse x and z. In the Poiseuille flow this symmetry is broken by the presence of cross flow that establishes a preferred direction. In this way it is then possible to distinguish between the intensity of disturbances along the streamwise (α) and spanwise (β) direction.
However, in the hydrostatic case there is no cross-flow and therefore there is no preferential direction.
The equations (3.19) have been simplified by deleting the velocity-base-flow terms.

$$\begin{cases} \omega(D_2 - \mathsf{k}^2)\hat{v} = \left[-\dfrac{1}{i}\dfrac{M^2}{T}(D_2 - \mathsf{k}^2)^2\right]\hat{v} + \dfrac{1}{i}M^2\left[\mathsf{k}^2\Phi_0'(D_2 - \mathsf{k}^2) - \mathsf{k}^2\Phi_0'''\right]\hat{\phi}, \\ \omega\hat{\eta} = \left[-\dfrac{1}{i}\dfrac{M^2}{T}(D_2 - \mathsf{k}^2)\right]\hat{\eta}, \\ \omega(D_2 - \mathsf{k}^2)\hat{\phi} = \Phi_0'''\hat{v} + \\ \quad + \left[-\dfrac{1}{i}(\Phi_0'''D_1 + 2\Phi_0''(D_2 - \mathsf{k}^2) + \Phi_0'(D_3 - \mathsf{k}^2 D_1)) - \dfrac{1}{i}\dfrac{1}{Fe}(D_2 - \mathsf{k}^2)^2\right]\hat{\phi}. \end{cases}$$

As it is both mathematically and physically clear, there is no point distinguishing from streamwise and spanwise disturbances do to the fact that there is no cross flow. The only disturbance parameter that still plays a role in the equations is its modulus k. Furthermore, if in the the Poiseuille's flow the normal velocity v couples the whole system by forcing the normal vorticity η, in the hydrostatic case the absence of the term ($U_0'\beta\hat{v}$) effectively decouples the vorticity reason why the system can be composed by only two equations.
The following study will focus on the system (5.1).

$$\begin{cases} \omega(D_2 - \mathsf{k}^2)\hat{v} = \left[-\dfrac{1}{i}\dfrac{M^2}{T}(D_2 - \mathsf{k}^2)^2\right]\hat{v} + \dfrac{1}{i}M^2\left[\mathsf{k}^2\Phi_0'(D_2 - \mathsf{k}^2) - \mathsf{k}^2\Phi_0'''\right]\hat{\phi}, \\ \omega(D_2 - \mathsf{k}^2)\hat{\phi} = \dfrac{1}{i}\Phi_0'''\hat{v} + \\ \quad + \left[-\dfrac{1}{i}(\Phi_0'''D_1 + 2\Phi_0''(D_2 - \mathsf{k}^2) + \Phi_0'(D_3 - \mathsf{k}^2 D_1)) - \dfrac{1}{i}\dfrac{1}{Fe}(D_2 - \mathsf{k}^2)^2\right]\hat{\phi}. \end{cases} \tag{5.1}$$

with its suitable boundary conditions

$$\hat{v}(\pm 1) = 0, \qquad \hat{v}'\Big|_{\pm 1} = 0, \qquad \hat{\phi}(\pm 1) = 0, \qquad \hat{\phi}''\Big|_{-1} = 0, \qquad \hat{\phi}'''\Big|_{1} = 0.$$

The parameters which determine the solution are k, M, T and Fe.
Recovering the discrete form notation we obtain

$$\begin{bmatrix} \mathbf{L}_{vv} & \mathbf{L}_{v\phi} \\ \mathbf{L}_{\phi v} & \mathbf{L}_{\phi\phi} \end{bmatrix} \begin{pmatrix} \mathbf{a}_v \\ \mathbf{a}_\phi \end{pmatrix} = \omega \begin{bmatrix} \mathbf{M}_{vv} & 0 \\ 0 & \mathbf{M}_{\phi\phi} \end{bmatrix} \begin{pmatrix} \mathbf{a}_v \\ \mathbf{a}_\phi \end{pmatrix} \tag{5.2}$$

Where the $M_{(.)}$ and $L_{(.)}$ operators are the following:

$$\mathbf{M}_{vv} = \mathbf{D}_2 - \mathsf{k}^2\mathbf{D_0}, \tag{5.3}$$

$$\mathbf{M}_{\phi\phi} = \mathbf{D}_2 - \mathsf{k}^2\mathbf{D_0}. \tag{5.4}$$

$$\mathbf{L}_{vv} = -\frac{1}{i}\frac{M^2}{T}(\mathbf{D}_4 - 2\mathsf{k}^2\mathbf{D}_2 + \mathsf{k}^4\mathbf{D_0}), \tag{5.5}$$

$$\mathbf{L}_{v\phi} = +\frac{1}{i}M^2\left[\mathsf{k}^2\mathbf{\Phi_0'}(\mathbf{D}_2 - \mathsf{k}^2\mathbf{D_0}) - \mathsf{k}^2\mathbf{\Phi_0'''}\mathbf{D_0}\right], \tag{5.6}$$

$$\mathbf{L}_{\phi v} = \frac{1}{i}\mathbf{\Phi_0'''}\mathbf{D_0}, \tag{5.7}$$

$$\begin{aligned} \mathbf{L}_{\phi\phi} = &-\frac{1}{i}(\Phi_0'''\mathbf{D} + 2\Phi_0''(\mathbf{D}_2 - \mathsf{k}^2\mathbf{D_0}) + \Phi_0'(\mathbf{D}_3 - \mathsf{k}^2\mathbf{D})) \\ &-\frac{1}{i}\frac{1}{Fe}(\mathbf{D}_4 - 2\mathsf{k}^2\mathbf{D}_2 + \mathsf{k}^4\mathbf{D_0}). \end{aligned} \tag{5.8}$$

5.2 Modal stability

5.2.1 Discrete Spectrum

The eigenvalues of the equation set (5.1) are shown in Figure 5.1. The eigenvalues are located on three main branches which have been labeled as A, B (*parabola*) and Z ($\omega_R = 0$) using a similar notation to the one used by [17]. Typical shape of eigenfunction labeled (1,2,3) in Figure 5.1 are shown in Figure 5.2. Since in the Hydrostatic case the wall normal vorticity is decoupled by the rest of the system, and the flow is essentially a 2D flow only the components $u(y, \mathsf{K})$, $v(y, \mathsf{K})$ and $\phi(y, \mathsf{K})$ will be shown.
As for the Poiseuille flow we can distinguish between *wall-modes* and *center-modes*. The only difference is that, starting from the least stable eigenvalue, as σ_I diminishes the modes tends to pass from center-modes to wall-modes. There are non differences between A and B's modes.

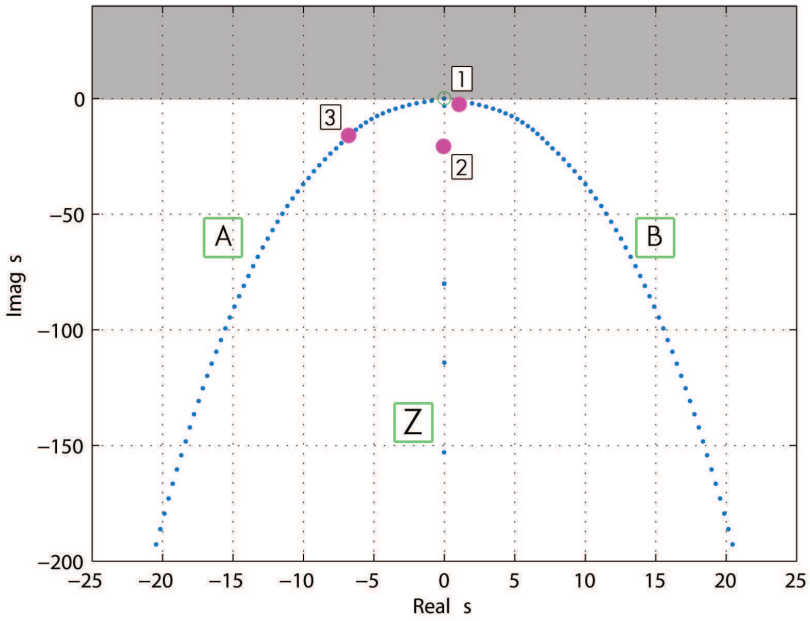

Figure 5.1: Hydrostatic case: *Spectrum*, $N = 250$, $\mathsf{K} = 2.5$, $Fe = 65$,$C = 10$, $M = 60$, $T = 110$

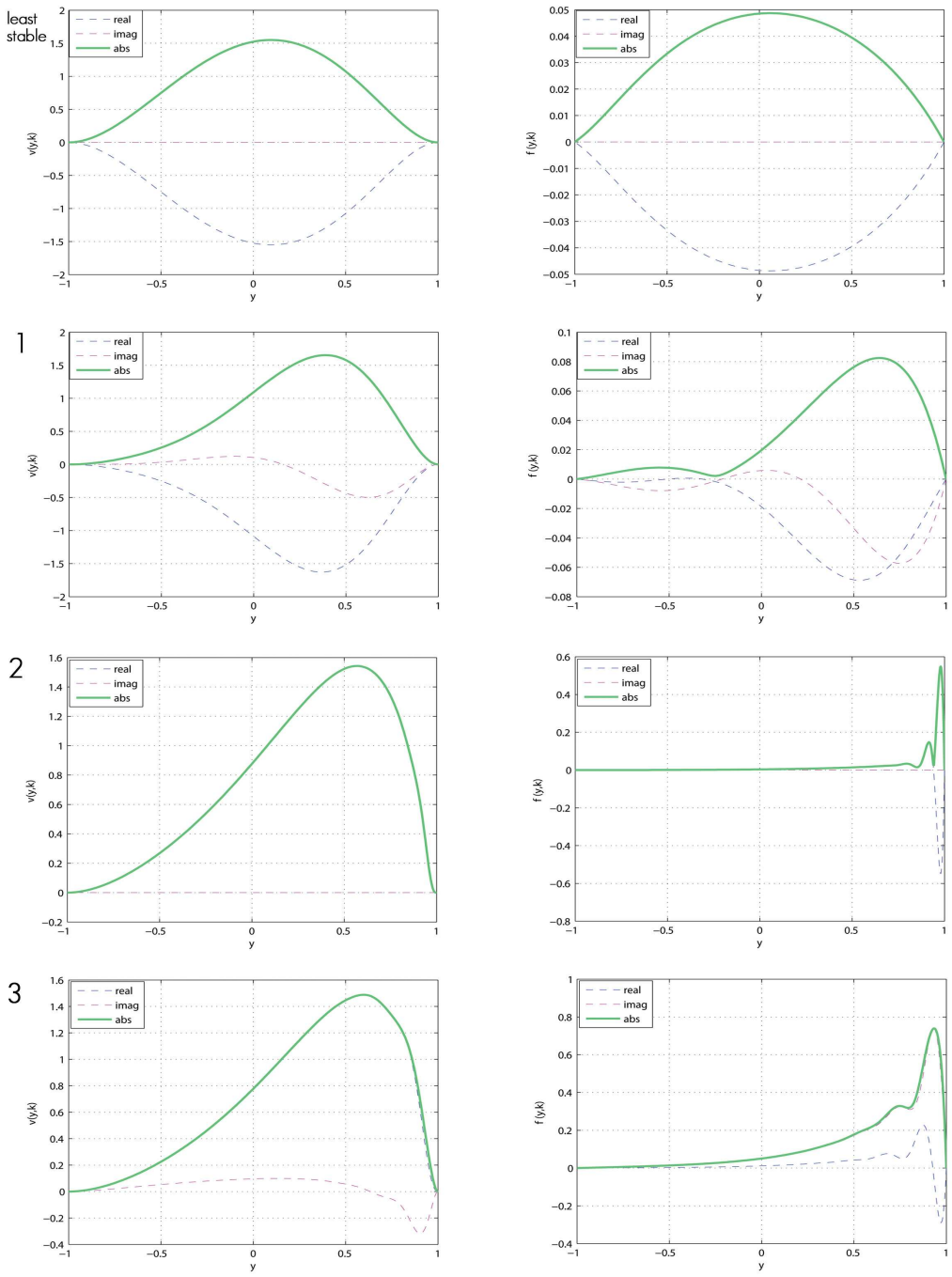

Figure 5.2: Hydrostatic case: *Eigenfunctions*, $N = 250$, $\mathsf{K} = 2.5$, $Fe = 65$,$C = 10$, $M = 60$, $T = 110$

resolution errors

Errors in the spectrum introduced by insufficient resolution have most of their effects on A and B branches as shown in Figure 5.3. As clearly explained on [17] with the decreasing of imaginary part of eigenvalues, one observes that the eigenfunctions become increasingly oscillatory. At a certain point the numerical resolution is insufficient to represent these oscillations. Now the eigenvalues corresponding to this ill-represented eigenfunctions fail to follow the asymptotic behavior of the two branches splitting. Reducing N the split clearly climbs back to the branches A and B not affecting the Z branch. Testing the code, neither M nor Fe values affects the resolution capability in the hydrostatic case.

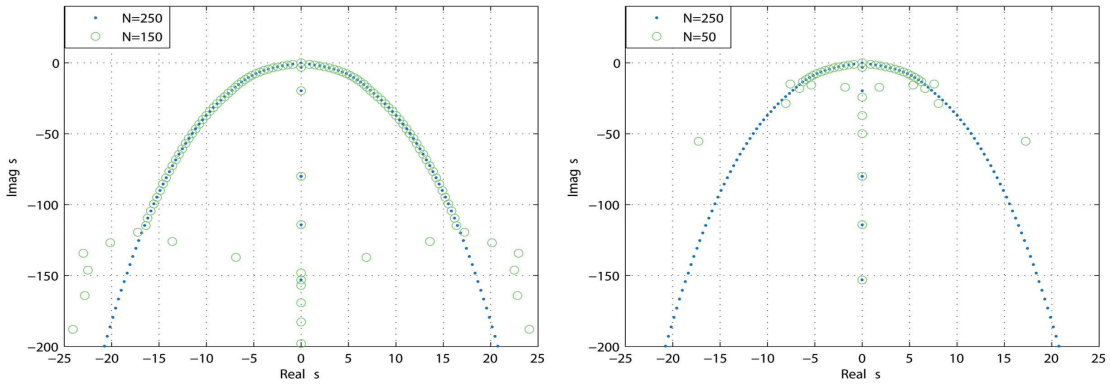

Figure 5.3: Hydrostatic case: *Discretization errors*, $\mathsf{K} = 2.5$, $Fe = 65$,$C = 10$, $M = 60$, $T = 110$

5.2.2 Neutral curves

The neutral curve shows the values of k, M, T and Fe for whose the system is unstable. In the EHD hydrostatic case the *principle of exchange of instabilities* is assumed to be valid [25]. This principle assumes that the transition from stability to instability occurs when the least stable eigenvalue becomes a positive pure imaginary number. The spectrum confirms this assumption. Keeping in mind this, it can be shown that the dimensionless ionic mobility has no effect on the neutral curve behavior.
Mathematically, assuming the critical eigenvalue null, the system (5.1) does not depends on M

$$\begin{cases} \left[\frac{1}{T}(D_2 - \mathsf{k}^2)^2\right]\hat{v} - \left[\mathsf{k}^2\Phi_0'(D_2 - \mathsf{k}^2) - \mathsf{k}^2\Phi_0'''\right]\hat{\phi} = 0, \\ \left[(\Phi_0'''D_1 + 2\Phi_0''(D_2 - \mathsf{k}^2) + \Phi_0'(D_3 - \mathsf{k}^2 D_1)) + \frac{1}{Fe}(D_2 - \mathsf{k}^2)^2\right]\hat{\phi} - \Phi_0'''\hat{v} = 0. \end{cases}$$

Physically, since $M = \tau_K/\tau_{EI}$ and no inertial processes are present in the base flow, one can assume that the M parameter does not make sense in this kind of problem and therefore the solution does not depend on it.
The neutral curve in Figure 5.4 confirms the assumption above, while the case studied in [25] has been considered as a benchmark case [C] in order to test the numerical code.

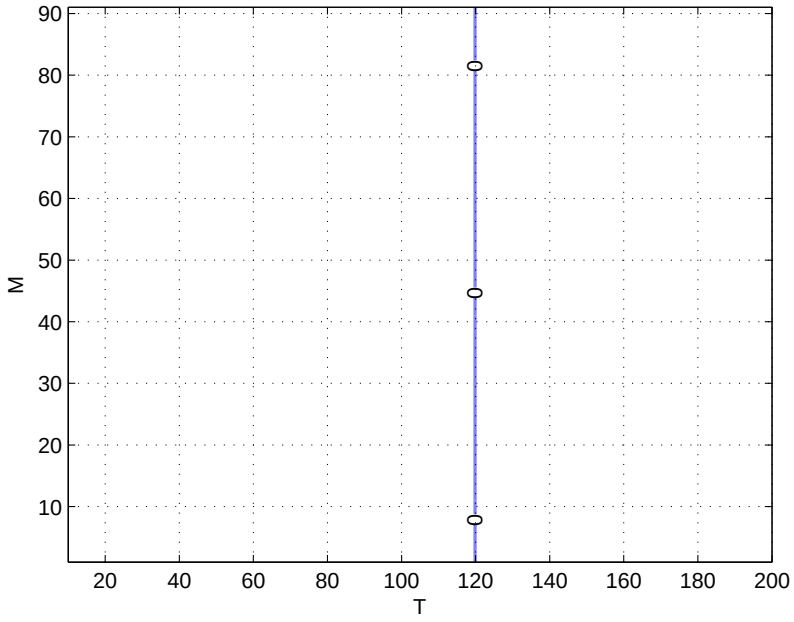

Figure 5.4: Hydrostatic Case: *Neutral curve*, Effect of M, $N = 150$, $k = 2$, $Fe = 65$, $C = 10$

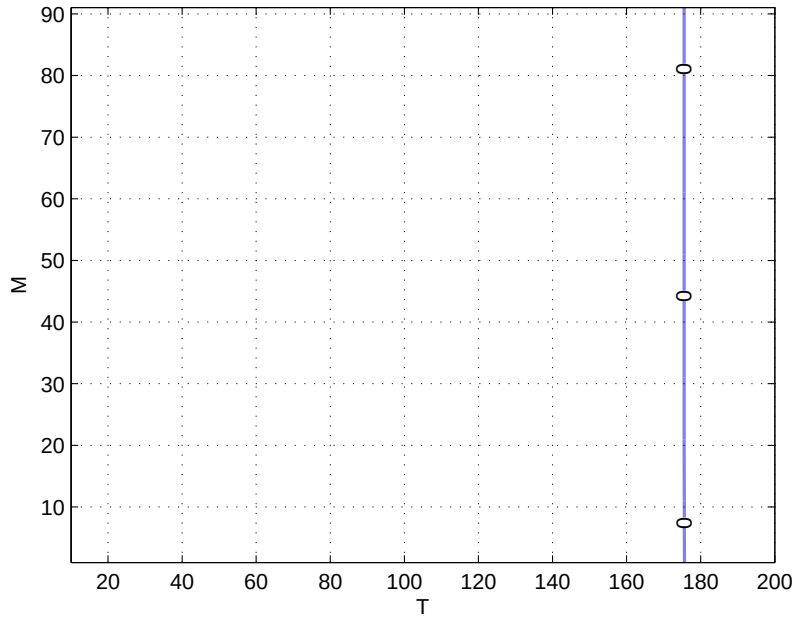

Figure 5.5: Hydrostatic case: *Neutral curve*, Effect of M, $N = 150$, $k = 2$, $Fe = 10^5$, $C = 10$

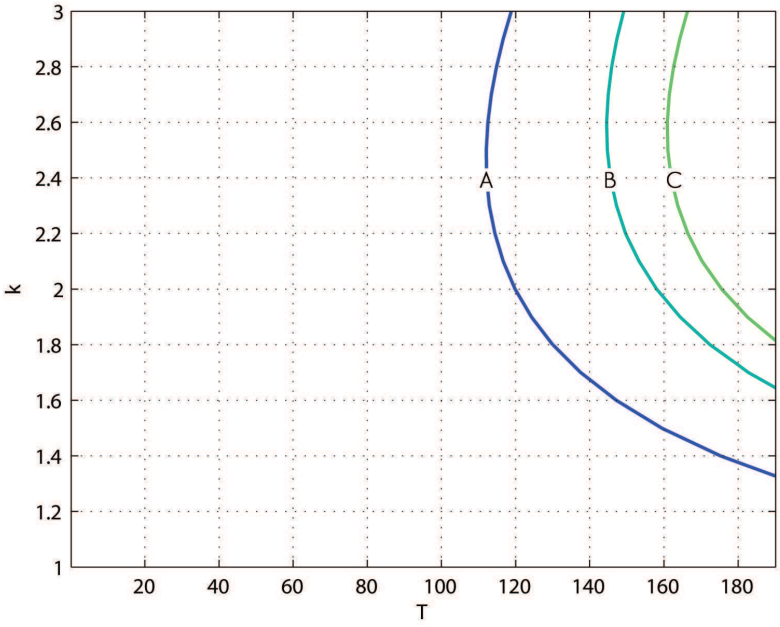

Figure 5.6: Hydrostatic case: *Neutral curve*, Effect of Fe. A for $Fe = 65$, B for $Fe = 10^3$, C for $Fe = 10^7$. Others parameters are $N = 150$, $C = 10$,$M = 60$

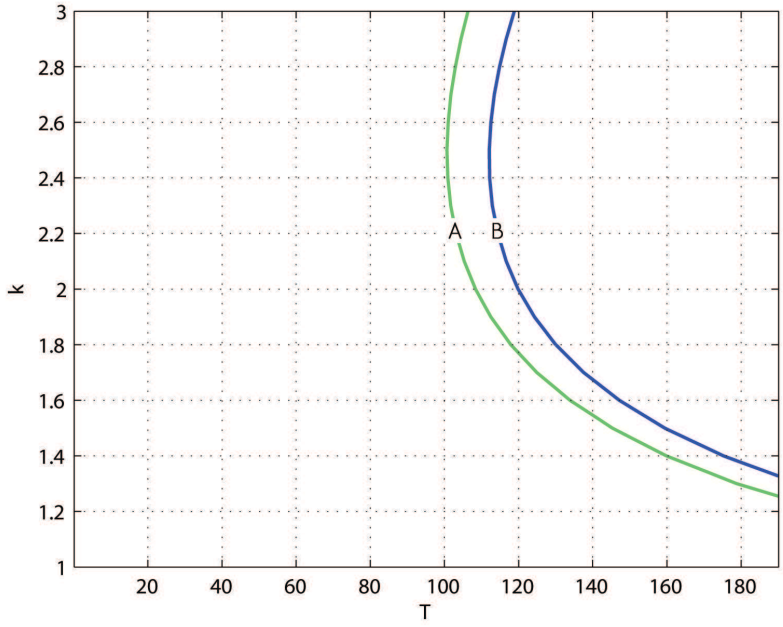

Figure 5.7: Hydrostatic case: *Neutral curve*, Effect of C. A for $C = 100$, B for $C = 10$, Others parameters are $N = 150$, $C = 10$,$M = 60$

Physically speaking, the charge density decreases from the emitter into insulating liquid and and this creates a potentially unstable situation. Considering a fluid portion under a velocity perturbation which conserves the charge, if it will be pushed toward collector it will be subjected to a greater Coulomb force than the fluid in its neighborhood which has a lower charge. Therefore it will have a tendency to continue to swing towards the collector. This tendency is counteracted by viscous drag and by relaxation of charge [6]. This excesses charge relaxation takes place via two physical mechanisms, i.e. molecular charge diffusion and Coulomb repulsion. Remarking that charge diffusion is destabilizing, the critical parameters become $T^\star \approx 112$, $\mathsf{K} \approx 2.5$ instead of $T^\star \approx 161$. Comparing the results of DNS by [8], the critical value of T is different, more precisely $T^\star \approx 132$. As the diffusive term tends to zero ($Fe \to \infty$) the behavior described in (D) is resumed. Experimental results confirm that $T^\star \approx 100$ in agreement with the ones above found.
As expressed in 3.3 there is a strong connection between the effect of C and the presence of the charge diffusivity. More $Fe \to 0$, or $C \to \infty$, more the *charge boundary layer* thickness decreases and so the diffusivity becomes important.

5.3 Non modal stability

The non modal analysis figures out a weak transient growth shown in Figure 5.8. The model has been reduced using the eigenmodes projection. The energy similitude of the original system and the reduced one has been demonstrated [21] for the critical case represented by the black point in Figure 5.8. In the same figure the grey area on the spectrum is the unstable part of the imaginary plane while in the $Gmax(t)$ convergence graph represents the *numerically spurious eigenmodes* which are neglected. In order to extract them a simple comparison between the spectra computed with $N = 300$ has been done.

5.3.1 Max growth

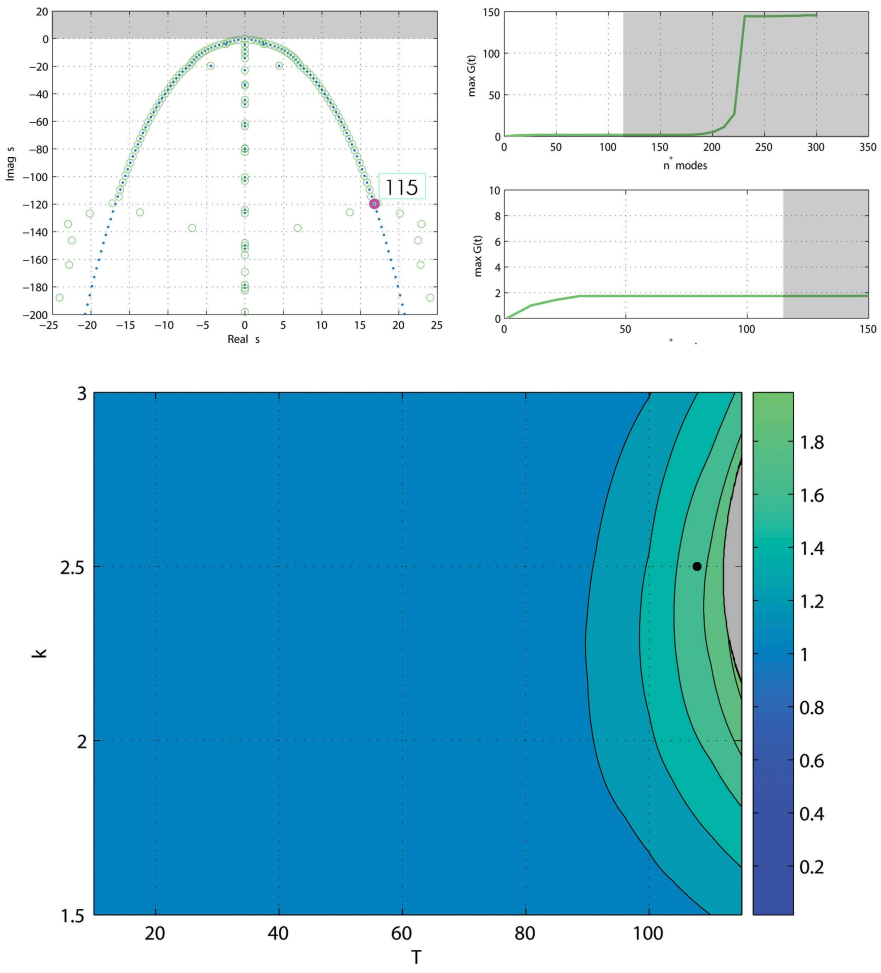

Figure 5.8: Hydrostatic case: *Max Growth*.$N = 150$, $Fe = 65$,$C = 10$, $M = 60$

5.3.2 Max growth rate

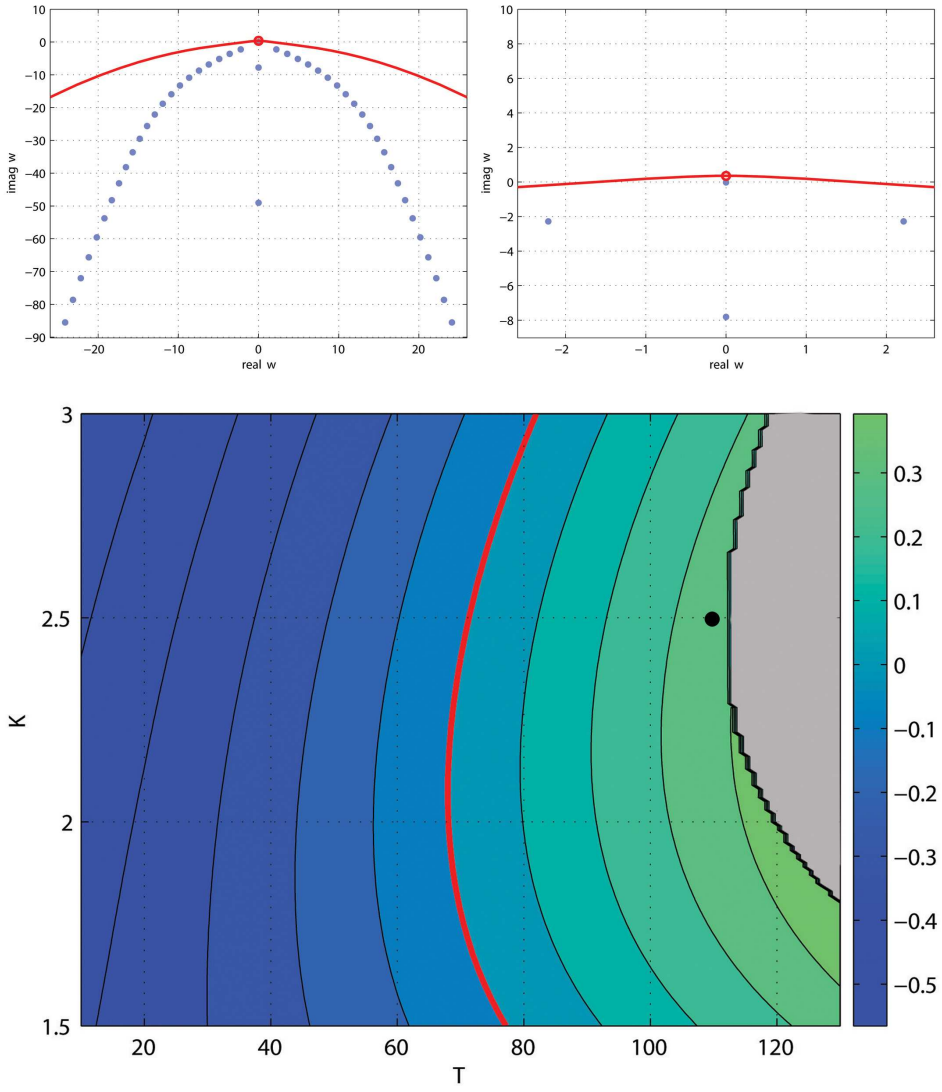

Figure 5.9: Hydrostatic case: *max growth rate*.$N = 150$, $Fe = 65$,$C = 10$, $M = 60$

5.3.3 Transient growth neutral curve

The black line in Figure (5.1) separates the area of asymptotic growth (dark grey) from the area of asymptotic decay (colored). The no growth rate curve (red line) defines the area of transient growth, but asymptotic decay (colored), from the area of no transient growth (light grey). The well-known critical $T^{\star} \approx 112$ can be easily determined from the graph. The largest T below which the initial perturbation energy for two-dimensional disturbances decays monotonically is given by $T^{\star}_{energy} \approx 65$.

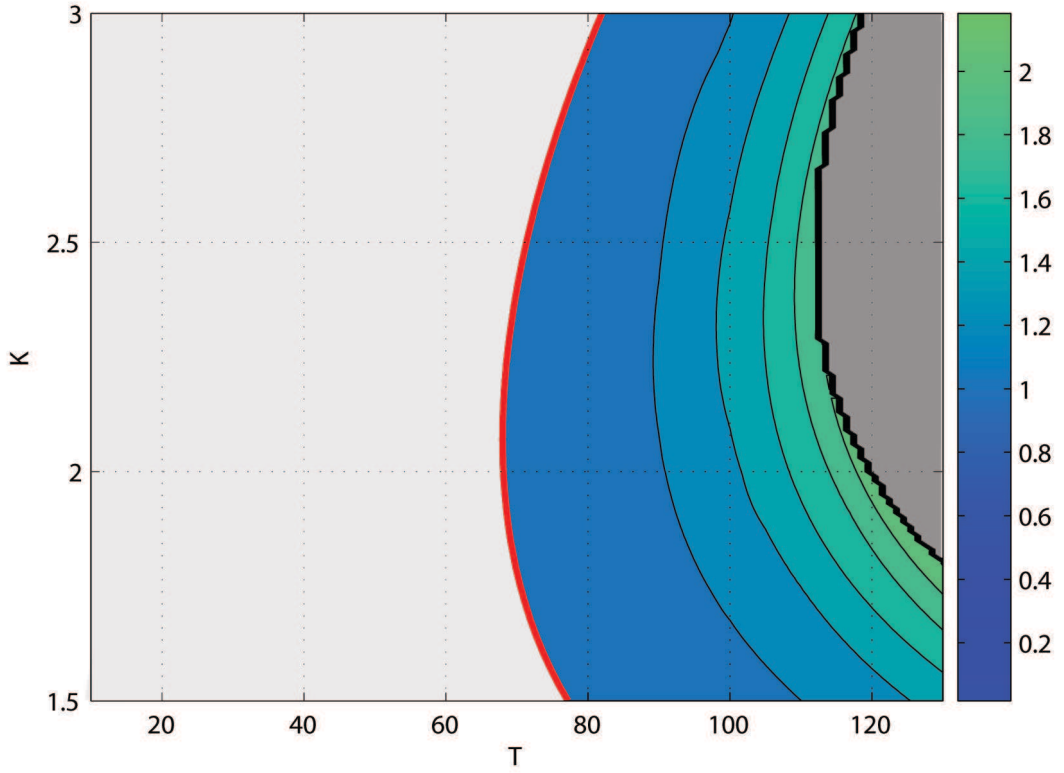

Figure 5.10: Hydrostatic case: *Neutral curves.*$N = 150$, $Fe = 65$,$C = 10$, $M = 60$

5.3.4 Optimal disturbance

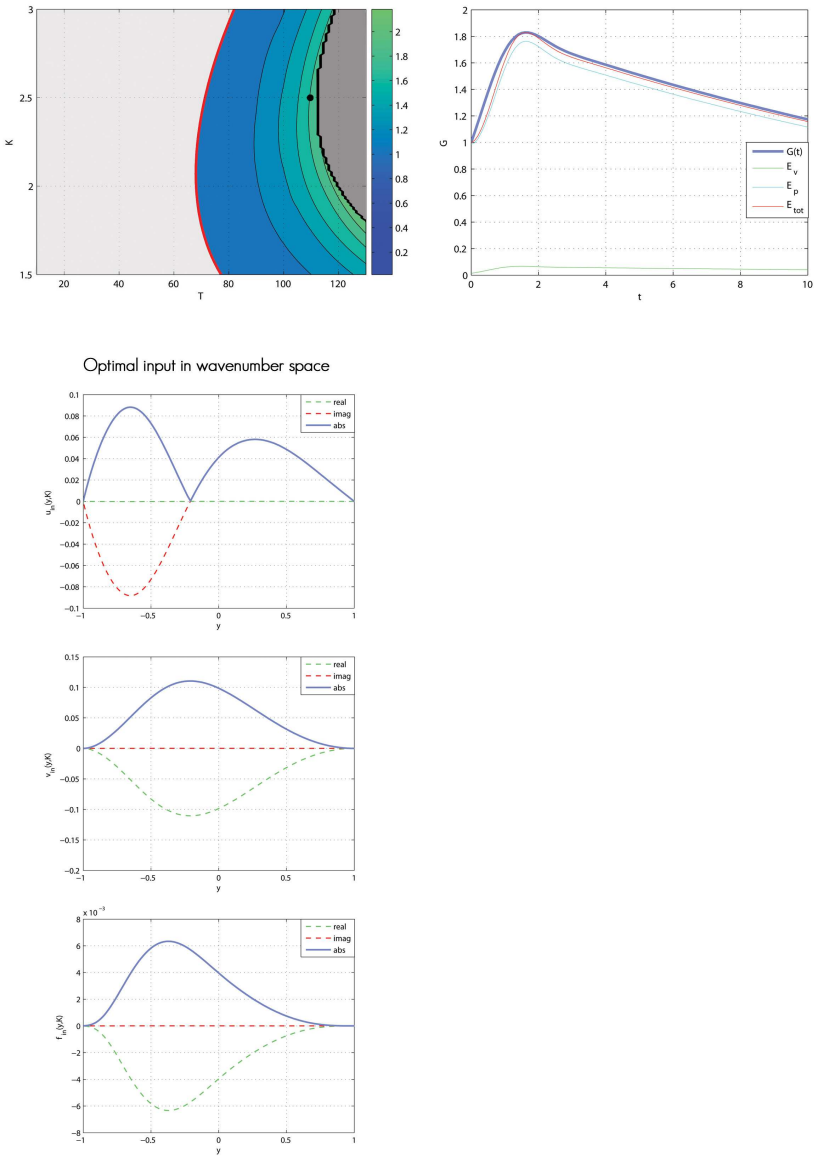

Figure 5.11: Hydrostatic case: *Optimal disturbance.*$N = 150$, $Fe = 65$,$C = 10$, $M = 60$, $T = 102$,$\mathsf{K} = 2.5$

5.3.5 Forced flow

Figure 5.12 displays the maximum response to a harmonic forcing. As in the simple Poiseuille flow without streamwise disturbances, we observe a pronounced peak for steady forcing, which means that the *pseudo-resonance* phenomena occurred. Increasing T the maximum response increases (Figure5.13).

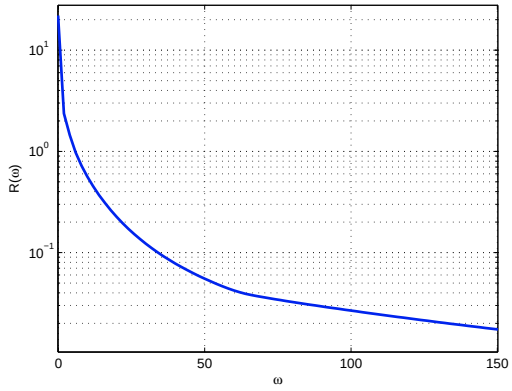

Figure 5.12: Hydrostatic case: *Forced flow*. Forced response. $N = 150$, $Fe = 65$,$C = 10$, $M = 60$, $T = 110$,$\mathsf{K} = 2.5$

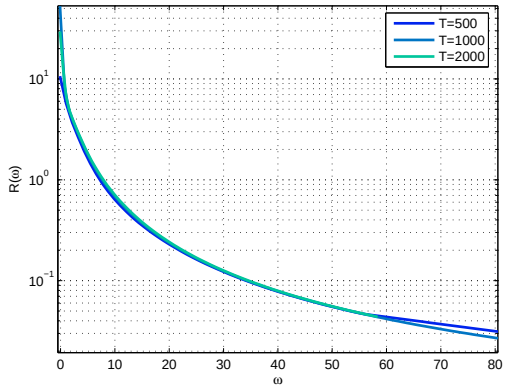

Figure 5.13: Hydrostatic case: *Forced flow*. Effect of T. $C = 10$, $Fe = 65$, $M = 60$, $N = 150$, $\mathsf{K} = 2.5$

5.4 Remarks

Through the use of electric timescales, it is shown that dimensionless ionic mobility has no physical meaning for the hydrostatic problem. Since the only way to achieved a M independence in (5.1) is to assume valid the instability exchange principle, the results confirm its applicability.
For the first time, the effect of charge diffusivity has been investigated in the hydrostatic EHD problem. Considering only its order of magnitude, it has been often suggested that its effect is relevant only close to the walls. However, thanks to a more precise identification of modes, and defining the system's total energy, we have proven that the energetically important modes are almost entirely *wall modes*. Thus using a simplified model which neglects diffusion, one does not take into account the most important energetic effects.
Sustaining the conclusion written above the most of the energetic content is related to the charge perturbation as shown in Figure 5.11.
As expected, the charge diffusivity shows a strong destabilizing character yielding a $T^\star$ lower than 30% compared to literature results.
Despite the outcome, the modal analysis results are not yet comparable with the experimental ones.
Using the non modal analysis tool, we prove that the system shows a mild non modal behavior where the maximum transient growth usually occurs in one dimensionless time unit. This could explain the earlier transition observed during the experiments.
A new and more useful curve which considers both transient and asymptotic fate of the modes has been in Figure 5.10.
Finally Figure 5.12 displays the maximum response to a harmonic forcing. As in the simple Poiseuille flow without streamwise disturbances, we observe a pronounced peak for steady forcing, which means *pseudo-resonance* occurred.

CHAPTER 6

POISEUILLE CASE

6.1 Equations

A laminar forced flow with direction normal to the electric field does not alter the unstable character of the charge distribution, but it modifies the turbulence structure of electroconvection which exists without forced flow [7].
Poiseuille's plane flow is unstable to infinitesimal disturbances for a critical Reynolds number of about 5772. This instability, which has a pure hydrodynamic nature, is due to the transfer of energy via Reynolds stresses. The superposition of a unipolar injection to this forced flow should enhance the instability of the liquid layer.
Complete set shown below

$$
\begin{cases}
\omega(D_2-\mathsf{k}^2)\hat{v} = \left[\alpha U_0(D_2-\mathsf{k}^2) - \alpha U_0'' - \dfrac{1}{i}\dfrac{M^2}{T}(D_2-\mathsf{k}^2)^2\right]\hat{v} + \\
\quad + \dfrac{1}{i}M^2\left[\mathsf{k}^2\Phi_0'(D_2-\mathsf{k}^2) - \mathsf{k}^2\Phi_0'''\right]\hat{\phi}, \\
\omega\hat{\eta} = \left[U_0'\beta\right]\hat{v} + \left[\alpha U_0 - \dfrac{1}{i}\dfrac{M^2}{T}(D_2-\mathsf{k}^2)\right]\hat{\eta}, \\
\omega(D_2-\mathsf{k}^2)\hat{\phi} = \Phi_0'''\hat{v} + \\
\quad + \left[\alpha U_0(D_2-\mathsf{k}^2) - \dfrac{1}{i}(\Phi_0'''D_1 + 2\Phi_0''(D_2-\mathsf{k}^2) + \Phi_0'(D_3-\mathsf{k}^2D_1)) - \dfrac{1}{i}\dfrac{1}{Fe}(D_2-\mathsf{k}^2)^2\right]\hat{\phi}.
\end{cases}
\tag{6.1}
$$

with its suitable homogeneous boundary conditions

6.1.1 Squire's theorem

Since the presence of the electric field has no effect on the squire equation [1], *Dumped Squire Modes theorem* can be applied. Therefore the solutions to the vorticity equation are always dumped, i.e. $\omega_I < 0$ for all α, β, and Re. The dimensionless parameters, explicitly, do not play any role in the charge continuity then the Squire's

[1] Normal vorticity equation

transformation can be applied just to v equation. Considering $\omega = \alpha c$, 3D and 2D cases are (6.2) and (6.3) respectively

$$c(D_2-\mathsf{k}^2)\hat{v} = \left[U_0(D_2-\mathsf{k}^2) - U_0'' - \frac{1}{i}\frac{M^2}{\alpha T}(D_2-\mathsf{k}^2)^2\right]\hat{v} + \frac{1}{i}\frac{M^2}{\alpha}\left[\mathsf{k}^2\Phi_0'(D_2-\mathsf{k}^2) - \mathsf{k}^2\Phi_0'''\right]\hat{\phi} \tag{6.2}$$

$$c(D_2-\mathsf{k}^2)\hat{v} = \left[U_0(D_2-\mathsf{k}^2) - U_0'' - \frac{1}{i}\frac{M_{2D}^2}{\alpha_{2D}T_{2D}}(D_2-\mathsf{k}^2)^2\right]\hat{v} + \frac{1}{i}\frac{M_{2D}^2}{\alpha_{2D}}\left[\mathsf{k}^2\Phi_0'(D_2-\mathsf{k}^2) - \mathsf{k}^2\Phi_0'''\right]\hat{\phi} \tag{6.3}$$

Comparing these two equations, it is evident that they have identical solutions if the following relations hold

$$\alpha_{2D}^2 = \mathsf{K}^2,$$

$$\frac{1}{\alpha_{2D}}\frac{M_{2D}^2}{T_{2D}} = \frac{1}{\alpha}\frac{M^2}{T},$$

$$\frac{M_{2D}^2}{\alpha_{2D}} = \frac{M^2}{\alpha}.$$

from which it follow

$$\alpha_{2D} = \sqrt{\alpha^2\beta^2},$$

$$M^{2D} = \sqrt{\frac{\mathsf{K}}{\alpha}}M,$$

$$T_{2D} = T.$$

Thus parallel shear flows become unstable to two dimensional wavelike perturbation at a critical values that are smaller than any value for which unstable three-dimensional perturbation exists.

6.1.2 Streamwise invariant perturbation

When $\alpha = 0$ the perturbation equation (3.19) simplifies to (6.4) that has stability properties similar to the hydrostatic case. In fact, the velocity base flow drops out from v and ϕ equation and the squire modes are always stable [17].

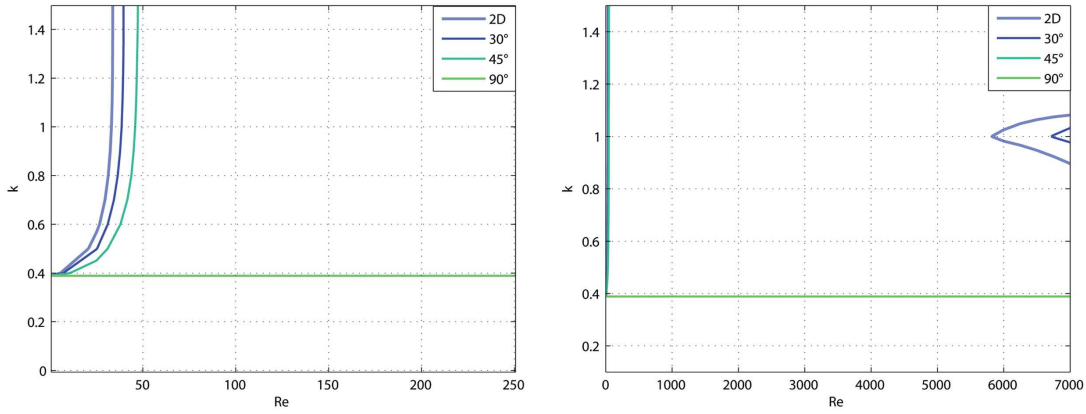

Figure 6.1: Poiseuille case: *Neutral Curve*. Squire's Theorem. $N = 150$, $Fe = 200$,$C = 10$, $M = 60$, $T = 2000$

$$
\begin{cases}
\omega(D_2 - \mathsf{k}^2)\hat{v} = \left[-\dfrac{1}{i}\dfrac{M^2}{T}(D_2 - \mathsf{k}^2)^2\right]\hat{v} + \\
\quad + \dfrac{1}{i}M^2\left[\mathsf{k}^2\Phi_0'(D_2 - \mathsf{k}^2) - \mathsf{k}^2\Phi_0'''\right]\hat{\phi}, \\
\omega\hat{\eta} = \left[U_0'\beta\right]\hat{v} + \left[\alpha U_0 - \dfrac{1}{i}\dfrac{M^2}{T}(D_2 - \mathsf{k}^2)\right]\hat{\eta}, \\
\omega(D_2 - \mathsf{k}^2)\hat{\phi} = \Phi_0'''\hat{v} + \\
\quad + \left[-\dfrac{1}{i}(\Phi_0'''D_1 + 2\Phi_0''(D_2 - \mathsf{k}^2) + \Phi_0'(D_3 - \mathsf{k}^2 D_1)) - \dfrac{1}{i}\dfrac{1}{Fe}(D_2 - \mathsf{k}^2)^2\right]\hat{\phi}.
\end{cases}
\tag{6.4}
$$

6.2 Modal stability

According to [7], neglecting charge diffusion, one can distinguish two different unstable regions. For a low-enough Reynolds number the EHD instability mechanism could be dominant, while for large values the destabilizing inertial mechanism would be the most important, with the electrical forces playing a minor role.
From [7] theoretical results, it may be stated that at low Reynolds numbers, the growth rate of transverse perturbations is strongly inhibited by the forced flow, whereas the perturbations to longitudinal wavenumbers β are unaffected.

6.2.1 Low Reynolds regime, discrete spectrum

In this subsection the eigenvalues of the equation set (3.19) will be shown. As already explained the system's behavior could be splitted in two regimes, low and high Reynolds. At low Reynolds numbers, and low values of M, it is still possible to recognize the three branches structure presented in the hydrostatic case (Figure E.2). However, with the cross flow, the eigenvalues on branch Z increased their real part and a new *cluster* path (related to the squire equation) appears (Figure 6.5). The branches and the G cluster, tend to fall down as Fe decreases (Figure E.3). Along with C's growth, the cluster tends to widen slightly (Figure E.5).
We can notice that M plays a fundamental role making the spectrum highly chaotic as it increases.

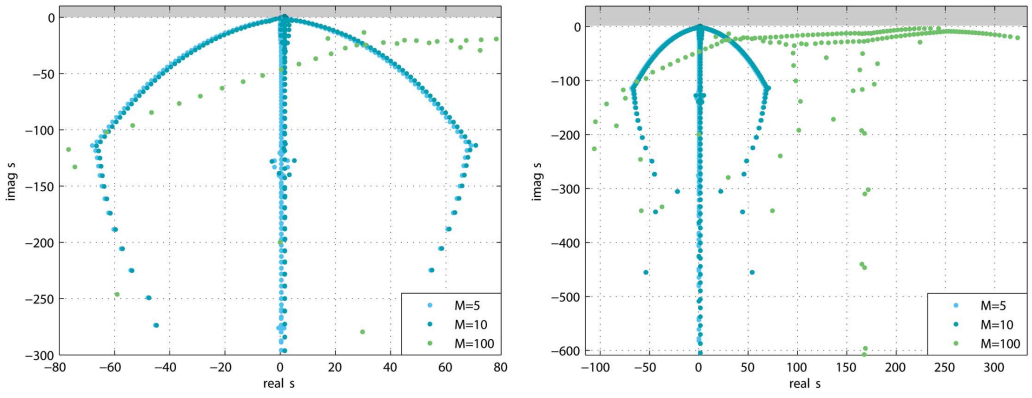

Figure 6.2: Poiseuille case: *Discrete Spectrum.* Effect of M. $\alpha = 1$, $\beta = 0$, $C = 50$, $Fe = 200$, $N = 150$, $Re = 50$, $T = 2000$

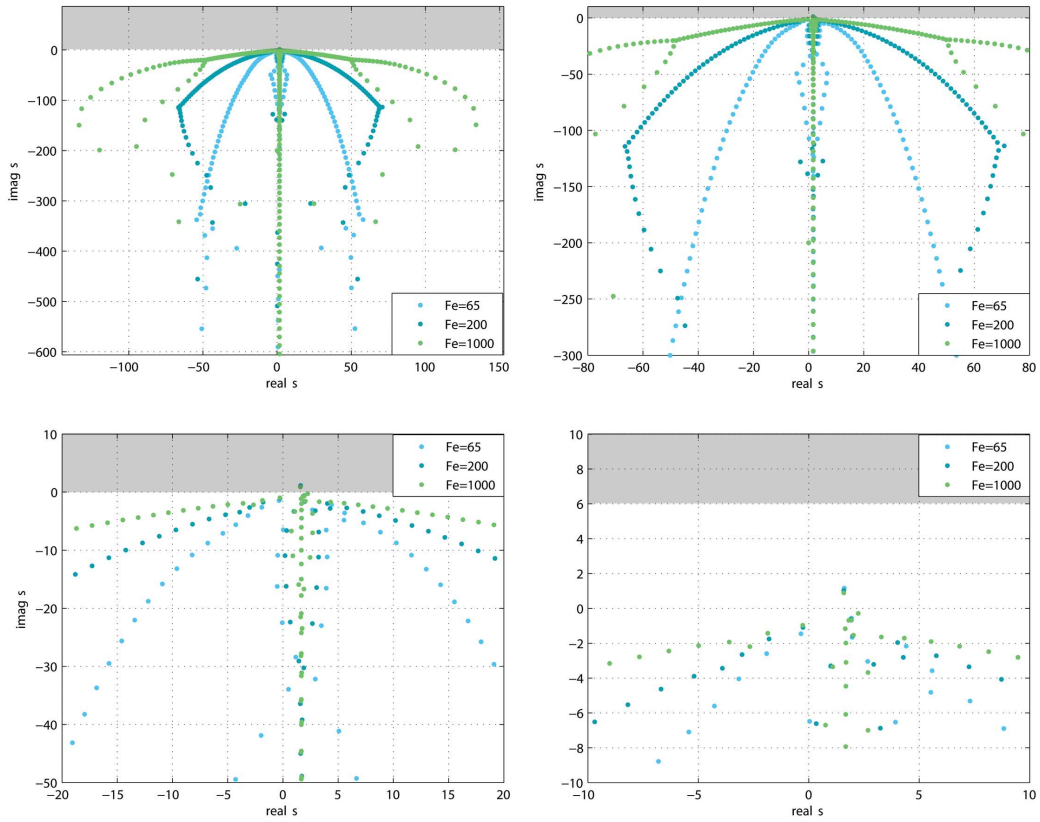

Figure 6.3: Poiseuille case: *Discrete Spectrum*. Effect of Fe. $\alpha = 1$, $\beta = 0$, $C = 50$, $M = 5$, $N = 150$, $Re = 50$, $T = 2000$

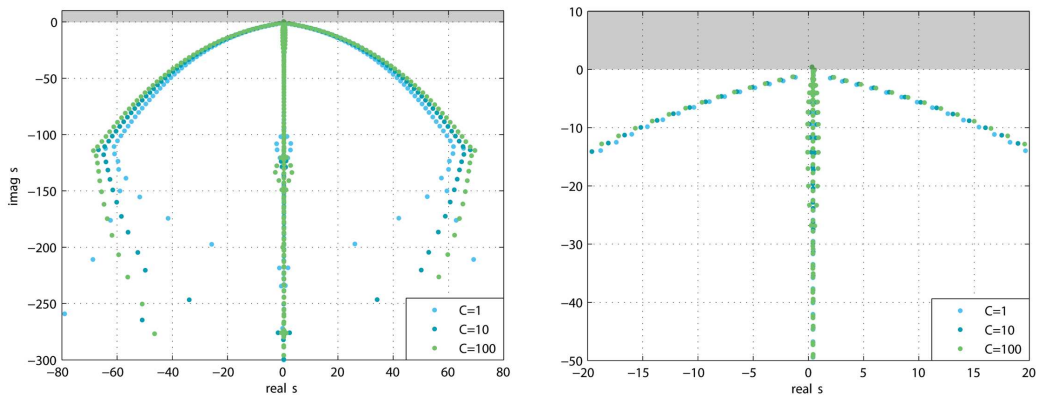

Figure 6.4: Poiseuille case: *Discrete Spectrum*. Effect of C. $\alpha = 1$, $\beta = 0$, $Fe = 200$, $M = 5$, $N = 150$, $Re = 5000$, $T = 2000$

Choosing a case not affected by resolution errors, a new identification of modes is possible. From Figure 6.6 to Figure 6.9 sample shapes of the eigenfunctions are shown. As in the hydrostatic case the least stable mode is a center-mode. While going downhill of the A-B branches, the eigenfunctions tends to become 2D wall-modes, this means that $w(y, \mathsf{K})$ velocity is null. Contrarily, Z's eigenfunctions show a purely 3D structure which means that there are no $\phi(y, \mathsf{K})$, $u(y, \mathsf{K})$ and $v(y, \mathsf{K})$ but only an high oscillating $w(y, \mathsf{K})$. The oscillation tends to increase as $\sigma_I \to -\infty$. On the G cluster, the modes neither center modes nor wall modes. They show a 2D high oscillating structure with the same asymptotic behavior of the Z branch.

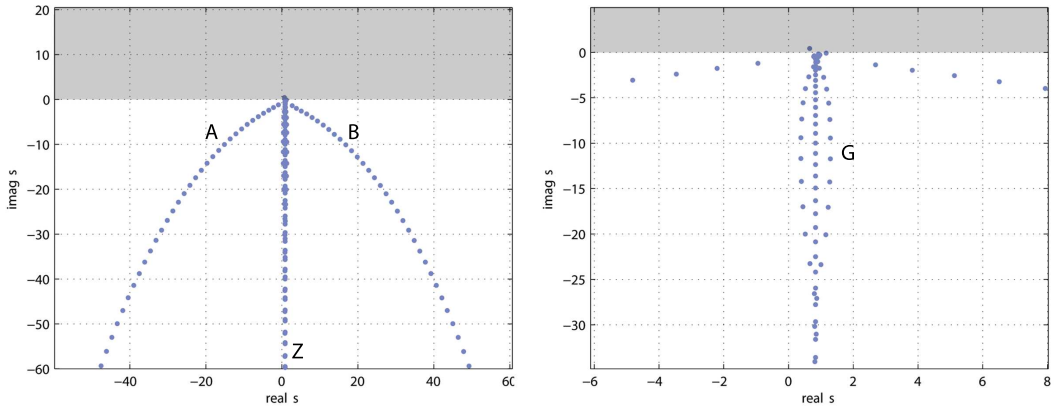

Figure 6.5: Poiseuille case:*Modal Identification.* Spectrum. $\alpha = 1$, $\beta = 0$, $C = 50$, $Fe = 200$, $M = 5$, $N = 250$, $Re = 100$, $T = 2000$

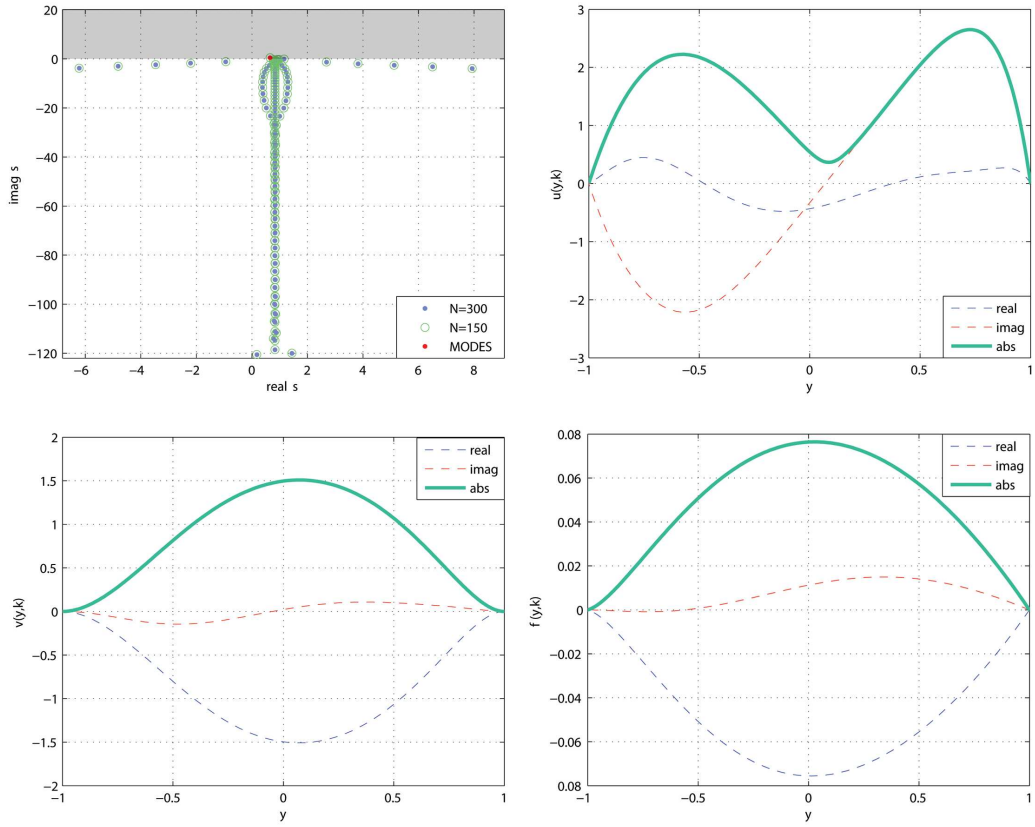

Figure 6.6: Poiseuille case:*Modal Identification.* Least stable mode. $\alpha = 1$, $\beta = 0$, $C = 50$, $Fe = 200$, $M = 5$, $N = 250$, $Re = 100$, $T = 2000$

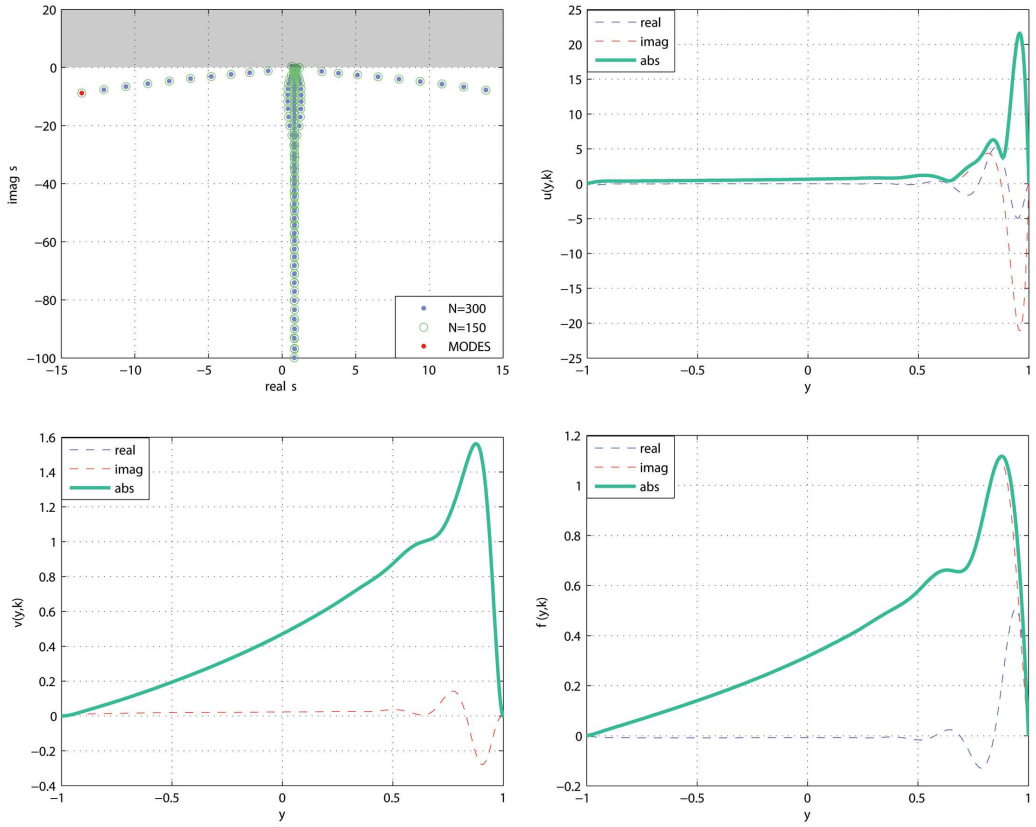

Figure 6.7: Poiseuille case:*Modal Identification.* A-B branches. $\alpha = 1$, $\beta = 0$, $C = 50$, $Fe = 200$, $M = 5$, $N = 250$, $Re = 100$, $T = 2000$

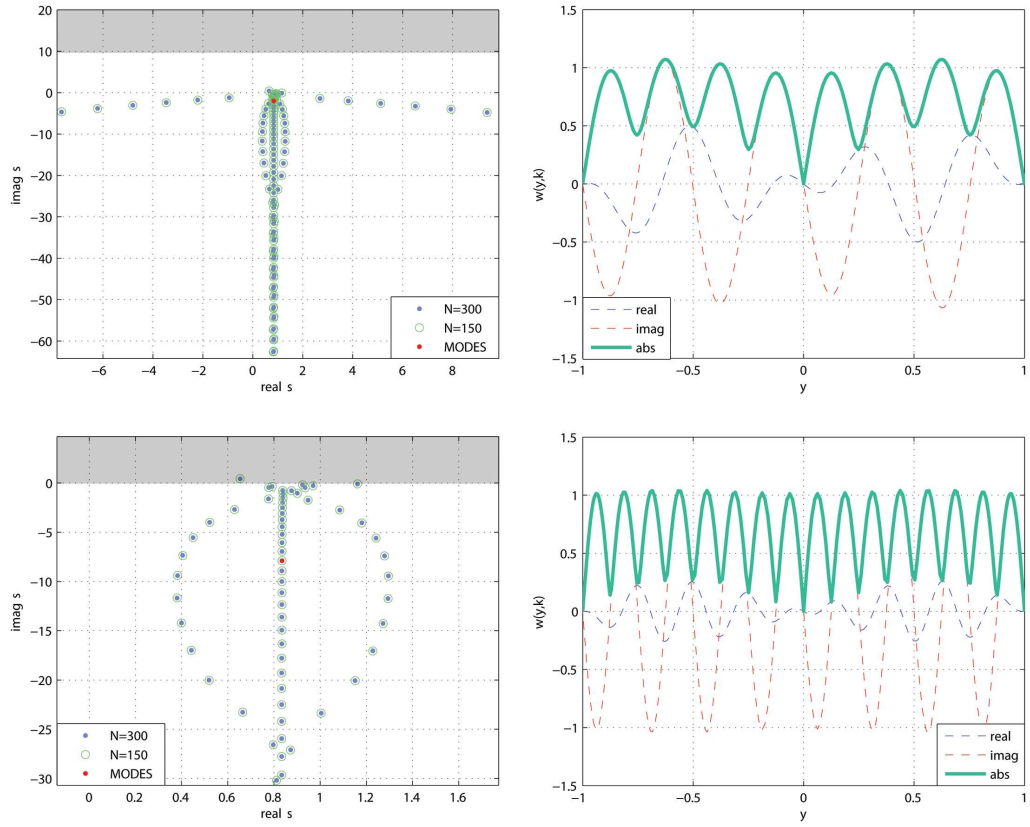

Figure 6.8: Poiseuille case:*Modal Identification.* Z branch. $\alpha = 1$, $\beta = 0$, $C = 50$, $Fe = 200$, $M = 5$, $N = 250$, $Re = 100$, $T = 2000$

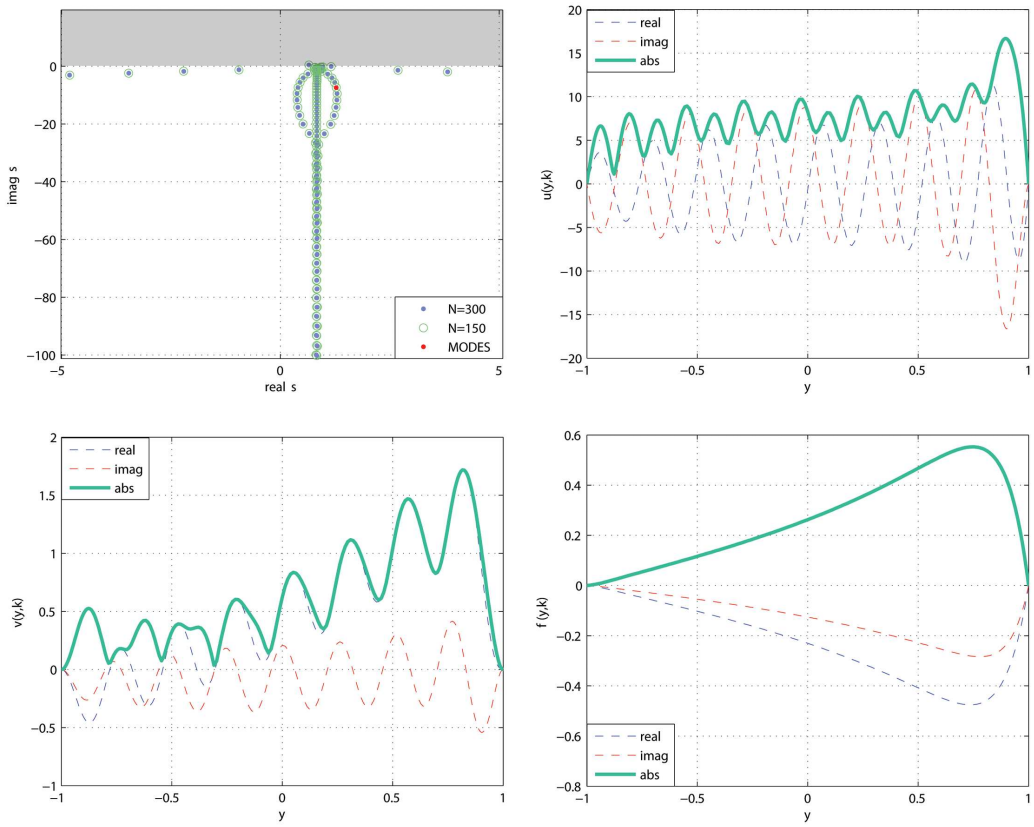

Figure 6.9: Poiseuille case:*Modal Identification.* G cluster. $\alpha = 1$, $\beta = 0$, $C = 50$, $Fe = 200$, $M = 5$, $N = 250$, $Re = 100$, $T = 2000$

Resolution error

As previously explained spectrum errors are introduced by insufficient resolution of numerical scheme. In Figure 6.10 the leak of resolution is strictly linked to the parameter M. If in the hydrostatic case, M played a secondary role, adding the cross flow, would turn it into a very important parameter. Matter of fact as M increases the spectrum tends to be chaotic, and the high mode's oscillations makes the spectral method unable to resolve the eigenvalue problem.
In physical terms a small M value corresponds to a low electric potential- fluid kinetic energy transforming efficiency liquid. In the other words if M has a high value, the electric potential interferes with the velocity oscillation making the non linear interference relevant. A better understanding of this phenomena is necessary.
In Figure 6.11 Fe determines relevantly the choice of N. If one considers Fe's physical values no critical layer phenomenons occur. Last but not least the injection parameter C has to be chosen higher than one (Figure 6.12). Contrarily, the autonomous injection assumption tends to fail and the numerical model does not represent the physical system.

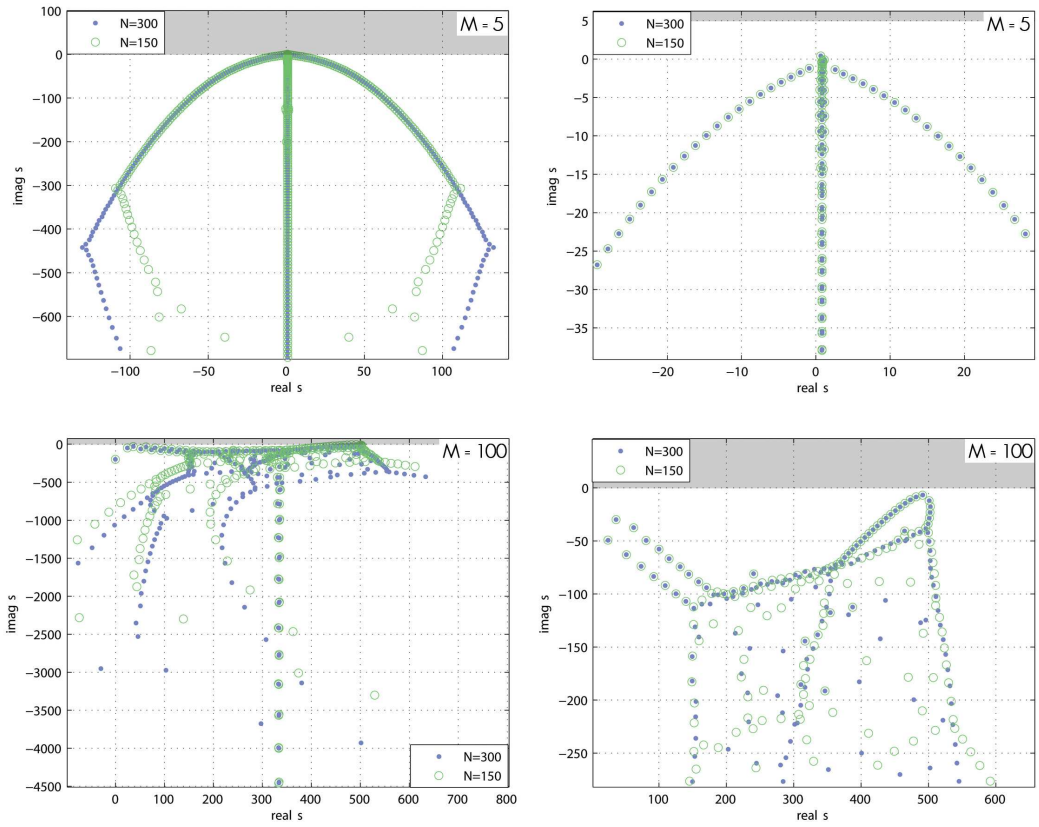

Figure 6.10: Poiseuille case: *Resolution.* Effect of M. $\alpha = 1$, $\beta = 0$, $C = 50$, $Fe = 200$, $Re = 100$, $T = 2000$

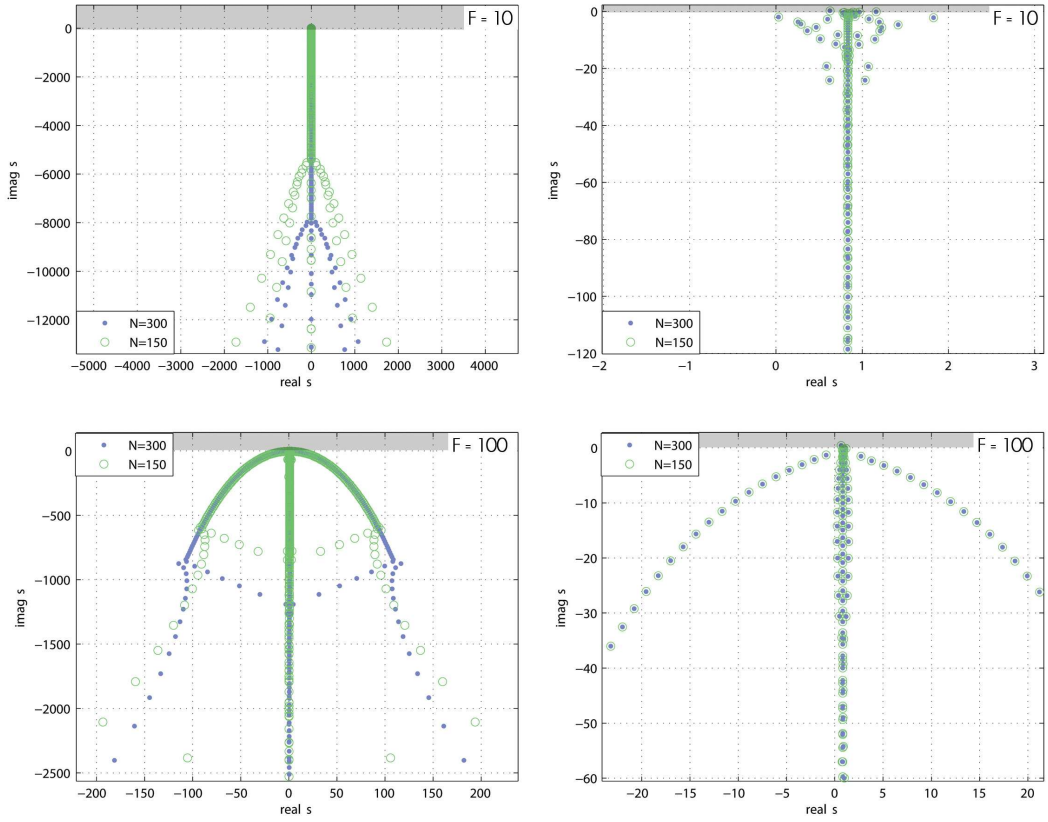

Figure 6.11: Poiseuille case:*Resolution.* Effect of F. $\alpha = 1$, $\beta = 0$, $C = 50$, $M = 5$, $Re = 100$, $T = 2000$

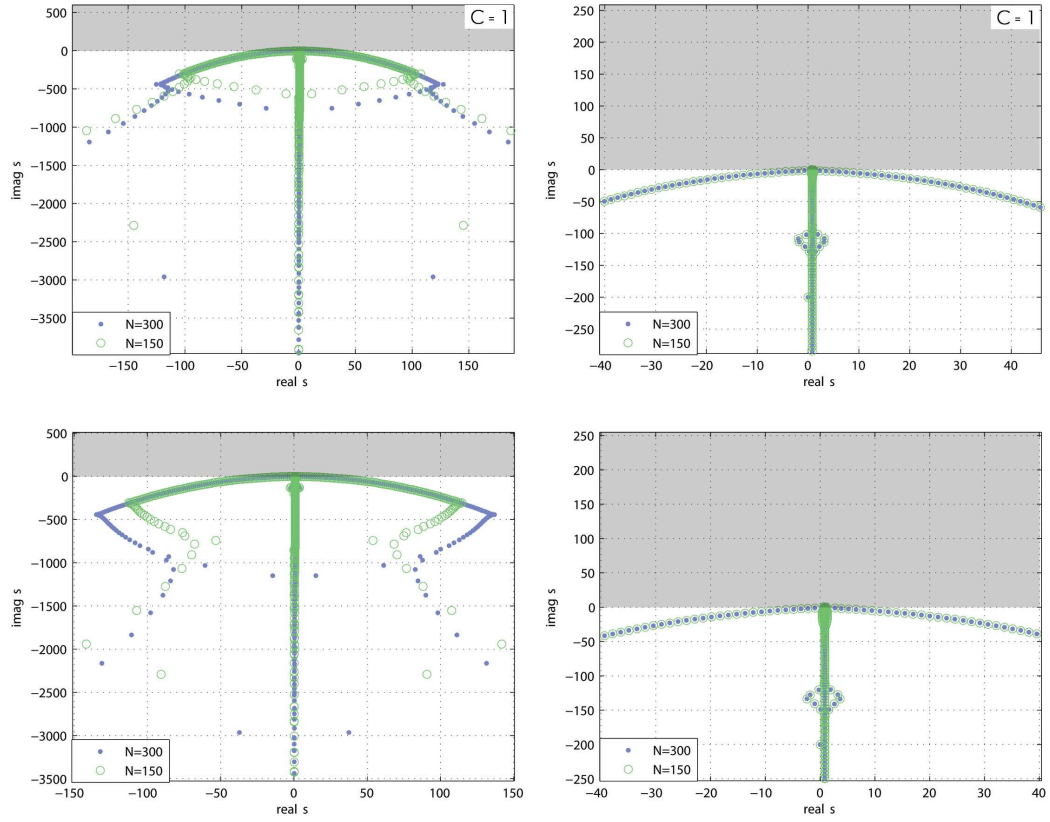

Figure 6.12: Poiseuille case: *Resolution.* Effect of C. $\alpha = 1$, $\beta = 0$, $Fe = 200$, $M = 5$, $Re = 100$, $T = 2000$

6.2.2 High Reynolds regime, discrete spectrum

As the Reynolds number increases, things get a bit more complicated. The Z branch tends to move from its original position ($\sigma_R = 0$) toward higher real values. The new path seems the classic Poiseuille Y spectrum combined with the parabolic branches A and B. Although at this Reynolds regime the transition is driven by fluid dynamics causes, the electrical parameters are still playing a key role. Therefore in Figure E.2 and E.3 the shape of the spectra presents important changes. The spectrum behavior is too chaotic to hazard any conclusion.

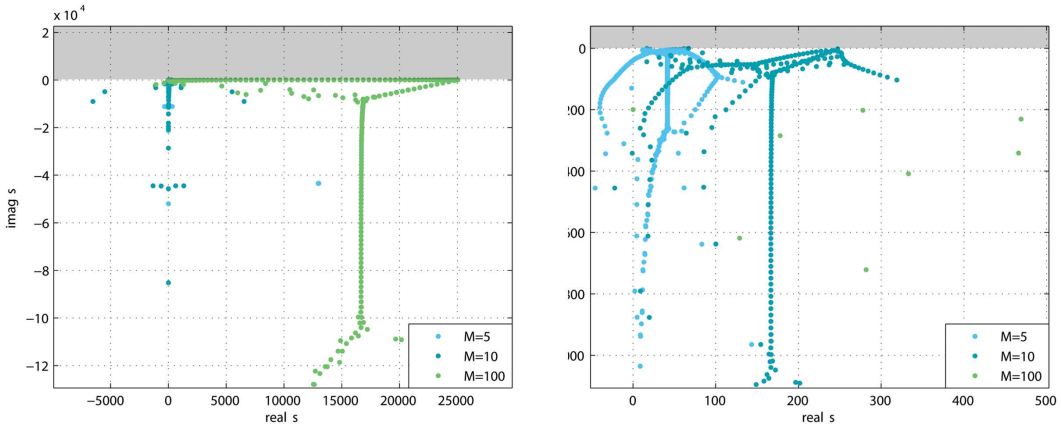

Figure 6.13: Poiseuille case: *Discrete Spectrum*. Effect of M. $\alpha = 1$, $\beta = 0$, $C = 50$, $Fe = 200$, $N = 150$, $Re = 5000$, $T = 2000$

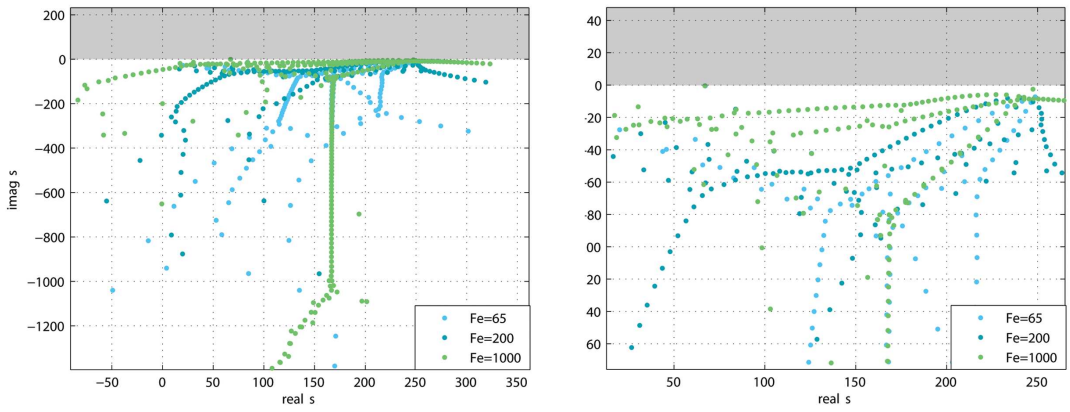

Figure 6.14: Poiseuille case: *Discrete Spectrum*. Effect of Fe. $\alpha = 1$, $\beta = 0$, $C = 50$, $N = 150$, $M = 5$, $Re = 5000$, $T = 2000$

Resolution error

Figure 6.15 recalls the undeniable role played by M within numerical solution. Regards the charge diffusivity, its effect is related to the charge distribution (6.16). If

diffusion tends to be null the charge density gradients will rise until they determine discontinuities, therefore bad resolution.
Contrarily if C respects the high injection assumption, it has a weak effect (Figure 6.17).

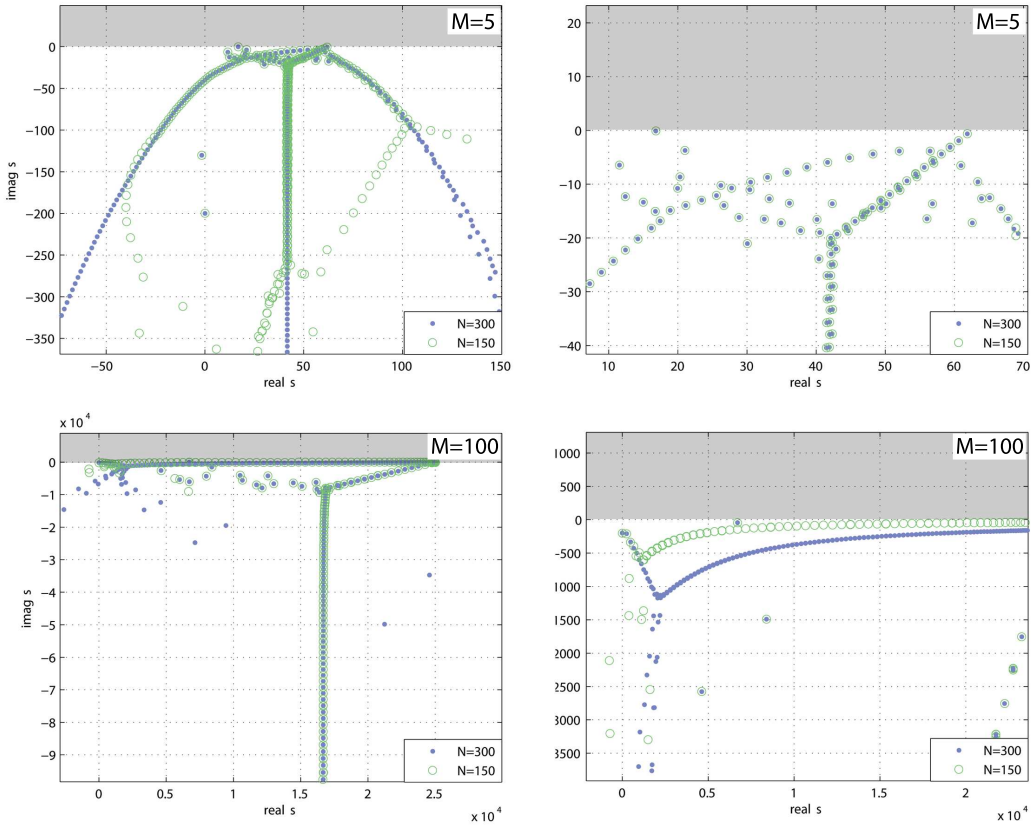

Figure 6.15: Poiseuille case: *Resolution at high Reynolds.* Effect of M. $\alpha = 1$, $\beta = 0$, $C = 50$, $Fe = 200$, $N = 250$, $Re = 5000$, $T = 2000$

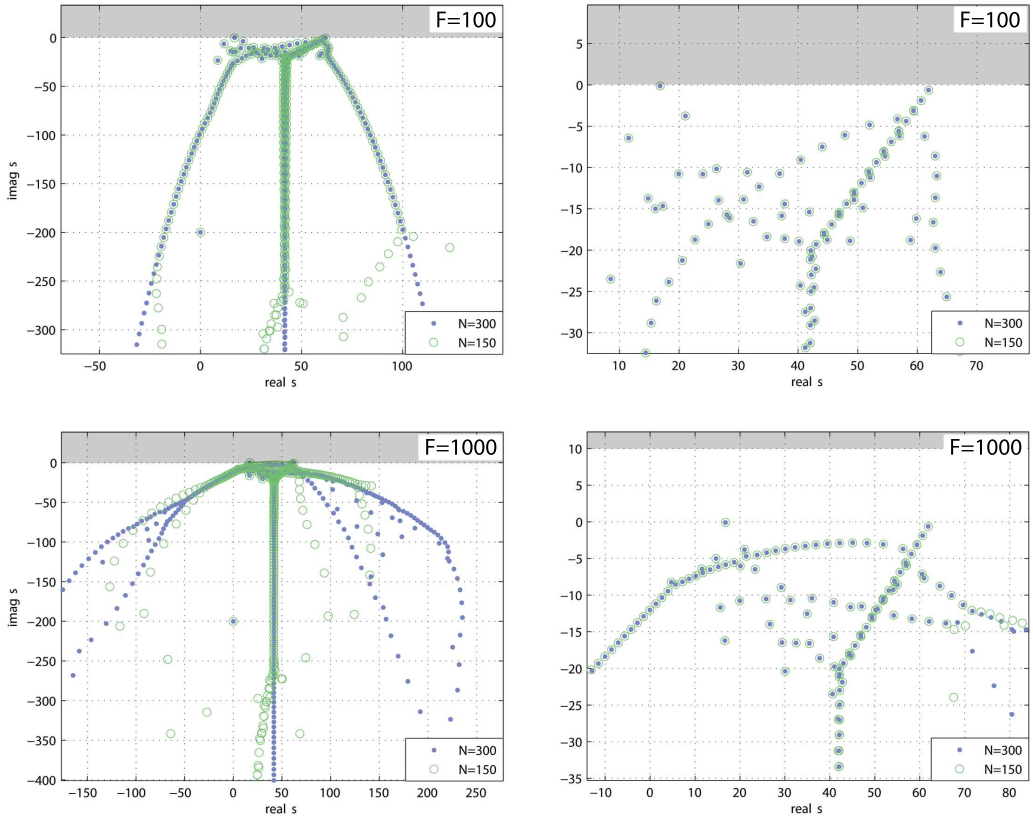

Figure 6.16: Poiseuille case:*Resolution at high Reynolds.* Effect of F. $\alpha = 1$, $\beta = 0$, $C = 50$, $M = 5$, $N = 250$, $Re = 5000$, $T = 2000$

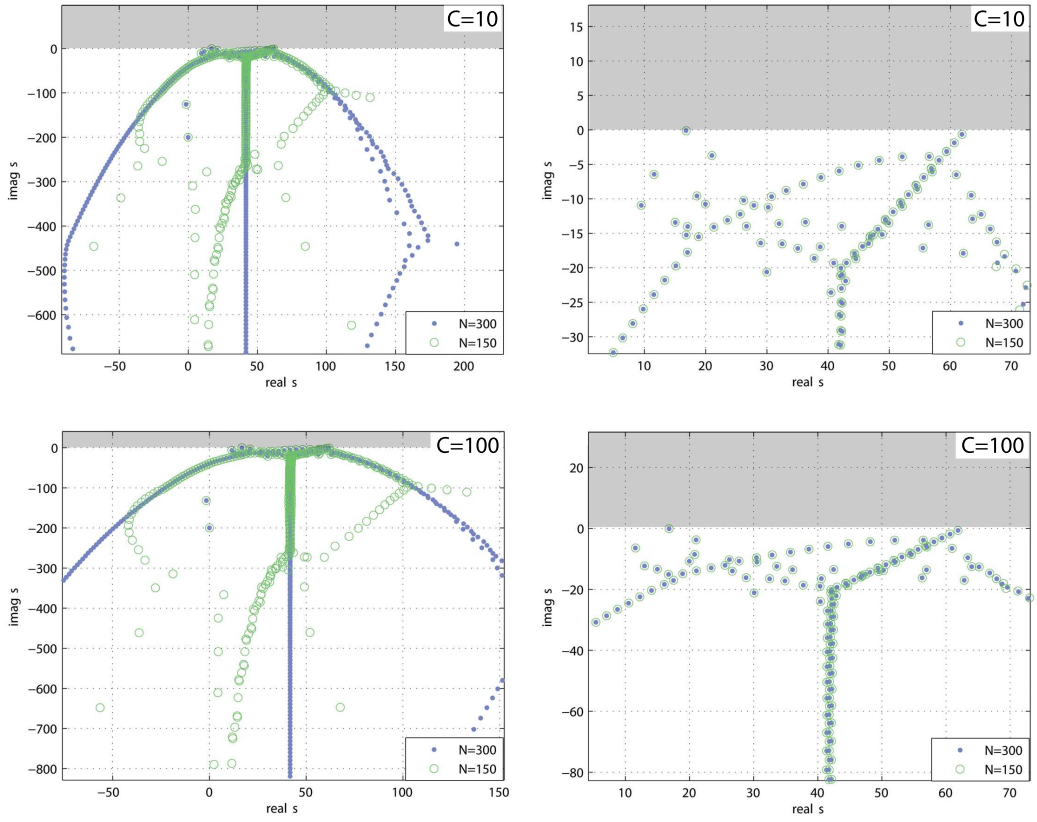

Figure 6.17: Poiseuille case: *Resolution at high Reynolds.* Effect of C. $\alpha = 1$, $\beta = 0$, $Fe = 200$, $M = 5$, $N = 250$, $Re = 5000$, $T = 2000$

6.2.3 Neutral curves

As suggested by [7], there are two critical regions. As shown in Figure 6.18, at low Reynolds number the cross flow tends to retard the EHD instabilities, while as Reynolds number increases, the effect of electrical disturbances and their parameters tend to be dominated by the velocity perturbations instabilities.

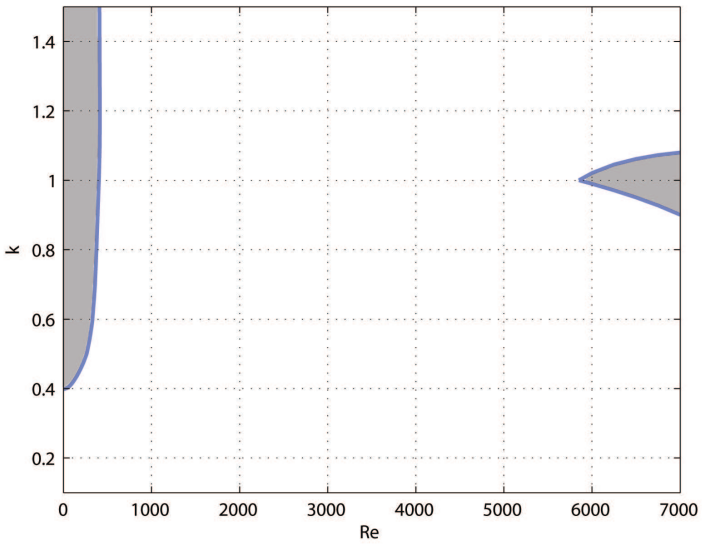

Figure 6.18: Poiseuille case: *Neutral Curve*. $\beta = 0$, $C = 50$, $Fe = 200$, $M = 5$, $N = 250$, $T = 2000$

Electric parameters effect

Form Figure 6.19 to Figure 6.22 the suggestion of [7] regard the strong influence of the fluid mechanics instabilities at high Reynolds number has been confirmed.

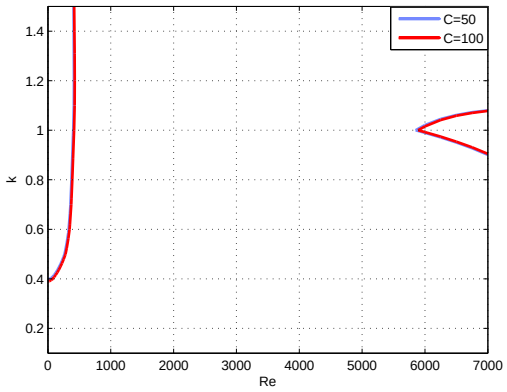

Figure 6.19: Poiseuille case: *Neutral Curve*. Effect of C. $\beta = 0$, $Fe = 200$, $M = 5$, $N = 250$, $T = 2000$

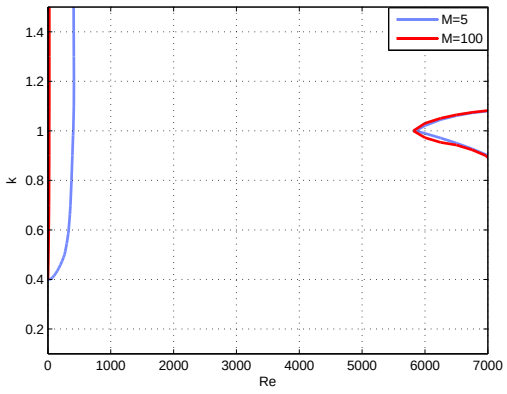

Figure 6.20: Poiseuille case: *Neutral Curve*. Effect of M. $\beta = 0$, $C = 50$, $Fe = 200$, $N = 250$, $T = 2000$

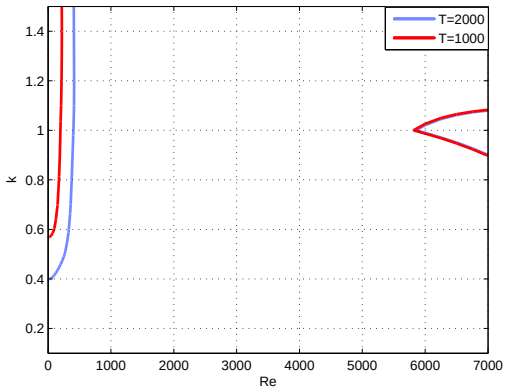

Figure 6.21: Poiseuille case: *Neutral Curve*. Effect of T.$\beta = 0$, $C = 50$, $Fe = 200$, $M = 5$, $N = 250$

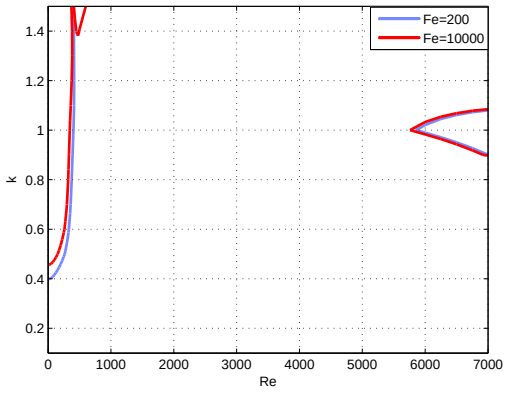

Figure 6.22: Poiseuille case: *Neutral Curve*. Effect of Fe. $\beta = 0$, $C = 50$, $M = 5$, $N = 250$, $T = 2000$

6.3 Non modal stability

The equation set has been reduced using the eigenmodes projection. The energy similitude of the original system and the reduced one has been demonstrated in two critical cases. The grey area on the spectrum is the unstable part of the imaginary plane while in the $Gmax(t)$ convergence graph it represents the numerically *spurious eigenmodes* which have to be neglected. In order to define them, a simple comparison with the spectra computed with $N = 300$ has been done. Usually, for ($M \leq 10$), a good resolution is achieved and the maximum modes's number that could be taken is $N_{max} \approx 200$. Unfortunately the transient growth needs an higher number of modes to converge as Reynolds number and α increase (from Figures 6.23 to Figure 6.24). Thus as shown in Figure 6.25 and Figure 6.28 the non-modal stability analysis allows us to affirm that the EHD system is capable to support transient growth of incresing intensity as the Reynolds number increases.

6.3.1 Max growth

2D Case

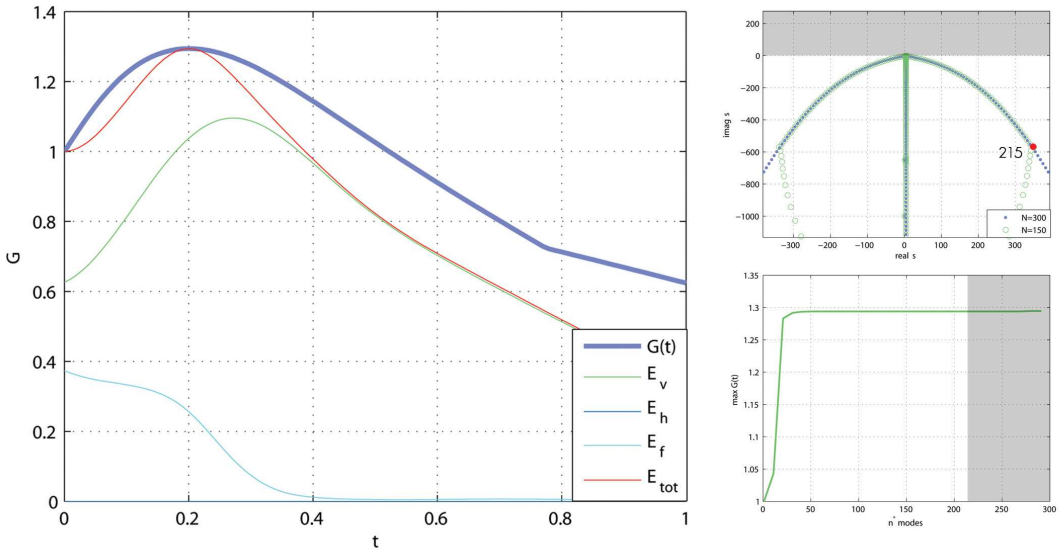

Figure 6.23: Poiseuille case: *Max Growth*. Case A, convergence. $\alpha = 0.2$, $\beta = 0$, $C = 50$, $Fe = 200$, $M = 5$, $N = 150$, $Re = 500$, $T = 2000$

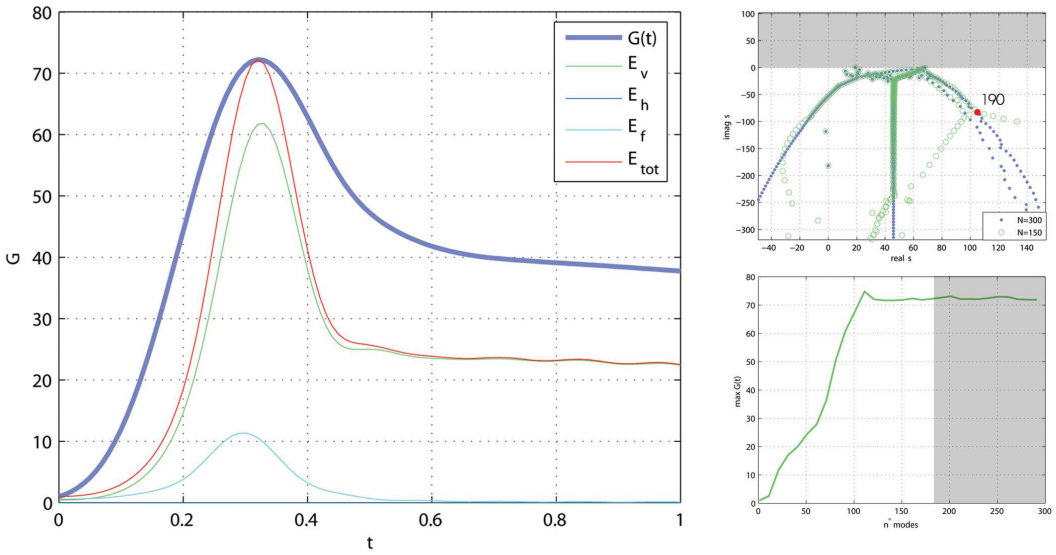

Figure 6.24: Poiseuille case: *Max Growth*. Case B, convergence. $\alpha = 0.2$, $\beta = 0$, $C = 50$, $Fe = 200$, $M = 5$, $N = 150$, $Re = 500$, $T = 2000$

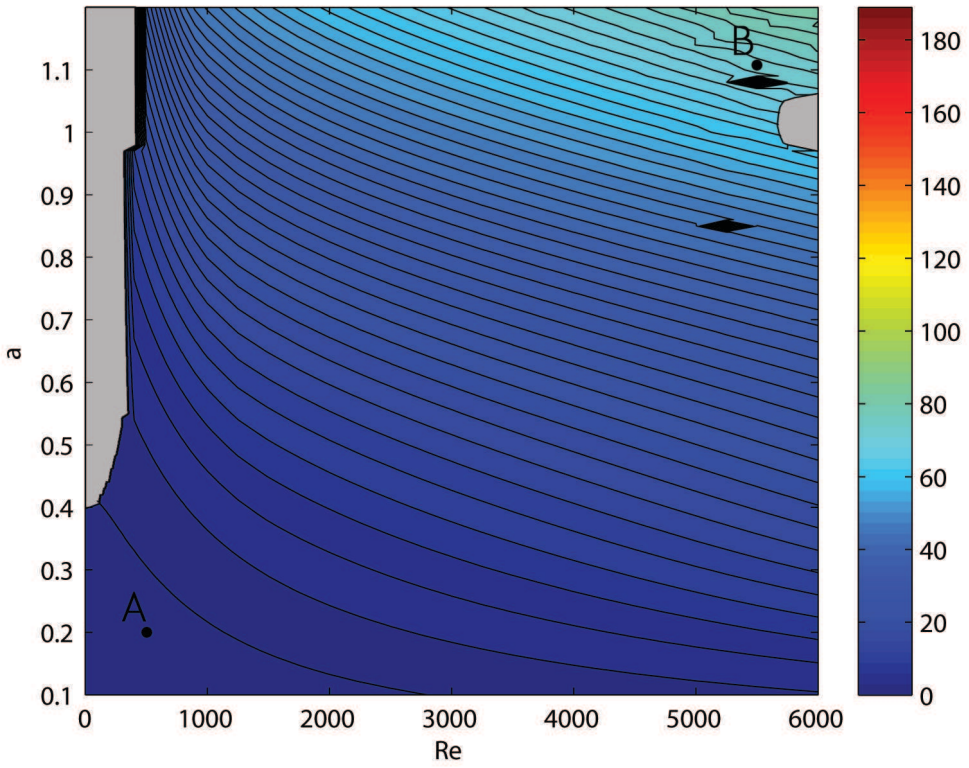

Figure 6.25: Poiseuille case: *Max Growth*. Reynolds-α behavior. $N = 150$, $M = 5$,,$Fe = 200$ $C = 50$, $T = 2000$

Streamwise independence

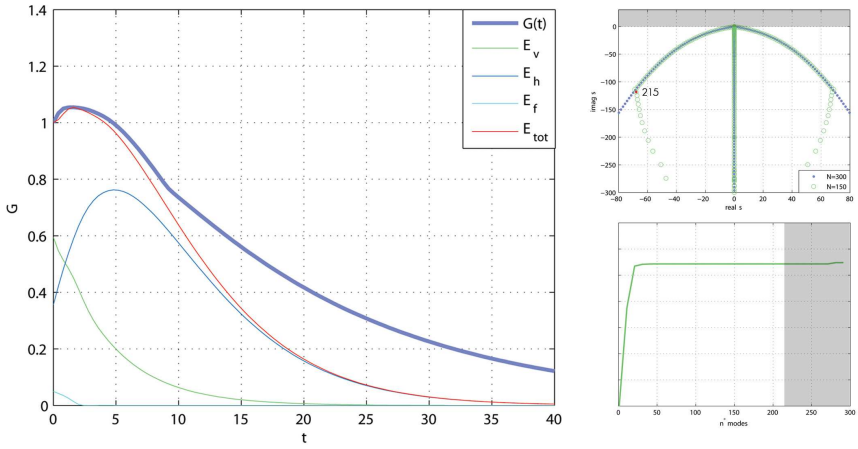

Figure 6.26: Poiseuille case: *Max Growth* $\alpha = 0$. Case A. $\alpha = 0$, $\beta = 0.1$, $C = 50$, $Fe = 200$, $M = 5$, $N = 150$, $Re = 600$, $T = 2000$

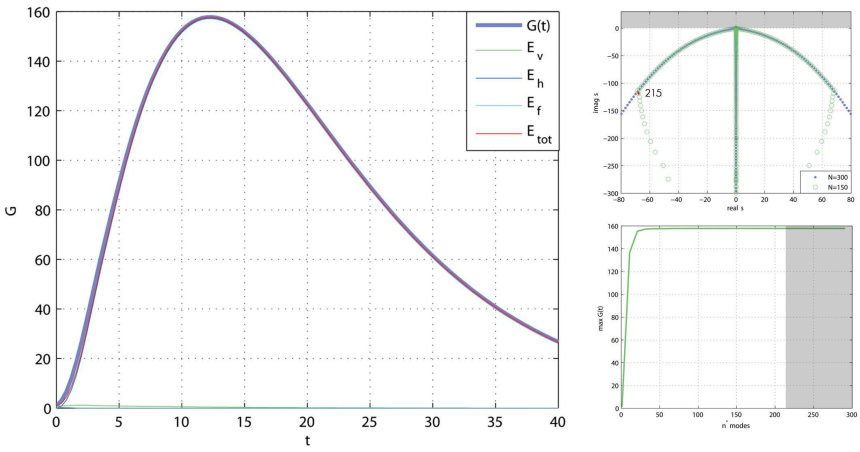

Figure 6.27: Poiseuille case: *Max Growth* $\alpha = 0$. Case B. $C = 50$, $Fe = 200$, $M = 5$, $N = 150$, $T = 2000$

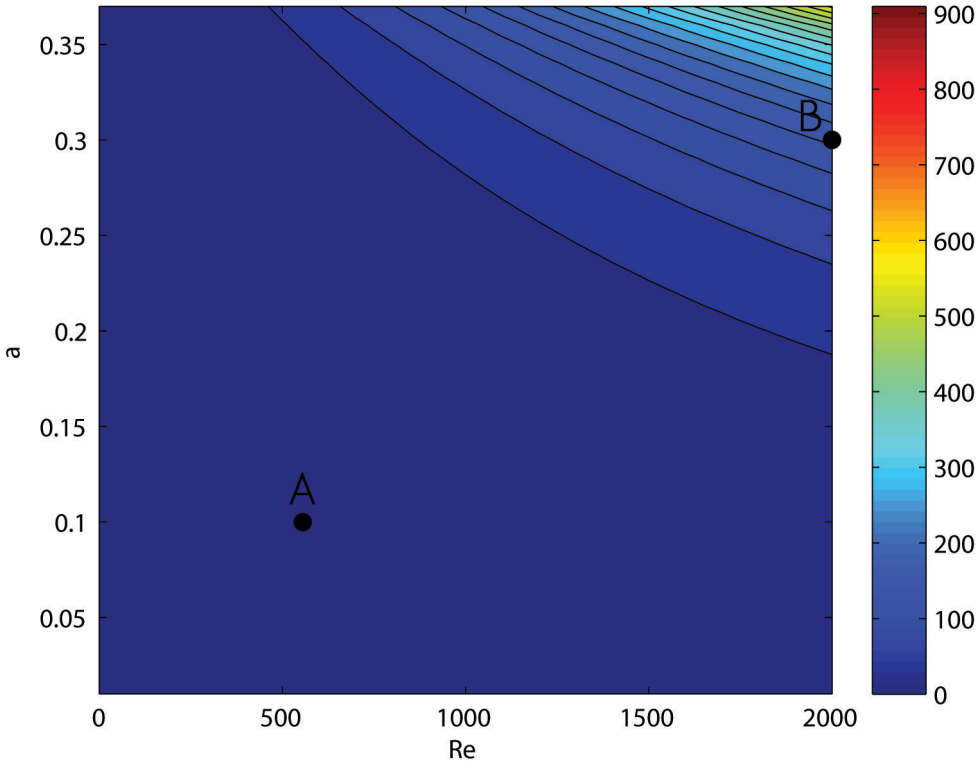

Figure 6.28: Poiseuille case: *Max Growth* $\alpha = 0$. Reynolds-β behavior. $C = 50$, $Fe = 200$, $M = 5$, $N = 150$, $T = 2000$

6.3.2 Max growth rate

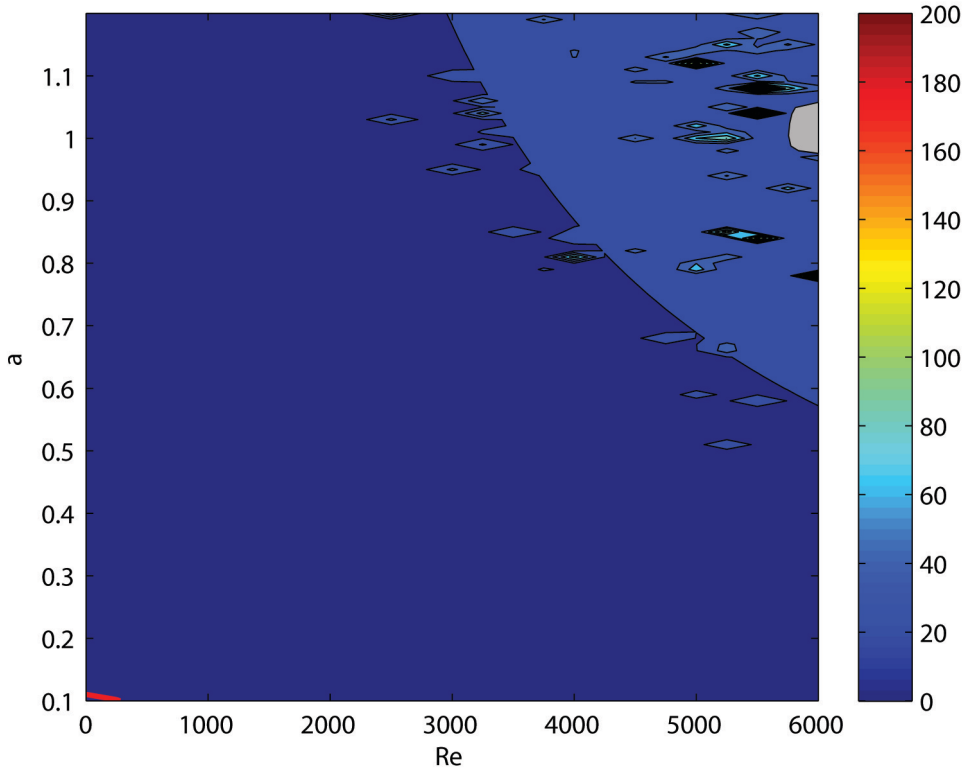

Figure 6.29: Poiseuille case: *Max Growth*. Reynolds-α behavior. $\beta = 0$, $C = 50$, $Fe = 200$, $M = 5$, $N = 150$, $T = 2000$

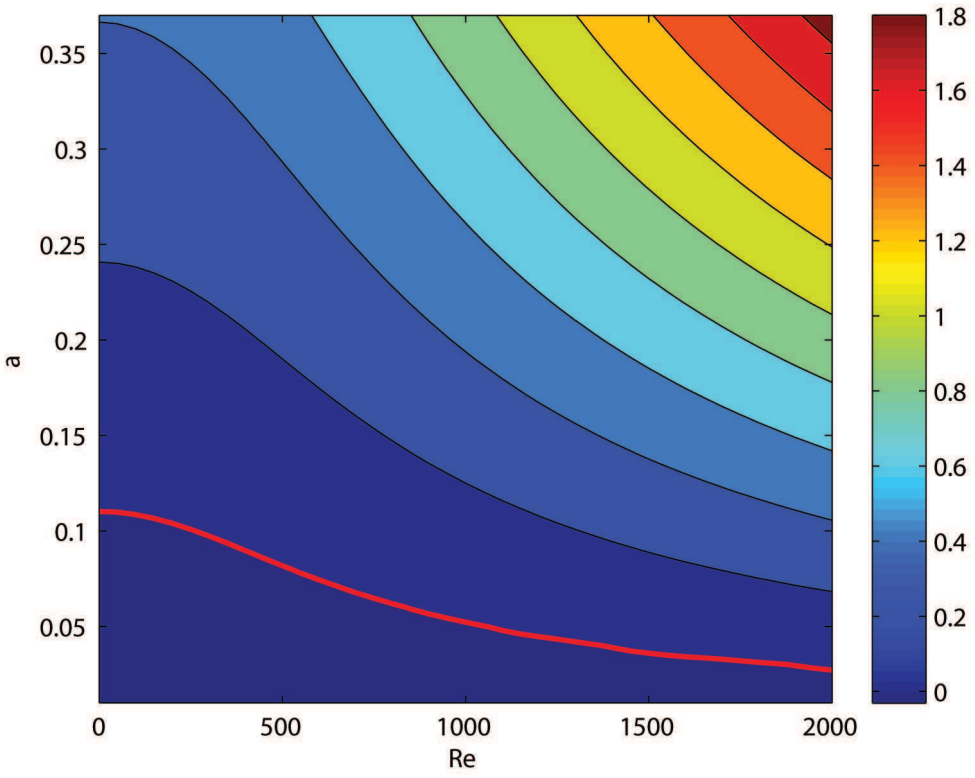

Figure 6.30: Poiseuille case: *Max Growth*. Reynolds-β behavior. $\alpha = 0$, $C = 50$, $Fe = 200$, $M = 5$, $N = 150$, $T = 2000$

6.3.3 Transient growth neutral curve

According to [14] a necessary and sufficient condition for growth of energy is that the numerical range extends into upper complex plane. This is a much stronger condition than eigenvalues's condition for the instability set in. In Figures 6.31 and 6.32 the limit for no grwth is shown as a red line while te limit for exponentila growt is described by the black line.

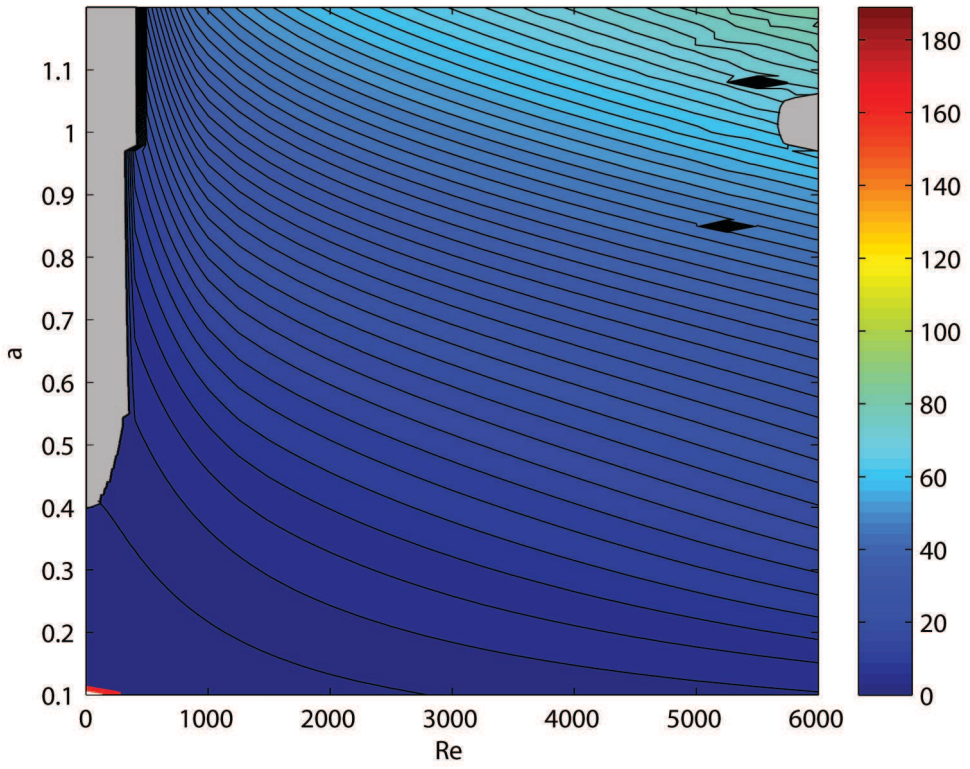

Figure 6.31: Poiseuille case: *Transient growth neutral curve.* Reynolds$-\alpha$ behavior. $\beta = 0$, $C = 50$, $Fe = 200$, $M = 5$, $N = 150$, $T = 2000$

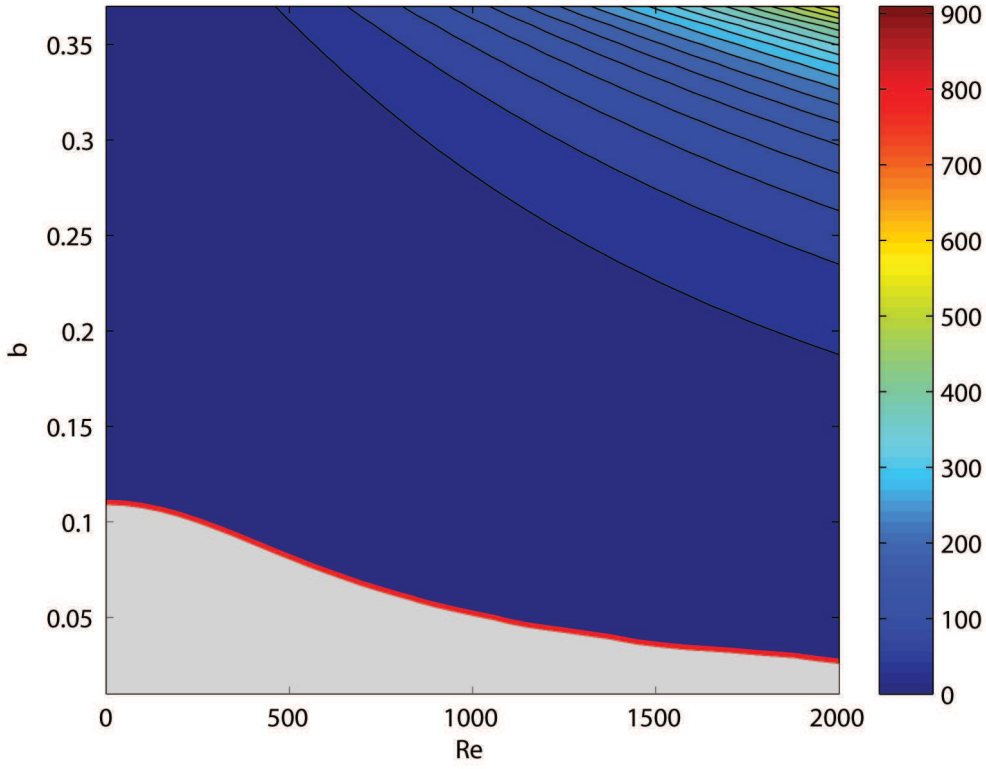

Figure 6.32: Poiseuille case: *Transient growth neutral curve.* Reynolds$-\beta$ behavior. $\alpha = 0$ $C = 50$, $Fe = 200$, $M = 5$, $N = 150$, $T = 2000$

6.4 Optimal disturbance

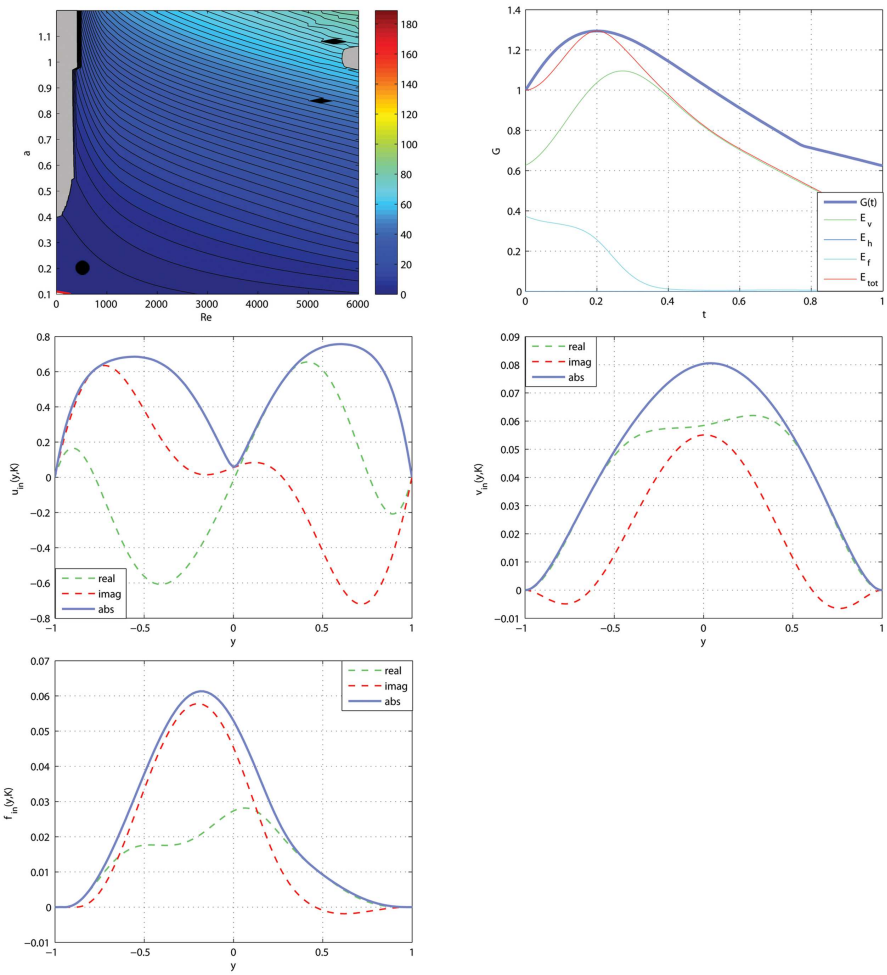

Figure 6.33: Poiseuille case: *Optimal Initial condition.* $\alpha = 0.2$, $\beta = 0$, $C = 50$, $Fe = 200$, $M = 5$, $N = 150$, $Re = 500$, $T = 2000$

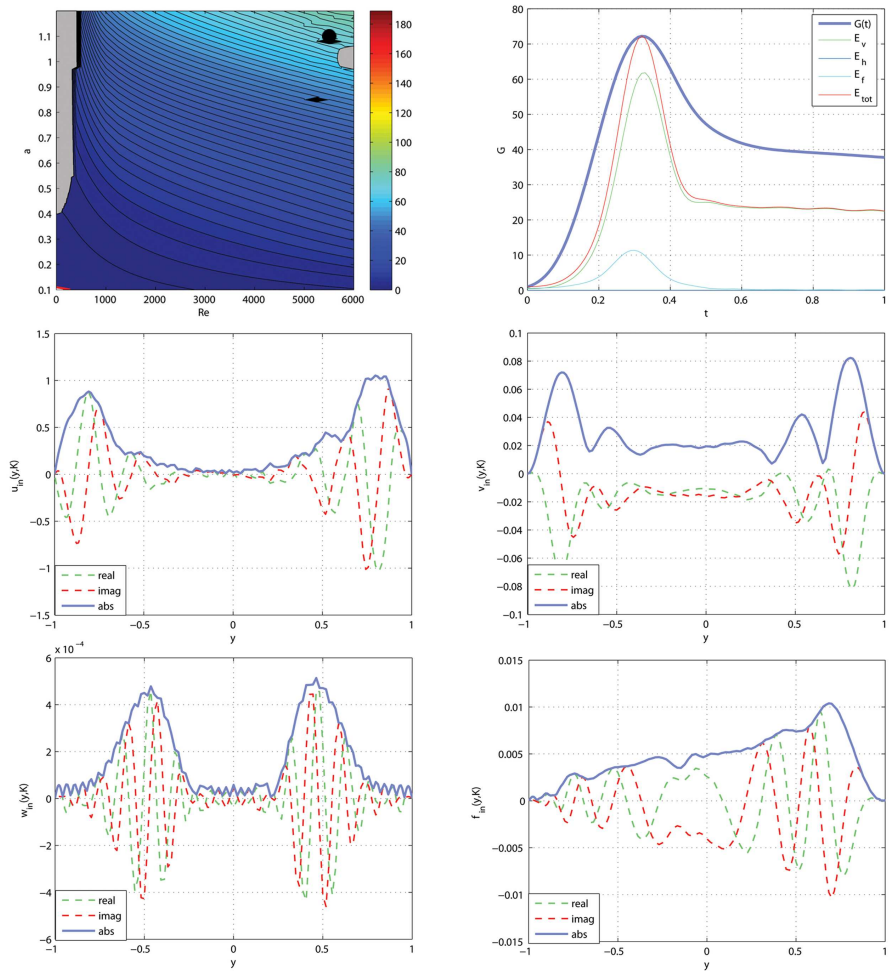

Figure 6.34: Poiseuille case: *Optimal Initial condition.* $\alpha = 1.1$, $\beta = 0$, $C = 50$, $Fe = 200$, $M = 5$, $N = 150$, $Re = 5500$, $T = 2000$

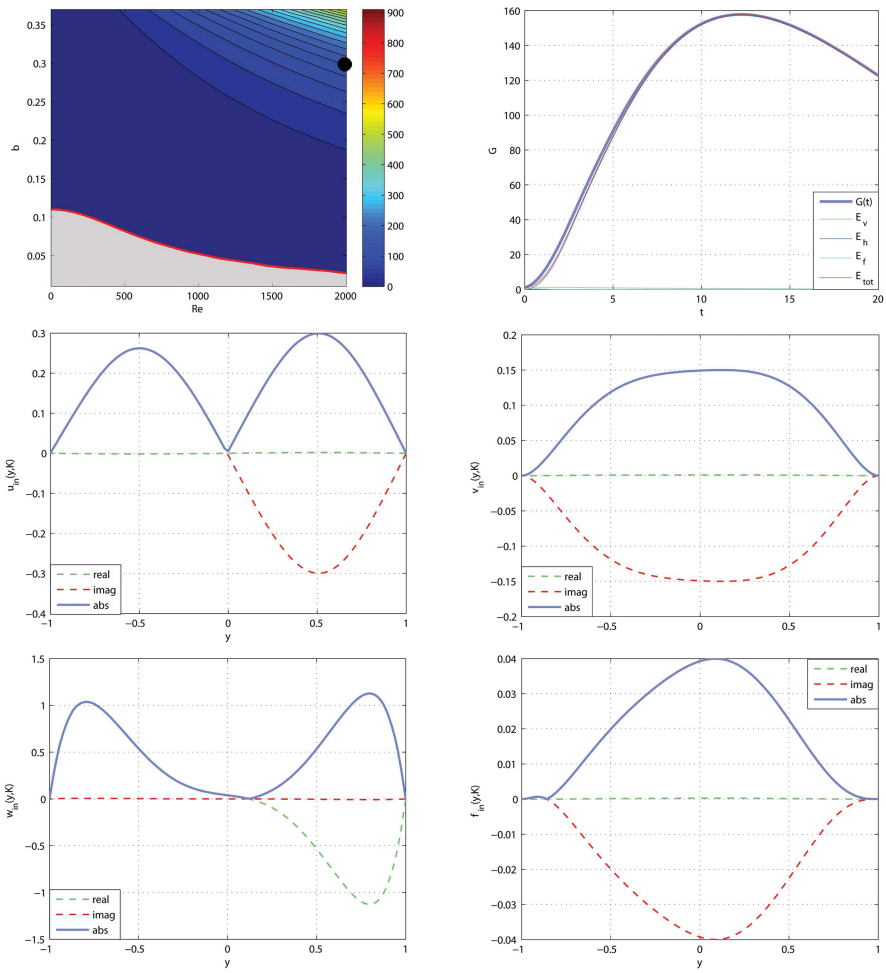

Figure 6.35: Poiseuille case: *Optimal Initial condition.* $\alpha = 0$, $\beta = 0.3$, $C = 50$, $Fe = 200$, $M = 5$, $N = 150$, $Re = 2000$, $T = 2000$

6.5 Forced flow

In both cases the maximum response to an harmonic force does not show a *pseudo resonance* behavior.

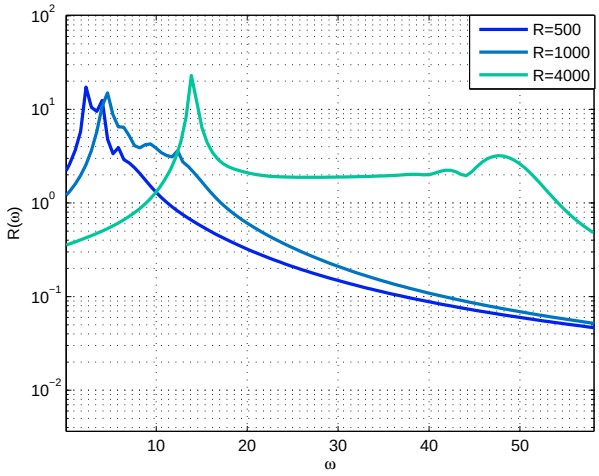

Figure 6.36: Poiseuille case: *Forced Response*. Effect of Reynolds. $\alpha = 1$, $\beta = 0$, $C = 50$, $Fe = 200$, $M = 5$, $N = 150$, $T = 2000$

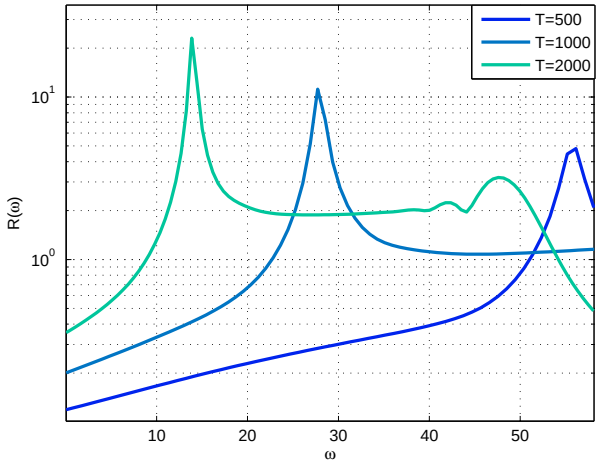

Figure 6.37: Poiseuille case: *Forced Response*. Effect of Reynolds. $\alpha = 1$, $\beta = 0$, $C = 50$, $Fe = 200$, $M = 5$, $N = 150$, $Re = 4000$

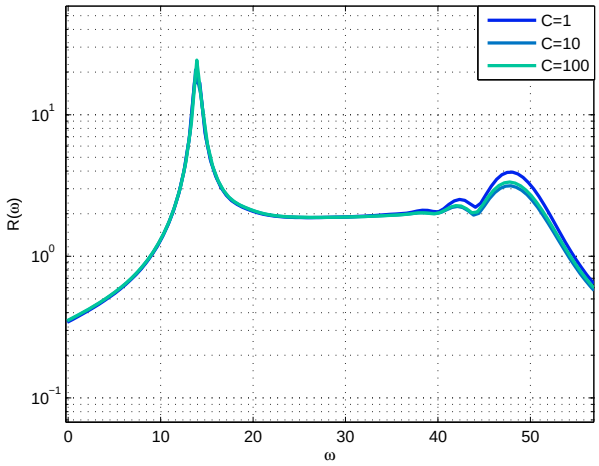

Figure 6.38: Poiseuille case: *Forced Response*. Effect of C. $\alpha = 0.2$, $\beta = 0$, $Fe = 200$, $M = 5$, $N = 150$, $Re = 4000$, $T = 2000$

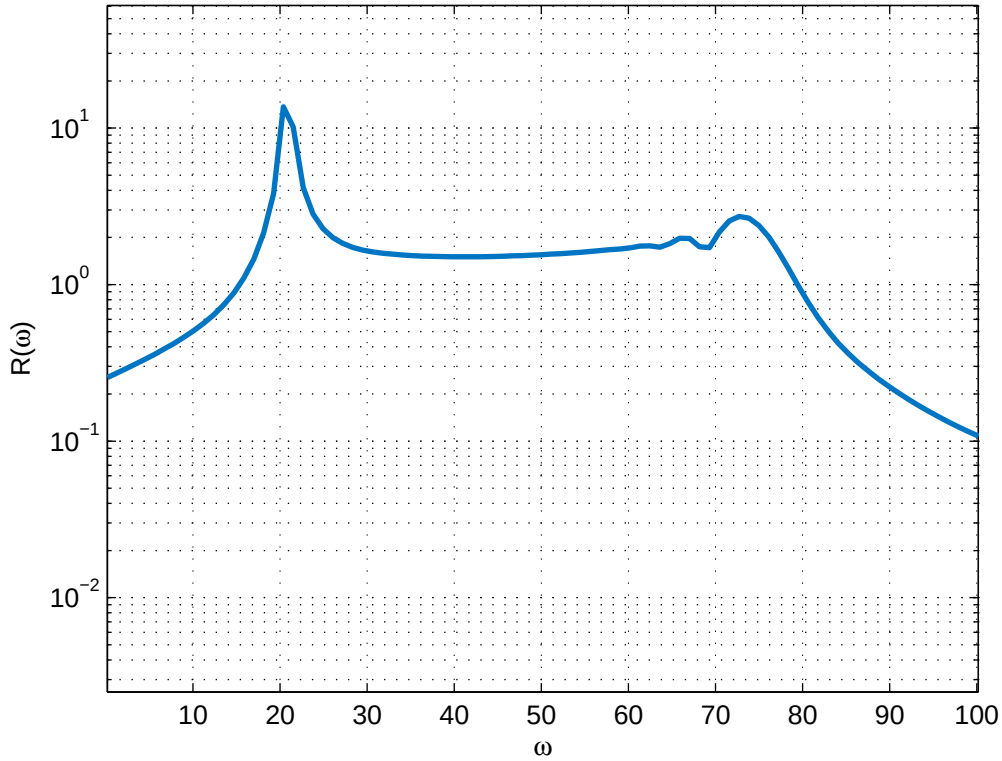

Figure 6.39: Poiseuille case: *Forced Response*. Case B. $\alpha = 0.2$, $\beta = 0$, $C = 50$, $Fe = 200$, $M = 5$, $N = 150$, $Re = 500$, $T = 2000$

6.6 Remarks

After proving that Squire's theorem can be applied for system (3.19), the 2D ($\beta = 0$) and streamwise invariant ($\alpha = 0$) cases were analyzed. While for $\beta = 0$ a distinction can be made between high and low Reynolds regime, for $\alpha = 0$ the Reynolds does not affect the transition from stable to unstable behavior. Unlike in the hydrostatic case, the dimensionless ionic mobility plays a key role by dictating the applicability limits of the numerical model here implemented. In fact, the error related to the numerical resolution remains acceptable only if $M \leq 10$. This means that for larger values of $M = \tau_K/\tau_{EI}$ the dynamics of the system are no longer well resolved.
Since the set up is studied for the first time including both charge diffusion and cross flow, no comparisons with known results is possible. However, as in the case without charge diffusivity the critical curve path suggested by [7], has been confirmed. In fact the linear stability of Poiseuille flow is significantly affected by the presence of the electric field at lowest Reynolds number and as the base flow velocity increases the charge perturbations tend to play a minor role in the transition.
When $\beta = 0$ and the Reynolds number is low, a modal identification is still possible but as soon as cross-flow's velocity increases it will be lost. The interesting fact is that with the cross flow, three-dimensional components of the disturbance appear. These modes lie on the Z branch and present only an high oscillating $w(y, k)$, without any other disturbance components. This means that they don't contribute to the system's potential energy. Furthermore the velocity modes have different behavior while the electrical perturbations tends to remain *wall-modes*. Once again the idea that the charge diffusivity plays an important role seems to be verified.
Significant energy transient growths are related to classical mechanisms (Figure 6.24) but the peaks of $G(t)$ are achieved for dimensionless timescales much lower than the classical Poiseuille flow. In addition, the Figure 6.31 shows that there is virtually no area where the system does not present energy growth.

The case in which $\alpha = 0$ presents slight differences. The transient growths achieved are higher than before ($\beta = 0$) but the transient mechanisms are still related only to the velocity perturbations (Figure 6.28). Moreover there is a wider area with no energy growth and the energy peaks are achieved at large time (Figure 6.32).
In both cases the maximum response to an harmonic force does not show a *pseudo resonance* behavior.

CHAPTER 7

CONCLUSIONS AND FURTHER STUDIES

For the first time, the EHD parallel plane problem has been studied with and without charge diffusion and with and without cross flow

As the charge diffusion tends to zero the results obtained agree very well with other works available in literature , (Figure 5.7), (C), (D). The possibility offered by the present code to include charge diffusion, short time transient growth and cross flow, has brought to light new aspects of the well-known EHD planar plane problem.

In the *hydrostatic case*, accounting the charge diffusion, the critical value $T^\star \approx 110$ associated with the linear stability criterion agrees with that predicted in [8]. Therefore it is significantly lower than the value reported in others papers according with the experimental results. Thus, once at all, it has been proven that the diffusion enhance the instability throughout an augmented mixing. Identifying the shape of eigenmodes, it is emerged that the energetically relevant modes are almost entirely *wall modes* and this confirms the importance of charge diffusivity.
The non-modal stability analysis has shown a mild transient growth dues to the potential disturbances. Moreover, for the first time Figure 5.10 shows the limit values of T and α for transient growth, and exponential growth. The harmonic forced response has been done as well but it doesn't show any relevant result.

In the *EHD-Poiseuille* the Squire's theorem has been proven allowing us to study the 2D case as the most critical one. Nevertheless, superimposing the cross flow, the higher number of parameters combination has forced us to impose some constrains at their values. If ($M \leq 10$), it ensures a good numerical resolution as well as $Fe \approx 10^2$. More over, according with the hydrostatic case, higher values of T comport lower $\mathsf{K}^\star$. Fixing $T = 2000$ the neutral curve in Figure 6.18 shows two different instability regions in accord to [7]. In the viscous dominated regime the effect of the electrical parameters on the linear stability criterion is relevant while at high Reynolds it tends to vanishing. Since non modal stability analysis involves an high number of modes, M and Fe dictate the applicability limits of the numerical model here implemented at both low and high Reynolds numbers. As previously explained a better understanding of this leak of resolution related to M is necessary. Avoiding the resolution error a non modal stability analysis has been performed revealing important transient growth, especially for $\alpha = 0$. Contrarily to the hy-

drostatic case, analyzing the different energetic contributes, the energy transient growth depends on the classical mechanisms related to the fluid dynamics, the Orr mechanism if $\beta = 0$, and lift-up if $\alpha = 0$. Moreover, as shown in Figure 6.31, the area with no transient growth tends to vanishing in the 2D case. The harmonic forced response has been done but it doesn't show any relevant result.

The analysis of the role played by M, it should be the natural follow up of this work as well as the identification of another growth mechanism mostly based on the electric dynamics.
Moreover, as explained in the introduction, the electric volume forcing might leads to a new brand of turbulence control techniques[1] or non-modal behavior control.

In conclusion, the present work has proved that charge diffusion effects are not negligible in both modal and non-modal stability analysis, and transient growth phenomena occur in both hydrostatic and Poiseuille EHD cases.

[1]such as Boundary control via distribution of perturbation potential

APPENDIX A

Notes on the quasi-stationary Maxwell equations

A.1 introduction

Quasi-steady electromagnetic systems are those systems not strictly stationary for which changes over time don't play a primary role. As every approximation, it is important to understand when is lawful to proceed in this way.
Considering the fundamentals Maxwell equation (A.1), the charge continuity equation (A.2), and constitutive laws (A.3) respectively

$$\nabla \times \mathbf{E} = -\frac{\partial \mathbf{B}}{\partial t},$$

$$\nabla \times \mathbf{H} = \frac{\partial \mathbf{D}}{\partial t} + \mathbf{J},$$

$$\nabla \cdot \mathbf{D} = Q,$$

$$\nabla \cdot \mathbf{B} = 0. \tag{A.1}$$

$$\frac{\partial Q}{\partial t} + \nabla \cdot \mathbf{J} = 0. \tag{A.2}$$

$$\mathbf{D} = \varepsilon \mathbf{E},$$

$$\mathbf{B} = \nu \mathbf{H},$$

$$\mathbf{J} = \sigma \mathbf{E} + \mathbf{J}_i. \tag{A.3}$$

Where physics quantities have been defined as

E, $[V/m]$, *Electric field*, caused by charge distribution,

D, $[C/m^2]$, *Electric induction*, caused by interaction between **E** and electric material,

H, $[Asp/m]$, *Magnetic field*, caused by the charge's movement,

B, $[Wb/m^2]$, *Magnetic induction*, caused by interaction between **B** and electric material,

J, $[A/m^2]$ *Conduction current density*, linked to the charge's movement.

and the material parameters[1] are

ε, $[F/m]$, *Dielectric constant or permittivity*,

μ, $[H/m]$, *Magnetic Permeability*,

γ, $[\Omega^{-1}/m]$, *Conductibility*,

Q, $[C/m^3]$, *Charge density*

Obviously the steady set is obtained neglecting the time derivatives in (A.1). Instead, for quasi-stationary fields, we proceed removing only *some* time derivatives. It remains to specify which part could be removed and which not.

A.2 Quasi-steady assumption

In (A.1) is possible to neglect *or* the time derivative of magnetic induction **B** *or* the time derivative of electric induction **D**. So one has to identify *a priori* the regions where no serious errors are committed neglecting the time derivatives.
Focusing just on the case where $\partial_t \mathbf{B}$ is negligible, the electric field is governed by the following relations (3.2):

$$\begin{cases} \nabla \cdot \mathbf{D} = Q(t), \\ \mathbf{E} = -\nabla \Phi, \\ \dfrac{\partial Q}{\partial t} + \nabla \cdot \mathbf{J} = 0. \end{cases}$$

[1]Thanks to isotropy, linearity and homogeneity assumptions the material parameters are scalar quantities.

The time still appears in $Q(t)$, but it plays a minor role as simple parameter. Therefore at each time the electric field has a *stationary-like* behavior with unsteady boundary conditions, without mutual time influence.
Neglecting $\partial_t \mathbf{B}$ equals to consider that $\mathbf{B}$ has a static response to external forcing represented by Q and $\mathbf{J}$. In that way the quasi-steady assumption neglects the propagation delay linked to magnetodynamics. Roughly speaking the characteristic time scale of $\mathbf{B}$ is much smaller than Q timescale, so in a $\mathbf{B}$ time unit Q doesn't change.

A.3 Quasi-steady condition

Neglecting the time delay means, that the forcing term Q doesn't vary in a $\Delta\tau_B$ time unit, namely

$$Q(t + \Delta\tau_B) \approx Q(t) \qquad \rightarrow |Q(t + \Delta\tau_B) - Q(t)| \ll |Q(t)| \,.$$

Using a series develop for Q

$$\left| \frac{\partial Q}{\partial t} \Delta\tau_B \right| \ll |Q(t)| \,.$$

Defining c_0 as the speed of light and $\Delta\tau_B = 2\delta/c_0$, the quasi-steady assumption can be applied each time that is possible to verify the follows condition.

$$\left| \omega \frac{2\delta}{c_0} \right| \ll 1 \tag{A.4}$$

where $\omega = \alpha\sigma$ and σ is the disturbance's phase speed. In the present work the liquid is a dielectric. Since the dielectric fluids have a very low electrical conductivity (low σ) but can sustain very high electric fields, the relation (A.4) is verified hence the induced magnetic fields could be neglected.

APPENDIX B

Spectral Discretization with Chebyshev Polynomials

B.1 Introduction to Spectral method

The term Spectral Method refers to a wide range of numerical methods to calculate the derivatives of a function. The fundamental concept is the ability to drop down the differential operator of a function, sometimes unknown, on an approximation of it. So a continuous differential problem becomes a discrete one. Unlike techniques such as finite difference or finite element, spectral methods have higher computational cost but provide an incomparable accuracy (infinite convergence order).
Hence, from this point of view, The question is not if spectral methods are the best or not but if the problem requires a so high accuracy. The implementation difficulty of spectral method varies widely. It depends by geometry, the basis set and how the residual is minimized. To solve the current problem a spectral collocation method has been used. The reasons for this choice are summarized in four rules of thumb formulated by J.P.Boyd [5].

- *Collocation is the simplest choice which is guaranteed to work, and if done right, nothing else is superior,*
- *When in doubt, use Chebyshev polynomials unless the solution is spatially periodic, in which case an ordinary Fourier series is better,*
- *Unless you're sure another set of basis functions is better, use Chebyshev polynomials,*
- *Unless you're really, really sure that another set of basis functions is better, use Chebyshev polynomials.*

B.2 Gauss-Lobatto's nodes

In the literature the standard nodes set of Gauss-Lobatto-Chebyshev has been given by the following

$$x_i = \cos\left(\frac{i\pi}{N}\right), \qquad i = 0, ..., N. \tag{B.1}$$

This set provides the highest order of accuracy that is possible for quadrature formulas and includes the nodes at the boundaries, making more agile the imposition of boundary conditions. Furthermore, using the Chebyshev polynomials, through the theorem of *minimum amplitude of Chebyshev* [5] it has been proven that this distribution of nodes minimizes the interpolation error. Unfortunately, in finite arithmetic, already with $N = 10$, this formulation does not guarantee symmetry around the origin. Although, using the trigonometric identity

$$\cos(\theta) = \sin\left(\frac{\pi}{2} - \theta\right)$$

Is possible to obtain a similar form of (B.1) that is symmetry errors free.

$$x_i = \sin\frac{\pi(N-2i)}{2N}, \qquad i = 0, ..., N. \tag{B.2}$$

In the present work the (B.2) implementation has been used.

B.3 Chebyshev Polynomial

The Chebyshev polynomials are defined as

$$T_n(x) = cos(n\theta), \qquad \theta = arccos(x) \tag{B.3}$$

and they can be computed in various ways, such as eigenfunction of the Sturm-Liumville problem, by Rodrigues formula, expansion in powers series and much more. The (B.3) is known as *trigonometric formulation* that can be implemented using the recursive formula

$$T_0(x) \equiv 1, \tag{B.4}$$
$$T_1(x) \equiv x, \tag{B.5}$$
$$T_{n+1}(x) = 2xT_n(x) - T_{n-1}, \tag{B.6}$$

Some Chebyshev polynomial properties are, domain $[-1, 1]$:

$$|T_n(x)| \leq 1 \tag{B.7}$$
$$T_n(\pm 1) = (\pm 1)^n \tag{B.8}$$
$$|T_n'(x)| \leq n^2 \tag{B.9}$$
$$T_n'(\pm 1) = (\pm 1)^{n+1} n^2 \tag{B.10}$$

Moreover the Chebyshev polynomial are orthogonal respect to $w(x) = (1-x^2)^{-1/2}$ weight function, yielding to

$$(T_n, T_m)_w \equiv \int_{-1}^{1} T_m(x)T_n(x)w(x)dx = d_n\frac{\pi}{2}\delta_{mn}, \quad \text{where} \quad d_n = \begin{cases} 2, & n = 0 \\ 1, & n \geq 1 \end{cases}$$

B.4 Spectral Method with Chebyshev polynomial

Given a function $f(y)$ defined for $1 \geq y \geq -1$, is possible approximate it as

$$f(y) = \sum_{n=0}^{N} a_n T_n(y)$$

where

$$T_n(y) = \cos(n\theta), \quad \theta = \cos^{-1}(y)$$

In matrix form

$$\mathbf{f}(y) = \mathbf{D_0}\mathbf{a}_f, \qquad \mathbf{f}^{(n)}(y) = \frac{d^{(n)}}{dy^{(n)}}(\mathbf{D_0})\mathbf{a}_f = \mathbf{D}_n\mathbf{a}_f \tag{B.11}$$

where

$$D_{0(kj)} = \cos(j\cos^{-1}(y_k)).$$

The truncation error committed using a truncated Chebyshev approximation is limited by the sum of the coefficients neglected

$$Err_(x) \quad = \quad \| \, u(x) - \sum_{n=0}^{N} a_n T_n(y) \, \|_\infty \quad \leq \quad \sum_{n=N+1}^{\infty} |a_n|, \qquad \forall \quad u(x), N \quad \text{e} \quad \forall \quad x \in [-1, 1] \tag{B.12}$$

Since in most practical applications the function is unknown, usually it is impossible to quantify these errors. An approximation consists to retain that the errors are limited by the series convergence. This is a very strong statement that *can not*

be proven, but that is always true in *viceversa*: *If a method is distinguished by a large truncation error then it will certainly a bad way to solve that particular problem.* [5]. Furthermore, the *Principle of Darboux* states that problems without singularity, or with weak singularity outside the domain of convergence will have a spectral (infinite) convergence order. Conversely problems with singularity may have a geometric or algebraic order of convergence.
Therefore, roughly speaking, the truncation error has the same order of magnitude of the last coefficient of the series.

B.5 Boundary condition

In the spectral method theory, the boundary conditions may be divided into two broad categories: *numerical* and *behavioral*. The first category has to be explicitly imposed, in contrast, the second one may be satisfied implicitly by choosing basis functions such that each have the required property or behavior.
In finite element theory, boundary conditions are classified as either *essential*, which must be explicitly imposed, or *natural* conditions, which are automatically satisfied by the approximate solution. Attention! There is no duality between the two classifications! In fact, both *essential* and *natural* conditions are numerical and the distinction is only between whether $u(x)$ or its derivative is set equal to a particular number at the endpoints. Nevertheless, from a programmers standpoint just *numerical* and *essential* conditions require work.
There are two strategies to impose the numerical conditions:

- **boundary bordering:** The *border* of the spectral matrixin this case, is used to explicitly enforces the boundary conditions, reducing the number of collocation conditions on the residual of the differential equation.
- **basis recombination** modifying the problem to get homogeneous boundary conditions and then altering the basis set so that the basis functions individually satisfy these conditions.

The boundary-bordering method is more simple and applicable to even the most bizarre boundary conditions. It gives a slightly larger matrix in comparison to the basis recombination method, but for the largest problem, this is compensated by the higher cost of calculating the matrix elements in the latter technique. These are good reasons to choose it.

B.6 Spurious eigenvalues

Solving a linear eigenvalue problem with a spectral method composed by $N + 1$ expansion function and reordering the eigenvalues in ascending order, generally, only the first $N/2$ eigenvalues will be accurate within a small error percentage.

Others may be deemed unusable. The only way to understand which eigenvalues are accurate and which are not consist in repeat the calculation with a different N and compare the results. Doing that sometimes may happens to get few accurate eigenvalues, less than $N/2$. In this case it is very likely that the solution contains singularities in the complex domain of method's convergence. In these cases the solutions may gives *boundary layer phenomena* and the spectral approach fails. An examples is non modal analysis of the EHD Poiseuille flow without charge diffusion. Graphic techniques are a good tools to check the results goodness. Some of them are shown in [5].

APPENDIX C

Benchmark Case I: Free surface case

C.1 Introduction

Investigating instabilities set in conditions, the *free-surface* case is a good benchmark to test our code. Both numerical and experimental results are reported in the literature [25], [27]. To take in count the previews works the charge diffusion has to be neglected.
In conduction experiments the liquid-electrode interface usually acts as a blocking contact than as injected one. Moreover injection may set in a very high fields and the microscopic asperities on the electrode could work as *disturbs*. The nonuniform charge emission causes local pumping in the liquid which may set up a more general convection pattern.
In order to obtain experimental results consistent with the numerical ones, it has been necessary to avoid the electrode-liquid interface phenomena not modeled in the equation set. Hence, the following problem is slightly different from what it has been shown before.
In free surface set up (fig. **??**) just the *collector* is present while on the *injector* side there is a *electron gun* also known as *electron beam*. Ideally speaking, the hydrostatic assumption lets say that the free surface is a plane, thus the electron beam creates a *virtual injector* on it avoiding the electrode-liquid interface phenomena.

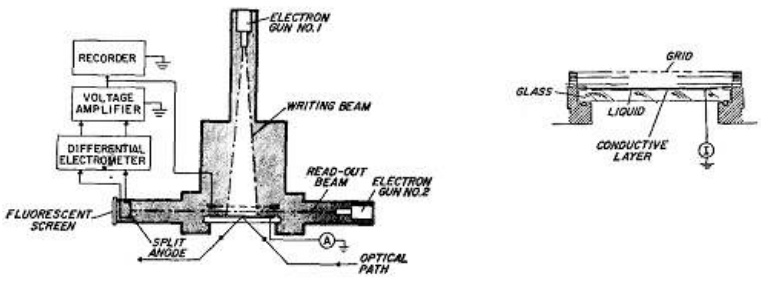

Figure C.1: Benchmark Case I:*Experimental setup*

C.2 Perturbation Equations

Following the derivation of (5.1), the equation set is presented below.

$$\begin{cases} \omega(D_2 - \mathsf{k}^2)\hat{v} = \left[-\dfrac{1}{i}\dfrac{M^2}{T}(D_2 - \mathsf{k}^2)^2\right]\hat{v} + \dfrac{1}{i}M^2\left[\mathsf{k}^2\Phi_0'(D_2 - \mathsf{k}^2) - \mathsf{k}^2\Phi_0'''\right]\hat{\phi}, \\ \omega(D_2 - \mathsf{k}^2)\hat{\phi} = \dfrac{1}{i}\Phi_0'''\hat{v} + \\ \quad + \left[-\dfrac{1}{i}(\Phi_0'''D_1 + 2\Phi_0''(D_2 - \mathsf{k}^2) + \Phi_0'(D_3 - \mathsf{k}^2 D_1)) - \dfrac{1}{i}\dfrac{1}{Fe}(D_2 - \mathsf{k}^2)^2\right]\hat{\phi}. \end{cases}$$

with its suitable boundary conditions as

$$v(-1) = 0, \qquad v'\Big|_{y=-1} = 0, \qquad v(1) = 0, \qquad v''\Big|_{y=1} = 0.$$

The third boundary conditions equals to assume that on the free surface the tangential stress is zero and the surface is flat.

C.3 Electric potential mean-flow

Rewriting the charge density evolution as a electric field's function, a non linear third order ODE equation has been found.

$$E_0\frac{d^2E_0}{dy^2} + \left(\frac{dE_0}{dy}\right)^2 = 0. \tag{C.1}$$

with variable changing:

$$\frac{dE_0}{dy} = t$$

$$\frac{d^2E_0}{dy^2} = \frac{dt}{dE_0}\frac{dE_0}{dy} = \frac{dt}{dE_0}t$$

the (D.2) solution as potential's function is

$$\Phi_0(y) = \frac{2}{3}\alpha(y+\beta)^{3/2} + \delta, \tag{C.2}$$
$$\Phi_0^{'}(y) = \alpha(y+\beta)^{1/2}, \tag{C.3}$$
$$\Phi_0^{''}(y) = \frac{1}{2}\alpha(y+\beta)^{-1/2}, \tag{C.4}$$
$$\Phi_0^{'''}(y) = -\frac{1}{4}\alpha(y+\beta)^{-3/2}. \tag{C.5}$$

Applying the follows boundary conditions [25],

$$\Phi_0(1) = 1, \qquad \Phi_0^{'}\Big|_{y=1} = 0, \qquad \Phi_0(-1) = 0.$$

the potential base flow is

$$\Phi_0(y) = 1 - \sqrt{\frac{1}{8}}(1-y)^{3/2},$$
$$\Phi_0^{'}(y) = \sqrt{\frac{9}{32}}(1-y)^{1/2},$$
$$\Phi_0^{''}(y) = -\sqrt{\frac{9}{128}}(1-y)^{-1/2},$$
$$\Phi_0^{'''}(y) = -\sqrt{\frac{9}{512}}(1-y)^{-3/2}.$$

C.4 Results

Comparing the results with those of [25] some differences have been founded.According to the experimental data the critical parameters are $T^\star \approx 95.196$ and $\mathsf{K}^\star \approx 2.175$ while by [25] $T^\star = 99$ and $\mathsf{K}^\star = 2$. It is to be remarked that in the both cases the agreement between theory and experiments is excellent.
In [25], Watson has assumed *a priori* the principle of exchange of stabilities. With this hypothesi the neutral curve is independent by M. In the present work no assumption has been made regarding $\omega^\star$ but the results confirm this independence.

C.4.1 Neutral curves

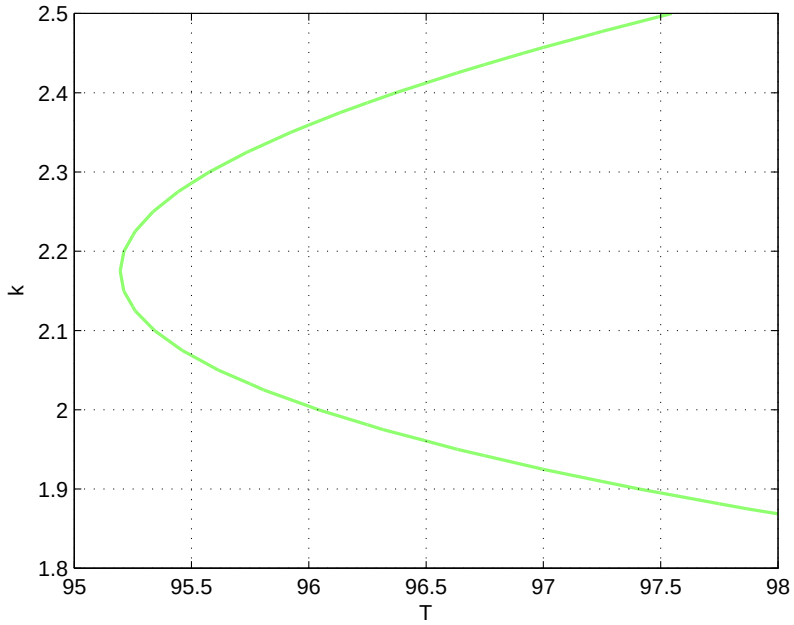

Figure C.2: Benchmark Case I: *Neutral Curve*

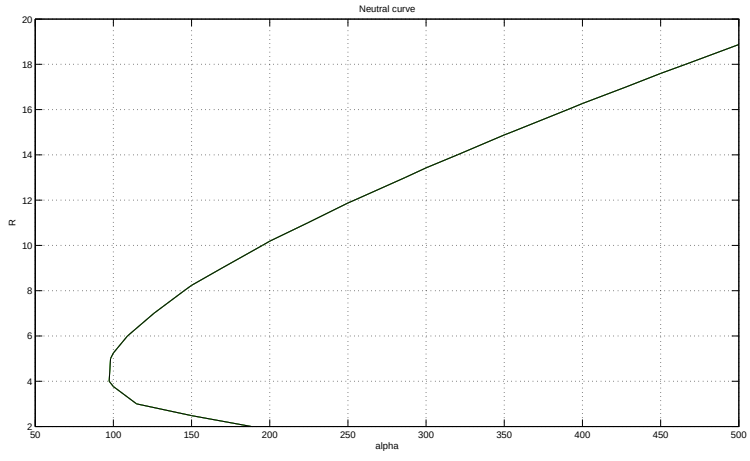

Figure C.3: Benchmark Case I:*Neutral curve*, Effect of M, *green* $M = 60$, *black* $M = 1000$

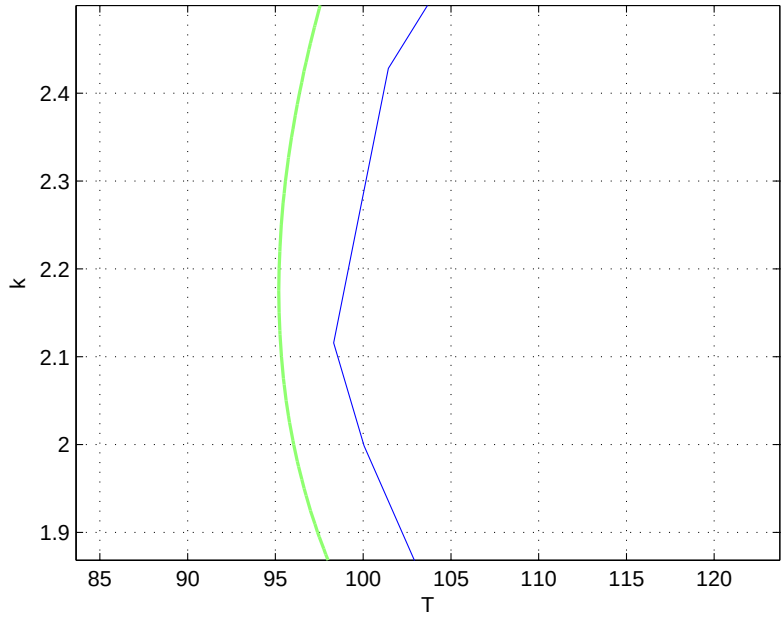

Figure C.4: Benchmark Case I: *Comparison of neutral curves*, *green line* is the present work, while *blue line* is [25]

APPENDIX D

Benchmark Case II: Poiseuille without charge diffusion

In the following appendix will be presented both hydrostatic and Poiseuille cases without the charge diffusion. Only the passages relates to the Poiseuille flow will be expose[1]. The only results available in literature regard the hydrostatic case in strong injection regime and most of them are summarized in [1][2]. Unfortunately if the electrical diffusivity is neglected, the numerical approach implemented here tends to fail, because the resulting the system presents singularities in charge density distribution. As explained in (B) the existence of these singularities can guessed testing the eigencvalue sensitivity to the number of grid points. In [7] Castellanos distinguishes two distinct regions. For a low-enough Reynolds number, the EHD instability mechanism would be dominant. Contrarily, for high enough Reynolds number, the destabilizing inertial mechanism would be the most relevant.

D.1 Perturbation equations

Neglecting the charge diffusion term the constitutive laws for the current density is

$$\mathbf{J} = Q\mathbf{V} + QK\mathbf{E}, \tag{D.1}$$

Following the same path which yields to (3.31), it is possible to write the same eigenvalue problem excepting for the charge density equation. Reasonably, the boundary conditions for the electric potential will be different.

$$\omega(D_2 - \mathsf{k}^2)\hat{\phi} = \Phi_0'''\hat{v} + + \left[\alpha U_0(D_2 - \mathsf{k}^2) - \frac{1}{i}(\Phi_0'''D_1 + 2\Phi_0''(D_2 - \mathsf{k}^2) + \Phi_0'(D_3 - \mathsf{k}^2 D_1))\right]\hat{\phi}.$$

where $U_0(y)$ is the same velocity base flow that has been obtained in the charge diffusion case, while Φ_0 will be deduced in the next section.

[1] in fact, for the hydrostatic case the C) are still valid.

[2] There are both numerical and experimental results

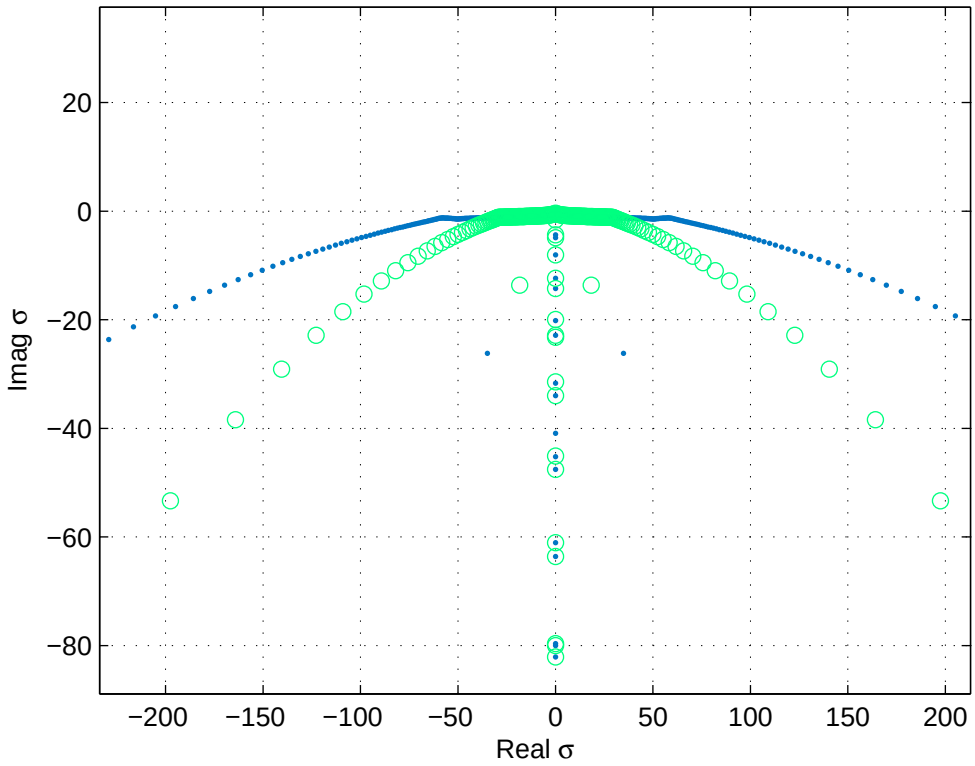

Figure D.1: Benchmark Case II: *Spectrum*, Discretization error

The homogeneous boundary conditions for the perturbations are

$$v(\pm 1) = 0, \qquad v^{'}(\pm 1) = 0, \qquad \eta(\pm 1) = 0, \qquad \phi(\pm 1) = 0, \qquad \phi^{''}\Big|_{y=-1} = 0.$$

D.1.1 Electric potential base flow

Hence, to close the system a new base flow must be provided for the electric potential. Rewriting the charge density evolution as a electric field's function, a non linear third order ODE equation has been found:

$$E_0 \frac{d^2 E_0}{dy^2} + \left(\frac{dE_0}{dy}\right)^2 = 0. \tag{D.2}$$

with variable changing:

$$\frac{dE_0}{dy} = t$$

$$\frac{d^2 E_0}{dy^2} = \frac{dt}{dE_0}\frac{dE_0}{dy} = \frac{dt}{dE_0} t$$

the (D.2) solution as potential's function is:

$$\Phi_0(y) = \frac{2}{3}\alpha(y+\beta)^{3/2} + \delta, \tag{D.3}$$

$$\Phi_0^{'}(y) = \alpha(y+\beta)^{1/2}, \tag{D.4}$$

$$\Phi_0^{''}(y) = \frac{1}{2}\alpha(y+\beta)^{-1/2}, \tag{D.5}$$

$$\Phi_0^{'''}(y) = -\frac{1}{4}\alpha(y+\beta)^{-3/2}. \tag{D.6}$$

Applying the follows boundary conditions,

$$\Phi_0(-1) = 1, \qquad \Phi_0^{''}\Big|_{y=-1} = \mathcal{C}, \qquad \Phi_0(1) = 0.$$

the integration constants are related in the follows way:

$$\begin{cases} \dfrac{2}{3}\alpha(\beta-1)^{3/2} - \dfrac{2}{3}\alpha(\beta+1)^{3/2} = 1, \\ \\ \alpha = -2\mathcal{C}(\beta-1)^{1/2} \end{cases}$$

Replacing the second equation in the first one, we'll get a cubic form for $\beta(\mathcal{C})$

$$6\beta^3 - (\frac{12\mathcal{C}+3}{2\mathcal{C}})\beta^2 + (\frac{2\mathcal{C}+3}{\mathcal{C}})\beta - (\frac{32\mathcal{C}^2+9+24\mathcal{C}}{16\mathcal{C}^2}) = 0 \tag{D.7}$$

SCL assumption

In space charge limited case $\mathcal{C} \to \infty$. To maintain A finite, B has to be equal one. Replacing it, an analytical form of the electric potential base flow has written below.

$$\alpha = -\frac{3}{4\sqrt{2}}, \qquad \beta = 1, \qquad \delta = 1.$$

$$\begin{cases} \Phi_0(y) = -\dfrac{1}{2\sqrt{2}}(y+1)^{3/2} + 1, \\ \\ \Phi_0^{'}(y) = -\dfrac{3}{4\sqrt{2}}(y+1)^{1/2}, \\ \\ \Phi_0^{''}(y) = -\dfrac{3}{8\sqrt{2}}(y+1)^{-1/2}, \\ \\ \Phi_0^{'''}(y) = \dfrac{3}{16\sqrt{2}}(y+1)^{-3/2} \end{cases} \tag{D.8}$$

D.2 Results

Since the cross flow effect have not been tested yet, a comparison could be attempted only for the hydrostatic case. According with the previous works, without cross flow, the critical values are $T^\star \approx 161$, $\mathsf{K} \approx 2.5$. The M independence is confirmed. Unfortunately in [6], $T^\star \approx 100$. This discrepancy is due probably to the simplicity of the model and to the electrode liquid interface. Indeed it has been shown that also using ion-exchange-membrane [6], its rapid deterioration, may affect the results. Nevertheless some controversy exists on the criterion to recognize the critical T.

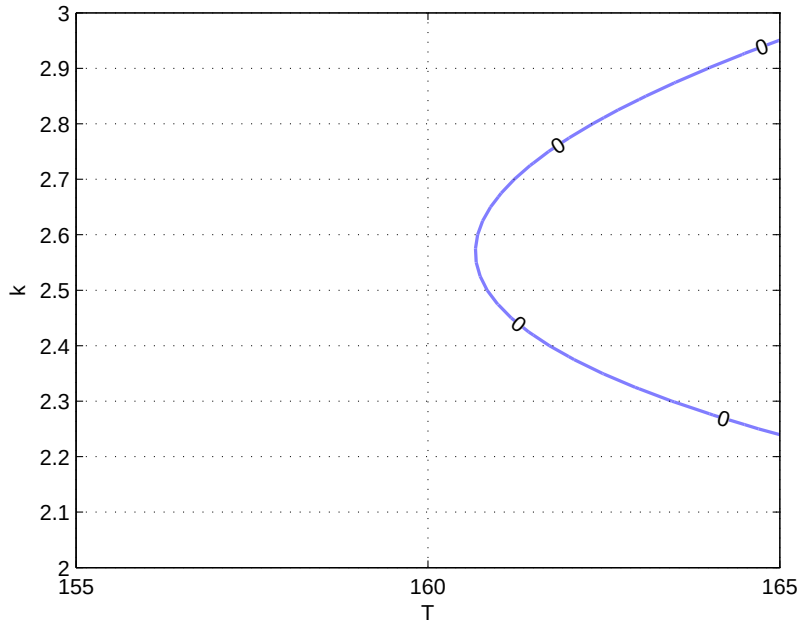

Figure D.2: Benchmark Case II: *Hydrostatic Neutral curve*

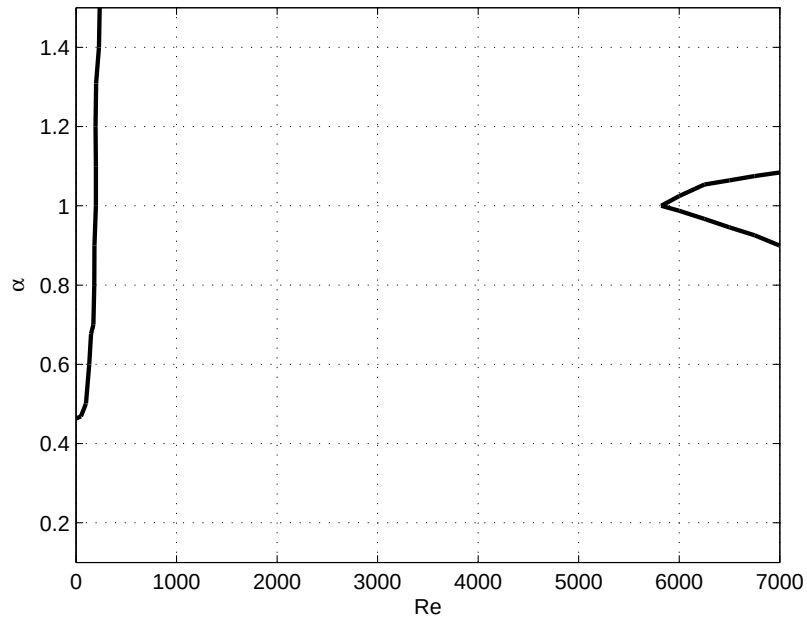

Figure D.3: Benchmark Case II: *Neutral curve*

APPENDIX E

High Reynolds number, discrete spectrum and eigenmodes

Since as the Reynolds number increases the spectrum behavior is too chaotic, no conclusions could be attempted regard the eigenmodes. For completeness has been decided to include a brief look to the modes in this appendix.
The Z branch tends to move from its original position ($\sigma_R = 0$) toward higher real values. The new path seems the classic Poiseuille Y spectrum combined with the parabolic branches A and B. Although at this Reynolds regime the transition is driven by fluid dynamics causes, the electrical parameters are still playing a key role. Therefore in Figure E.2 and E.3 the shape of the spectra presents important changes.

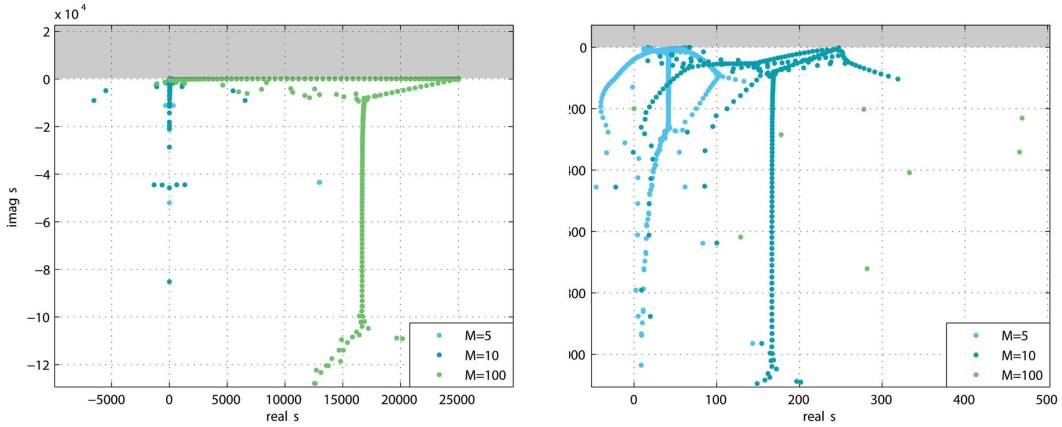

Figure E.1: Poiseuille case: *Discrete Spectrum.* Effect of M. $\alpha = 1$, $\beta = 0$, $C = 50$, $Fe = 200$, $N = 150$, $Re = 5000$, $T = 2000$

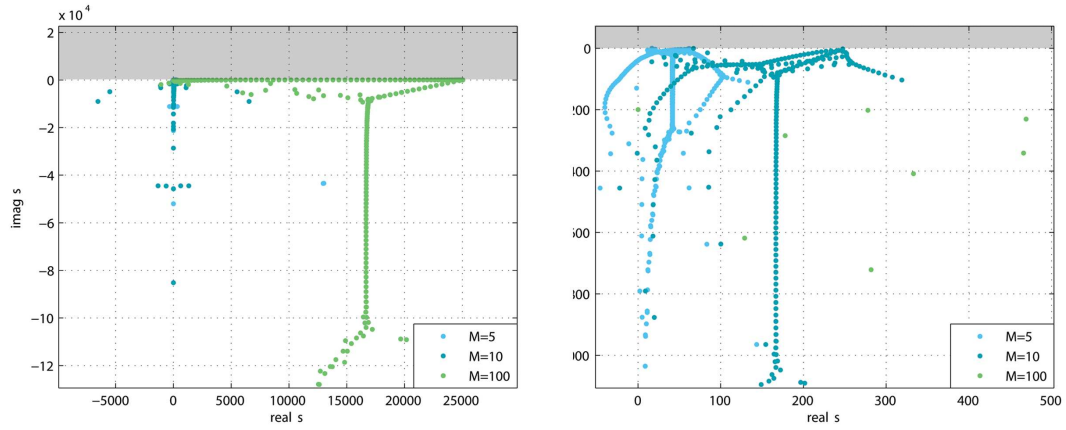

Figure E.2: Poiseuille case: *Discrete Spectrum*. Effect of M. $\alpha = 1$, $\beta = 0$, $C = 50$, $Fe = 200$, $N = 150$, $Re = 5000$, $T = 2000$

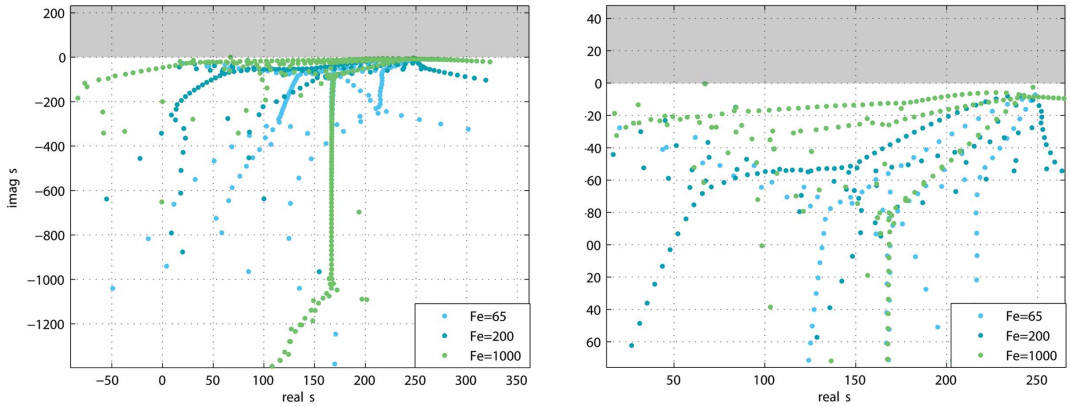

Figure E.3: Poiseuille case: *Discrete Spectrum*. Effect of Fe. $\alpha = 1$, $\beta = 0$, $C = 50$, $N = 150$, $M = 5$, $Re = 5000$, $T = 2000$

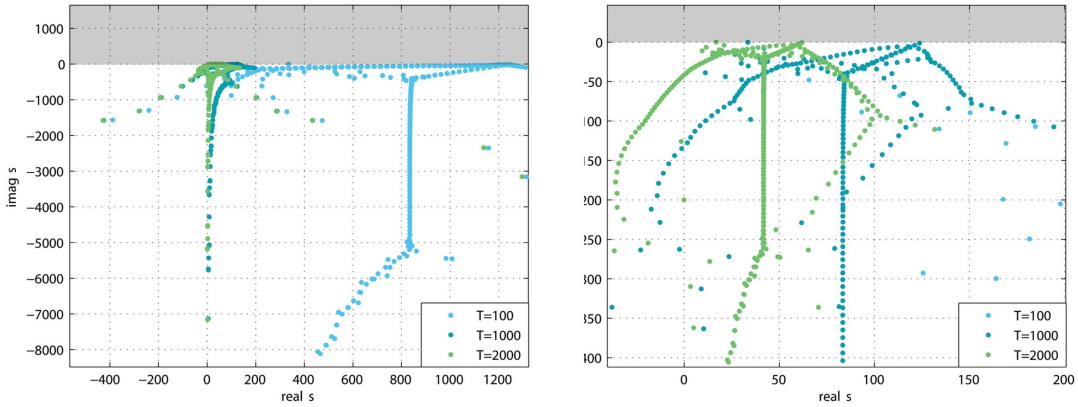

Figure E.4: Poiseuille case: *Discrete Spectrum*. Effect of T. $\alpha = 1$, $\beta = 0$, $C = 50$, $Fe = 200$, $N = 150$, $M = 5$, $Re = 5000$

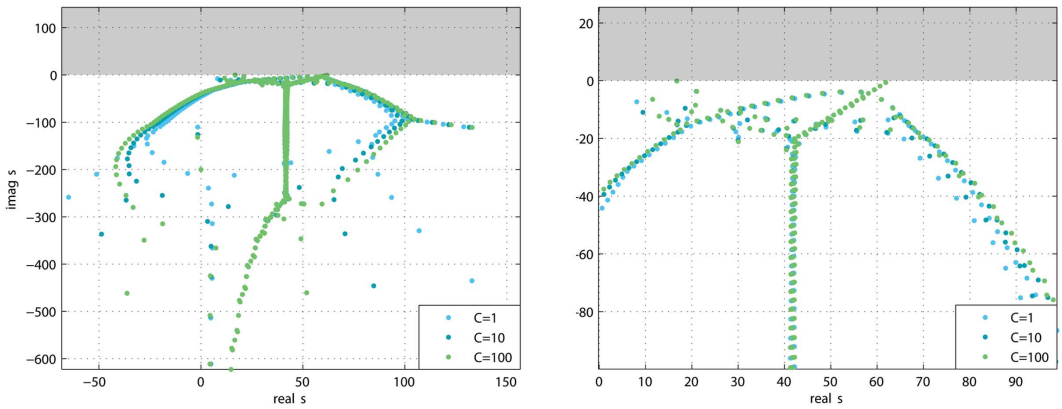

Figure E.5: Poiseuille case: *Discrete Spectrum.* Effect of C. $\alpha = 1$, $\beta = 0$, $Fe = 200$, $N = 150$, $M = 5$, $Re = 100$, $T = 2000$

As in the low Reynolds regime, a well solved case has been chosen to analyze in detail the eigenfunction. The least stable mode is still a *center mode*.

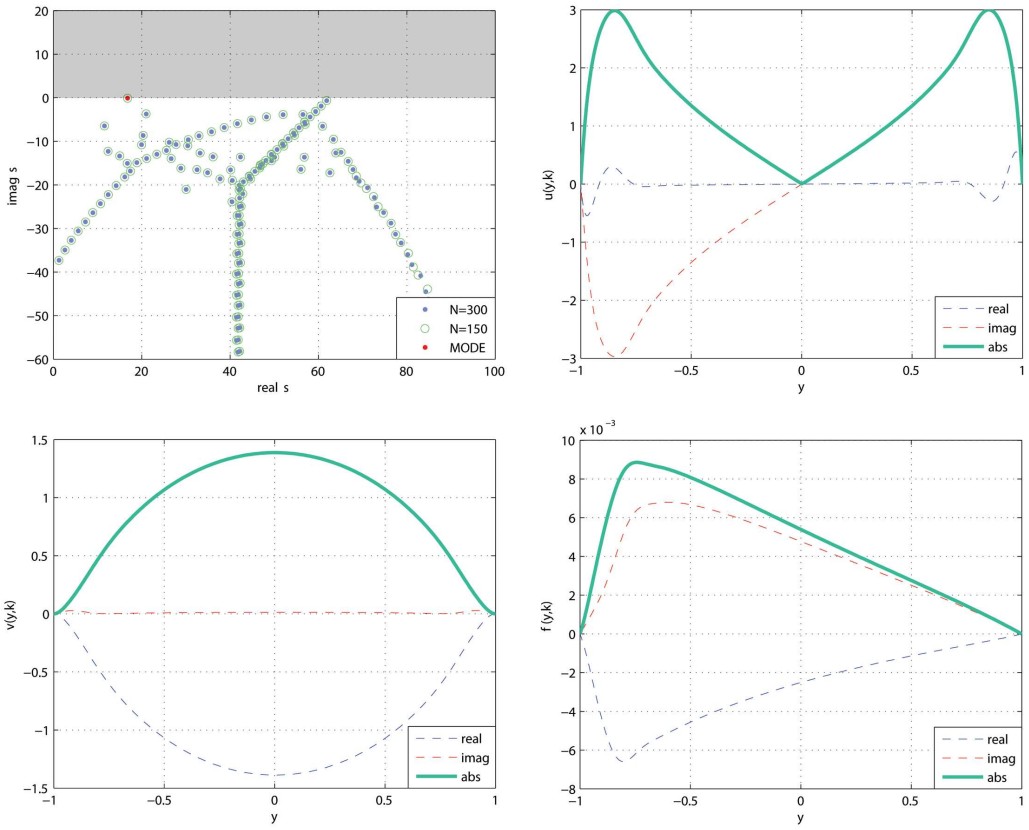

Figure E.6: Poiseuille case:*Modal Identification.* Least stable mode. $\alpha = 1$, $\beta = 0$, $C = 50$, $Fe = 200$, $M = 5$, $N = 250$, $Re = 5000$, $T = 2000$

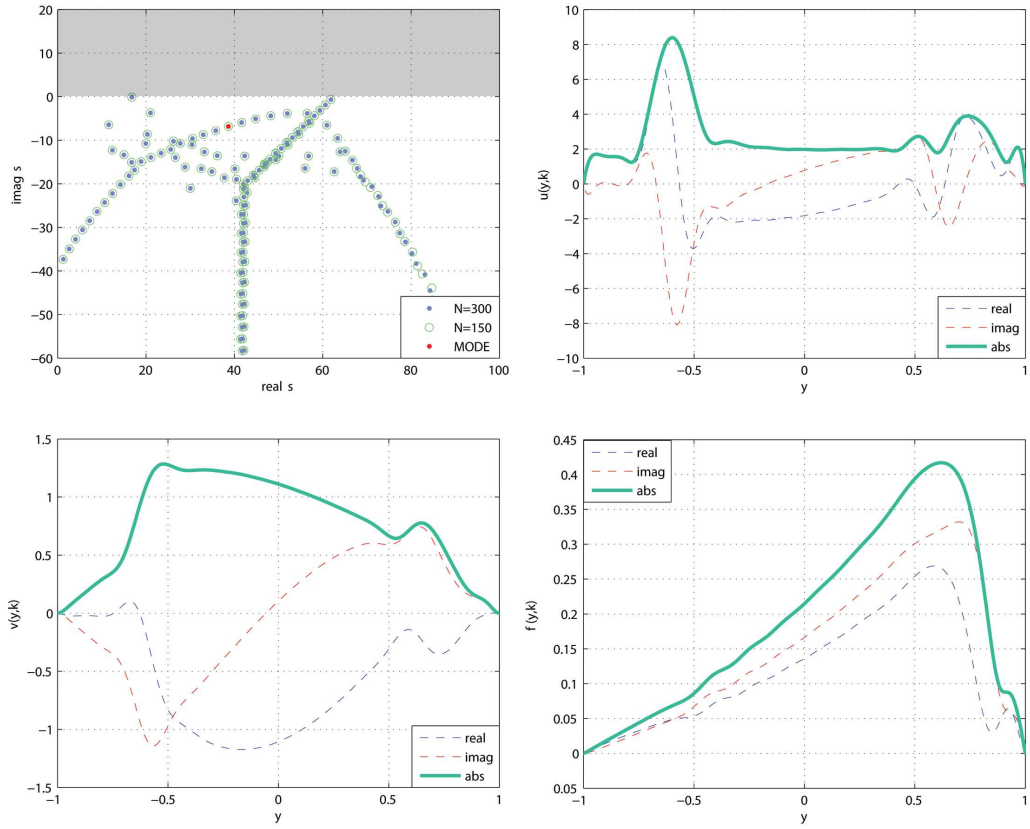

Figure E.7: Poiseuille case:*Modal Identification.* Mode $n20$. $\alpha = 1$, $\beta = 0$, $C = 50$, $Fe = 200$, $M = 5$, $N = 250$, $Re = 5000$, $T = 2000$

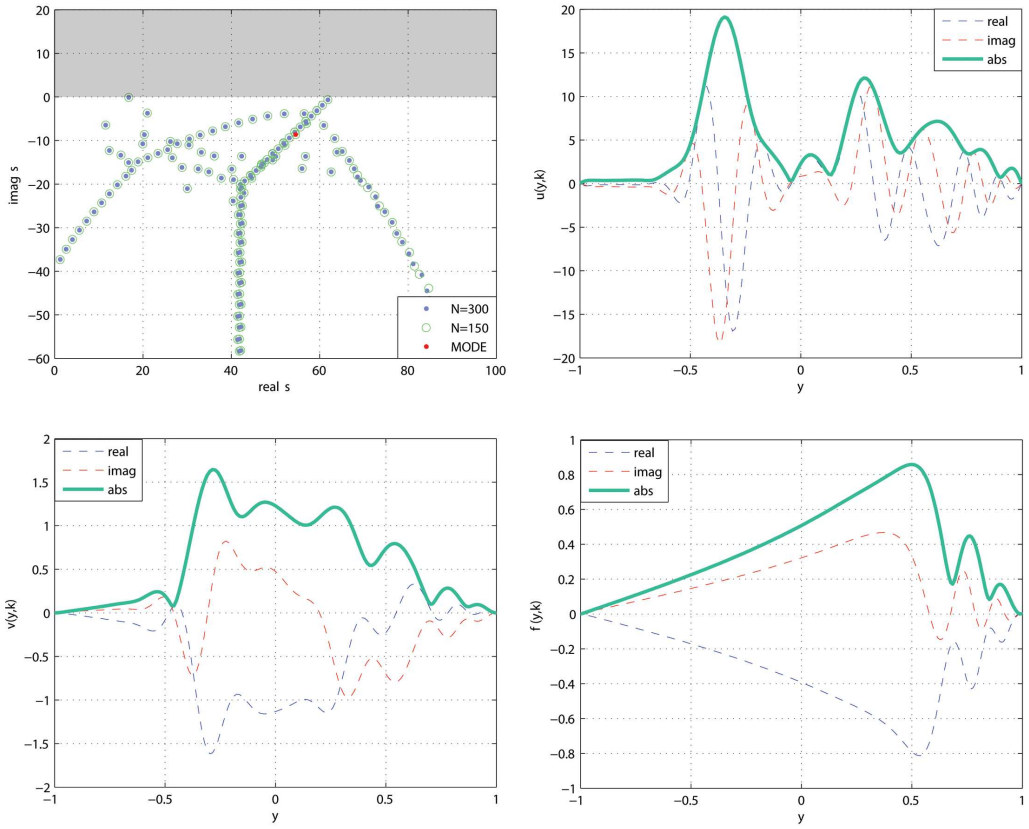

Figure E.8: Poiseuille case:*Modal Identification.* Mode $n25$. $\alpha = 1$, $\beta = 0$, $C = 50$, $Fe = 200$, $M = 5$, $N = 250$, $Re = 5000$, $T = 2000$

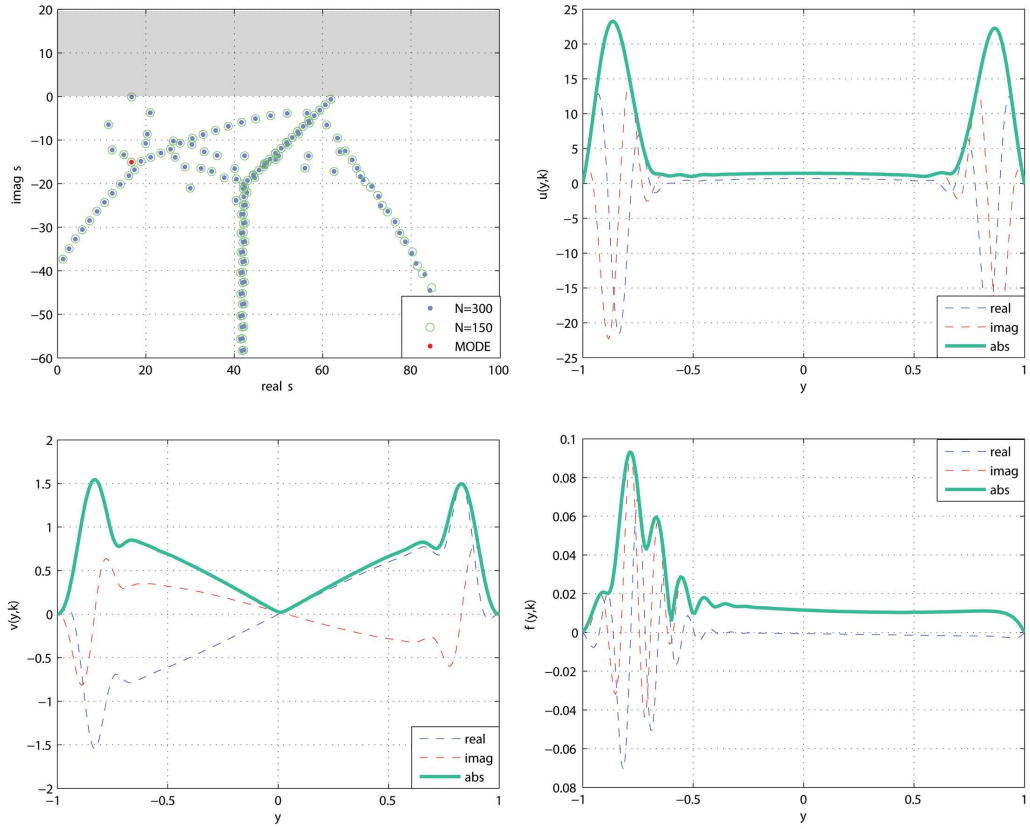

Figure E.9: Poiseuille case:*Modal Identification.* Mode $n60$. $\alpha = 1$, $\beta = 0$, $C = 50$, $Fe = 200$, $M = 5$, $N = 250$, $Re = 5000$, $T = 2000$

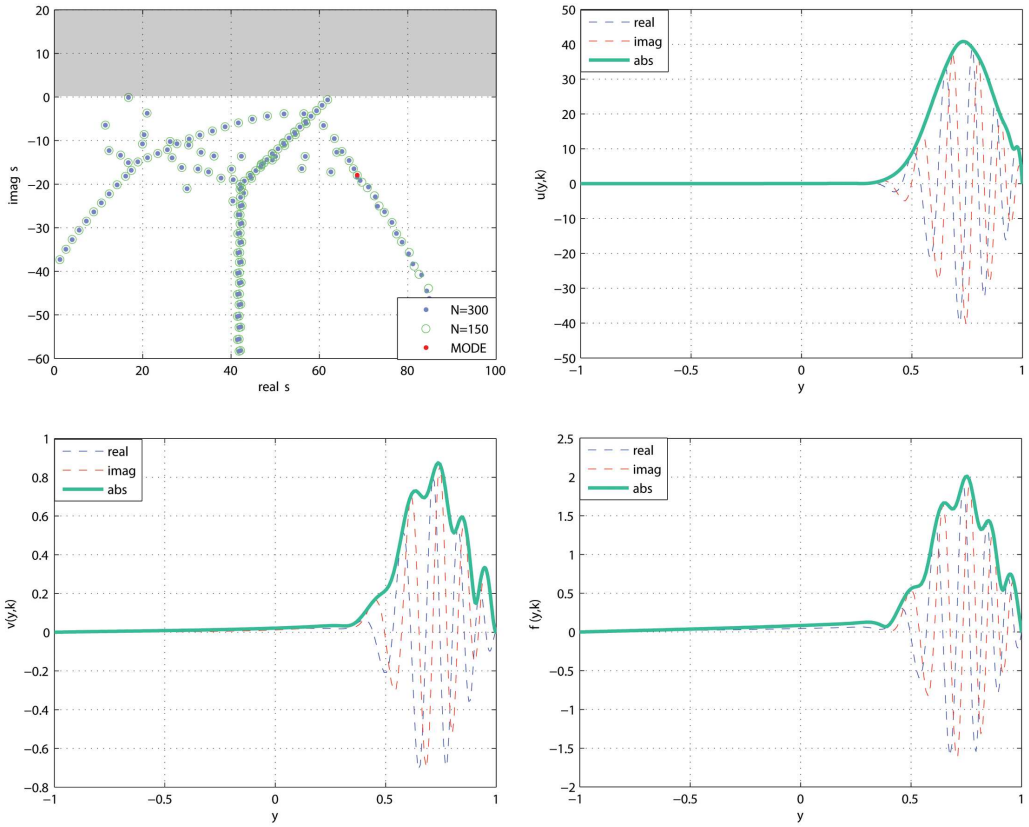

Figure E.10: Poiseuille case:*Modal Identification.* Mode $n75$. $\alpha = 1$, $\beta = 0$, $C = 50$, $Fe = 200$, $M = 5$, $N = 250$, $Re = 5000$, $T = 2000$

Bibliography

[1] P. Atten. Electrohydrodynamic instability and motion induced by injected space charge in insulating liquids. *Conduction and Breakdown in Dielectric Liquids,1993., ICDL '93., IEEE 11th International Conference on*, pages 20 –29, jul 1993.

[2] P. Atten and J.C. Lacroix. Non-linear hydrodynamic stability of liquids subjected to unipolar injection. *Journal de Mecanique*, 18(3):469–510, 1979.

[3] P. Atten, F.M.J. McCluskey, and A.T. Perez. Electroconvection and its effect on heat transfer. *Electrical Insulation, IEEE Transactions on*, 23(4):659 – 667, aug 1988.

[4] P. Atten and R. Moreau. Stabilité electrohydrodynamique des liquides isolants soumis une injection unipolaire. *Journal de Mecanique*, 11(3):471521, 1972.

[5] John P. Boyd. *Chebyshev and Fourier Spectram Methods*. Springer-Verlag, first edition edition, 1989.

[6] A. Castellanos. Coulomb-driven convection in electrohydrodynamics. *Electrical Insulation, IEEE Transactions on*, 26(6):1201 –1215, dec 1991.

[7] A. Castellanos and N. Agrait. Unipolar injection induced instabilities in plane parallel flows. *Industry Applications, IEEE Transactions on*, 28(3):513 –519, may/jun 1992.

[8] M. Quadrio D. Cerizza. Direct numerical simulation of two way 3D EHD coupling. Master's thesis, Aerospace Engineering dept. Politecnico of Milan, Italy, 2008.

[9] S.A. Orszag D. Gottlieb. *Numerical Analysis Of Spectral Methods - Theory And Applications*.

[10] N. Felici. Dc conduction in liquid dielectrics: Electrohydrodynamic phenomena. *Dir. Current*, 2(3):147–165, 1972.

[11] Ardeshir Hanifi, Peter J. Schmid, and Dan S. Henningson. Transient growth in compressible boundary layer flow. *Physics of Fluids*, 8(3):826–837, 1996.

[12] B. Gosse J.P. Gosse and A. Denant. La conduction electrique des liquides diélectriques. *Rev. Generale Électricité*, 10(85):733–744, 1985.

[13] L. Reddy T. Driscoll L. Trefethen, A. Trefethen. Hydrodynamic stability without eigenvalues. *Sciences*, (261):578–584, 1993.

[14] M. Embree L. Trefethen. *Spectra and Pseudospectra: the behavior of nonnormal matrices and operators*. Princeton university press, 2005.

[15] H. Omidvarborna, A. M. Zeinabad, and M. N. Esfahany. Effect of electrohydrodynamic (ehd) on condensation of r-134a in presence of non-condensable gas. *International Communications in Heat and Mass Transfer*, 36(3):286 – 291, 2009.

[16] A. T. Perez and A. Castellanos. Role of charge diffusion in finite-amplitude electroconvection. *Phys. Rev. A*.

[17] D.S. Henningson P.J. Schmid. *Stability and transition in shear flow*. Springer, applied mathemethical sciences 142 edition, 2001.

[18] F. Pontiga, A. Castellanos, and B. Malraison. Some considerations on the instabilities of nonpolar liquids subjected to charge injection. *Physics of Fluids*, 7(6):1348–1356, 1995.

[19] A. Castellanos R. Chicon and E. Martin. Numerical modelling of coulomb-driven convection in insulating liquids. *Journal of Fluid Mechanics*, (344):43–66, 1997.

[20] J. Johnson R. Horn. *Topics in matrix analysis*. Cambridge University Press, 1991.

[21] S.C. Reddy and D.S. Henningson. Energy growth in viscous channel flows. *Journal of Fluid Mechanics*, (252):209–238, 1993.

[22] M. Quadrio S. Ceccon. Interazione fra campo fluidodinamico e campo elettrico. Master's thesis, Aerospace Engineering dept. Politecnico of Milan, Italy, 2005.

[23] V. Schenested. Contribution to the theory of hydrodynamic stability. Master's thesis, Phd tesis, University of Michighan, Ann Arbor, 1961.

[24] Peter J. Schmid. Nonmodal stability theory. *Annual Review of Fluid Mechanics*, 39(1):129–162, 2007.

[25] J. M. Schneider and P. K. Watson. Electrohydrodynamic stability of space-charge-limited currents in dielectric liquids. i. theoretical study. *Physics of Fluids*, 13(8):1948–1954, 1970.

[26] V. I. Yudovich V. G. Babskii. *Mathematical Theory of Electrophoresis*. Springer Science, 1989.

[27] P. K. Watson, J. M. Schneider, and H. R. Till. Electrohydrodynamic stability of space-charge-limited currents in dielectric liquids. ii. experimental study. *Physics of Fluids*, 13(8):1955–1961, 1970.

[28] Xiaohong Nancy Xu. Modern electrochemistry. *Journal of the American Chemical Society*, 122(9):2144–2144, 2000.

[29] J.B. Hull Y.Y. Yan, H.B. Zhang. *Numerical modelling of electrohydrodynamic (EHD) effect on natural convection in an enclosure*. Taylor and Francis, numerical heat transfer, part a: applications: an international journal of computation and methodology edition, 2004.